Inaugural dissertation
for
obtaining the doctoral degree
of the
Combined Faculty of Mathematics, Engineering and Natural Sciences
of the
Ruprecht - Karls - University
Heidelberg

Presented by M.Sc. Bogac Aybey
born in Istanbul, Turkey
Oral examination: 23.05.2025

Comprehensive characterization of gene expression response to type-I and type-II interferon in healthy and diseased conditions

Referees: **Prof. Dr. Benedikt Brors**

Prof. Dr. Nina Papavasiliou

Abstract

Interferons (IFNs) are critical regulators of the immune system, with special importance for viral infections, autoimmune diseases, and cancer. However, there are challenges in distinguishing the effects of different IFN types and understanding their cell-type-specific responses. Single-cell sequencing can address these gaps but requires robust tools for cell-type classification and precise analysis of IFN-mediated effects. To better characterize IFN- and cell-type-specific gene expression responses, novel bioinformatics approaches are needed.

One of the main challenges in single-cell analysis is cell-type classification. Most approaches use expression information of all expressed genes to provide cell type labels. However, they often introduce bias into statistical procedures when testing the same genes for differential expression that were already used for cell typing. In the first chapter of my thesis, I addressed this issue by using only small sets of robust immune cell-type-specific genes for cell typing within a random forest model. While most studies have generated such gene expression signatures (GESs) from single gene expression datasets, I developed a novel GES discovery workflow based on similarities in gene expression across seven single-cell cancer datasets. Compared to existing algorithms and published GESs, my approach showed superior or comparable performance, significantly improved the classification of myeloid cells and enhanced downstream analysis of peripheral blood mononuclear cell (PBMC) datasets. Thereby, I establish an unbiased method for classifying immune cells and statistical investigation of expression differences between cell types.

In the second part, I dissected distinct effects of IFN-I and IFN-II across different cellular, experimental, and disease contexts. Published IFN GESs have been purely generated from only single gene expression datasets within specific cellular contexts and primarily comprise genes induced by IFN-I. I used five different bulk tissue RNA-sequencing datasets of IFN stimulation and applied a novel meta-analysis workflow to resolve GESs with specificity for IFN-I and IFN-II response. My IFN GESs had greater functional relevance to IFN-type-specific response and higher coherence than most published signatures. My IFN-II GES detected IFN-II response of not only myeloid cells but also B cells, hematopoietic cells, and naïve T cells. Further, I demonstrated the relevance of IFN-I GES in disease severity of lupus nephritis, and IFN-II GES as predictive biomarker for immune checkpoint inhibitor response. I provide a more precise distinction between IFN-I and IFN-II responses at the cell type level, as well as their relevance to disease progression and therapy outcomes.

In the final part, I characterized immune cell-type-specific responses to IFNs as comprehensive and objective studies of these responses are still lacking. Previous studies do

not provide cellular or temporal resolution, nor compare responses across different IFNs within a single study. To address this gap, I applied the tool sets established in Chapter 1 and 2 on a novel temporal CITE-seq dataset of IFN-I and IFN-II stimulation of human PBMCs. I showed that all immune cell types exhibited transient responses to IFN-I stimulation while only myeloid and B cells responded to IFN-II, with distinct dynamic patterns. Furthermore, I identified five unique temporal gene groups specific to monocyte responses to IFN-I or IFN-II. Those groups consist of genes that play key roles in distinct immunological pathways. My findings enable a more detailed characterization of IFN-mediated responses in distinct immune cell populations compared to those provided by published datasets or GESs.

In this thesis, I introduce novel bioinformatics tools that address key challenges in immune cell classification and the study of IFN responses. These methods advance the resolution of immune profiling in single-cell data and provide more precise insights into IFN-mediated immune cell type responses in both health and disease. My approaches overcome the limitations of existing workflows, offering new insights into IFN biology and its relevance to disease mechanisms, as well as potential applications in biomarker research and therapy.

Zusammenfassung

Interferone (IFNs) sind kritische Regulatoren des Immunsystems und spielen eine zentrale Rolle bei viralen Infektionen, Autoimmunerkrankungen und Krebs. Um diese kritischen Regulatoren therapeutisch zugänglich zu machen, muss es möglich werden die Effekte von verschiedenen IFN-Typen zu unterscheiden und ihre zelltypspezifischen Antworten zu verstehen. Einzelzell-Sequenzierung bietet zwar diese Möglichkeit, aber erfordert robuste Methoden zur Zelltypklassifizierung und eine präzise Analyse der Effekte von IFNs. Um IFN- und zelltypspezifische Genexpressionsprofile besser zu charakterisieren, sind daher neuartige bioinformatische Ansätze nötig.

Eine der größten Herausforderungen bei der Einzelzellanalyse ist die Zelltypklassifizierung. Die meisten Methoden verwenden die Expressionsinformation aller exprimierten Gene, um Zelltypen zu bestimmen. Dabei entsteht jedoch häufig ein Bias, wenn dieselbe Gene sowohl für die Zelltypbestimmung als auch für die Analyse differentieller Expression verwendet werden. Im ersten Kapitel meiner Dissertation bin ich dieses Problem angegangen, indem ich eine kleine Anzahl von robusten Genen, die spezifisch für Immunzellen sind, in einem Random-Forest-Modell eingesetzt habe. Während andere Studien solche Genexpressionssignaturen (GESs) auf Basis einzelner Datensätze erstellt haben, entwickelte ich eine neuartige Methode zur Entdeckung von GESs basierend auf den Genexpressionsmustern von über sieben Einzelzell-Krebsdatensätzen. Mein Ansatz übertraf die Ergebnisse bestehender Algorithmen und bereits veröffentlichter GESs. Außerdem konnte ich mit diesem Ansatz eine signifikante Verbesserung der Klassifizierung von myeloider Zellen erreichen und optimierte die Downstream-Analyse von mononukleäre Zellen des peripheren Blutes (PBMC) wesentlich. Damit führe ich eine unvoreingenommene Methode ein, die präzisere Zelltypklassifizierung und differentielle Genexpressionsanalyse ermöglicht.

Im zweiten Teil meiner Arbeit untersuchte ich die spezifischen Effekte von IFN-I und IFN-II in verschiedenen zellulären, experimentellen und krankheitsspezifischen Kontexten. Publizierte IFN-GESs basieren in der Regel auf einzelnen Datensätzen und bestehen oft aus IFN-I-induzierten Genen. Ich habe fünf verschiedene Bulk RNA-Sequenzierungsdatensätze analysiert und einen neuen Metaanalyse-Workflow angewandt, um GESs für IFN-I- und IFN-II spezifische Antworten zu ermitteln. Im Ergebnis dieser Analyse zeigten meine GESs eine hohefunktionelle Relevanz und Kohärenz und übertrafen damit die meisten publizierten GESs. Die IFN-II-GES erkannte nicht nur myeloide Zellantworten, sondern auch die Antworten von B-Zellen, hämatopoetischen Zellen und naiven T-Zellen. Außerdem konnte ich mit dieser Vorgehensweise aufzeigen, dass die IFN-I-GES mit der klinischen Krankheitsaktivität von Lupusnephritis korreliert, während die IFN-II-GES als prädiktiver Biomarker für die Wirksamkeit von Immuncheckpoint-Inhibitoren

dient. Zusammengefasst konnte ich eine präzisere Unterscheidung der IFN-Antworten auf Zelltypenebene ermöglichen und einen klaren Bezug zu ihrer Bedeutung für Krankheitsverläufe und Therapieerfolge herstellen.

Im dritten und letzten Teil meiner Arbeit adressierte ich dann die Tatsache, dass es bis zu diesem Zeitpunkt keine umfangreichen und objektiven Studien zur zelltypspezifische IFN-Antwort gibt. In den bisherigen Studien fehlen entweder die zelluläre oder zeitliche Auflösung oder es wurde kein Vergleich der Antworten verschiedener IFNs innerhalb einer einzelnen Studie durchgeführt. Um diese Lücke zu schließen, habe ich die in den ersten beiden Kapiteln entwickelten Methoden auf einen neuartigen zeitlichen CITE-seq-Datensatz angewandt, der die IFN-I- und IFN-II-Behandlung menschlicher PBMC untersucht. So konnte ich zeigen, dass alle Immunzellen vorübergehend auf IFN-I reagierten, während nur myeloide Zellen und B-Zellen auf IFN-II reagierten, jedoch mit unterschiedlichen dynamischen Mustern. Zudem identifizierte ich fünf zeitliche Genmuster, die für die IFN-Antwort in Monozyten entscheidend sind und zentrale immunologische Funktionen regulieren. Meine Ergebnisse liefern eine präzisere Charakterisierung der IFN-vermittelten Antworten als bisher verfügbare Datensätze oder Signaturen.

In dieser Dissertation stelle ich neuartige bioinformatische Methoden vor, die zentrale Herausforderungen in der Klassifizierung von Immunzellen und Untersuchung von IFN-Antworten angehen. Diese Methoden verbessern die Auflösung der Immunprofilierung in Einzelzelldaten und erschaffen genauere Einblicke in die IFN-vermittelten Immunreaktionen, sowohl im gesunden Zustand als auch in Krankheiten. Meine Ansätze überwinden die Einschränkungen bestehender Methoden und bieten neue Perspektiven in die IFN-Biologie und ihre Relevanz für Krankheitsmechanismen sowie mögliche Anwendungen in der Biomarkerforschung und -therapie.

Acknowledgements

As I mention in the first chapter of my thesis, "no man is an island." People come into our lives and impact us in different ways. No single person can make you whole, but it is the unison of all that truly makes the difference. I am so grateful to have encountered such diverse individuals who fulfill different parts of my life like puzzle pieces, each fitting into different corners of my journey.

I want to thank my TAC members, Benedikt Brors and Nina Papavasiliou, for your curiosity, interest, and feedback. Ich möchte mich herzlich bei Benedikt Brors und Eike Staub für eure sorgfältige Betreuung seit meiner Masterarbeit bedanken. Besonders mein Mentor bei Merck, Eike, hat mich immer gefordert, mich weiterzuentwickeln. Ich bin auch dankbar für die finanzielle Unterstützung von Merck KGaA für meine Doktorarbeit. I am also grateful for nice discussions, motivation, and curiosity of Data Science group at Merck especially Felix, Julian, Johanna, Olga, Dila, and Sheng.

İlk başta bana desteklerinden dolayı aileme teşekkür etmek istiyorum, özellikle her sorunda beni dinleyen ve bana yardımcı olan anneme. Çocukluğumdan beri beni her konuda geliştiren, okumaya ve başka kültürleri anlamaya iten kişiye... Bu yolculukta hep yanımda olan arkadaşlarıma da buradan seslenmek istiyorum: Dilara ve Ece. Her şey hakkında konuşabildiğim, gezileri, hayatı ve her şeyi paylaştığım en yakın arkadaşlarım... Öneminizi satırlara sığdıramam, Almanya'daki ailemsiniz çünkü. Bu ailenin diğer üyeleri Ecem, Simge, Aysu ve Pelin de Heidelberg'i yaşanır kılan insanlar arasında.

Eine der tapfersten, klügsten, witzigsten, freundlichsten, abenteuerlichsten, intelligentesten und intellektuellsten Personen ist Simona. Sie ist seit 10 Jahren immer in meinem Leben. Danke, dass du existierst und dass ich dich meine beste Freundin nennen darf.

Ich möchte auch eine wichtige Person erwähnen, mit der ich mein Leben geteilt habe: Lukas. Er hat mich immer gefordert, und hat immer an mich geglaubt, auch wenn ich es selbst nicht konnte. Du wolltest immer das Beste für mich. Dafür und für die schönen Erinnerungen werde ich immer dankbar sein.

Life is at the end a give-and-take relationship. During my doctoral thesis many people have come into different eras of my life and allowed me look into the life from their 'windows'. I am incredibly grateful that they opened their 'houses' for me to observe.

Thank you! Danke! Teşekkürler! Grazie! ¡Gracias! Obrigado! Dank je! Tack! Ευχαριστώ! Merci!

Contents

List of Figures

List of Tables

Abbreviations

BRCA	Breast cancer
CLR	Centered log ratio
CRC	Colorectal cancer
CS	Coherence score
DBSCAN	Density-Based Spatial Clustering of Applications with Noise
DCs	Dendritic cells
DGE	Differential gene expression
DEGs	Differentially expressed genes
FACS	Fluorescence-Activated Cell Sorting
FC	Fold-change
FDR	False discovery rate
FN	False negatives
FP	False positives
FPKM	Fragments Per Kilobase of transcript per Million mapped reads
GEO	Gene Expression Omnibus
GES	Gene expression signature
HSC	Hematopoietic stem cells
HVGs	Highly variable genes
ICI	Immune checkpoint inhibitor
IFN	Interferon
IFN-a	IFN-alpha
IFN-b	IFN-beta
IFN-g	IFN-gamma
IFN-I	Type-I IFN
IFN-II	Type-II IFN
IFN-III	Type-III IFN
IFN-λ	IFN-lambda
ISGs	IFN stimulated genes
KIRC	Kidney renal clear cell carcinoma
log	logarithm
LIHC	Liver hepatocellular carcinoma
minPts	Minimum number of points
NK	Natural killer cells
NMA	Network meta-analysis
NPV	Negative predictive value
NSCLC	Non-small cell lung cancer
PBMC	Peripheral blood mononuclear cell

PCA	Principal component analysis
pDCs	Plasmacytoid dendritic cells
PPV	Positive predictive value
RF	Random forest
RNA-seq	RNA sequencing
RPCA	Reciprocal principal component analysis
SC	Spearman correlation
scRNA-seq	Single-cell RNA sequencing
SKCM	Skin cutaneous melanoma
SLE	Systemic lupus erythematosus
SLEDAI	Systemic lupus erythematosus disease activity index
TCGA	The Cancer Genome Atlas
TLRs	Toll-like receptors
TME	Tumor microenvironment
TN	True negatives
TP	True positives
TPM	Transcripts Per Million
UMAP	Uniform manifold approximation and projection

My publications and conference contributions

Publication related to Chapter 1:
Aybey, B., Zhao, S., Brors, B., and Staub, E. (2023). Immune cell type signature discovery and random forest classification for analysis of single cell gene expression datasets. Front Immunol *14*, 1194745.

I extended the initial conceptualization and ideas from my published paper and my master thesis (unpublished) titled "Exploratory Meta-Analysis of Single Cell RNAseq Cancer Expression Datasets: Characterizing Cancer Immune Response and Evasion" (Aybey, 2020) for the discovery part of the first chapter of my doctoral thesis.

Manuscript related to Chapter 2:
Aybey, B., Brors, B., and Staub, E. (2025). Expression signatures with specificity for type I and II IFN response and relevance for autoimmune diseases and cancer. *Manuscript in preparation.*

Manuscript related to Chapter 3:
Aybey, B., Brors, B., and Staub, E. (2025). Single cell analysis revealed immune cell type specific temporal IFN activation patterns of blood monocytes. *Manuscript in preparation.*

Contributed publications not related to the doctoral thesis

Kreis, J., Aybey, B., Geist, F., Brors, B., and Staub, E. (2024). Stromal Signals Dominate Gene Expression Signature Scores That Aim to Describe Cancer Cell-intrinsic Stemness or Mesenchymality Characteristics. Cancer Res Commun *4*, 516-529.

Markowska, M., Cakała, T., Miasojedow, B., Aybey, B., Juraeva, D., Mazur, J., Ross, E., Staub, E., and Szczurek, E. (2022). CONET: copy number event tree model of evolutionary tumor history for single-cell data. Genome Biol *23*, 128.

Posters

Aybey, B., Zhao, S., Brors, B., and Staub, E. (2022). Machine learning for improved immune cell type classification as a basis to better understand effects of cell type specific interferon stimulation. *Merck Science Academy, Merck KGaA-online*

Aybey, B., Zhao, S., Brors, B., and Staub, E. (2023). Machine learning for improved immune cell type classification as a basis to better understand effects of cell type specific interferon stimulation. *ECCB, Sitges, Spain*

Talk

Aybey, B., Zhao, S., Brors, B., and Staub, E. (2023). Immune cell type signature discovery and random forest classification for analysis of single cell gene expression datasets. *Genes 2023 Single-Cell Genomics Moving Forward, Barcelona, Spain*

1 Introduction

1.1 Interferons: brief history

IFNs are proteins classified as cytokines, signaling molecules that regulate both the adaptive and innate immune systems. In the 1950s, Isaacs and Lindenmann observed acquired immunity upon primary infection in non-infected cells through an unknown substance in the medium (Isaacs and Lindenmann, 1957). They named this substance IFN meaning it 'interfered' with influenza cells. Later, the anti-viral properties of IFNs were extended to other viruses, increasing their importance as antiviral agents (Katze et al., 2002). IFNs were originally suggested to be anti-viral molecules. Later, their basic relevance for many immunity-related processes, especially in autoimmune diseases, became clear. Their anti-tumor effects have since been demonstrated in the context of cancer, not only in tumors of viral origin but in various tumors of different origins (Taylor, 2014). Although IFNs are broadly relevant and important for immune system regulation, IFNs are still an enigma in the immunology field. Despite many studies, a thorough and complete characterization of their transcriptional effects, particularly responses to different IFNs in different cellular and disease contexts, is still lacking. Understanding those effects and related mechanisms could provide novel strategies for targeting different aspects of disease biology: development, progression, therapy, and prevention (Aricò et al., 2019).

1.2 Transcription of IFN genes

The IFN family is a diverse group of immune-modulatory proteins consisting of three major types: type-I IFN (IFN-I), type-II IFN (IFN-II), and type-III IFN (IFN-III) (Platanias, 2005). IFN-I comprises seven types (α, β, ε, ω, ϰ, τ, and δ), as well as various isoforms of IFN-α (IFN-alpha/alfa, IFN-a). IFN-II contains only IFN-γ (IFN-gamma, IFN-g), while IFN-III consists solely of IFN-λ (IFN-lambda) and its isoforms. Together, these types and isoforms regulate diverse immune responses, each contributing uniquely to immune modulation.

Originally, IFNs were discovered by their induction upon viral infection. Further studies demonstrated that IFNs are released upon various cellular stimuli. IFN-I production can be triggered by microbial or viral glycolipids, viral RNA or DNA, and aberrant DNA or RNA from dying cells (Jorgovanovic et al., 2020; Borden, 2019; Perry et al., 2005). Pattern recognition receptors, such as Toll-like receptors (TLRs), located on the surface or inside the cell, detect extracellular stimuli and trigger downstream signaling pathways that lead to the expression of IFN-I types. Additionally, there are several intracellular

sensor pathways, such as the STING-cGAS pathway, which is activated by viral or host DNA from damaged cells. On the other hand, interleukins, tumor- or pathogen- secreted antigens and IFN-II stimulate IFN-II production. Notably, IFN types differ in terms of their production patterns. IFN-I is produced in the early phase of an infection, playing a central role in innate immune system, while IFN-II is secreted later, linking innate and adaptive immunity (Lee and Ashkar, 2018). IFN-I and IFN-III can be produced by various cells, while mainly immune cells such as T and natural killer (NK) cells secrete IFN-II (Jorgovanovic et al., 2020; Swiecki and Colonna, 2011). These temporal and cellular differences in IFN production indicate the specialized and complementary roles of IFN types in immunity.

1.3 IFN signaling and response: distinct activation pathways for different types of IFNs

IFNs initiate their signaling processes through binding to specific receptors on target cells, which activates downstream signaling pathways. These pathways are broadly classified into two types: the canonical and non-canonical pathways (Lee and Ashkar, 2018). The canonical IFN pathway is IFN type-specific with distinct receptors, kinases, transcription factors, and response elements responsible for the response. The signaling pathway involves three main steps: receptor binding, activation of receptor-associated kinases, and downstream signaling in which transcription factors and response elements activate multiple IFN stimulated genes (ISGs).

Each IFN type binds to distinct receptors: IFNAR1-IFNAR2 for IFN-I, IFNGR1-IFNGR2 for IFN-II, and IFNLR1-IL-10R2 for IFN-III (Chow and Gale, 2015; Mesev et al., 2019). Notably, IFN-I and IFN-III share the same downstream signaling pathway: the activation of TYK2-JAK1 kinases, formation of the STAT1-STAT2-IRF9 complex, and binding of the complex to IFN-stimulated response elements in the nucleus. Despite the similarities in signaling cascade and overlapping ISGs, IFN-I and IFN-III can lead to different signaling outcomes (Lazear et al., 2019). In contrast, IFN-II uses different downstream signaling elements, including JAK1-JAK2 kinases, formation of STAT1 homodimers, and activation of gamma-activated sequences on the promoters of ISGs (Mesev et al., 2019). Further, earlier studies (reviewed in Castro et al. (2018); McNab et al. (2015); Chow and Gale (2015)) suggest that while almost all nucleated cells are responsive to IFN-I and IFN-II, only non-hematopoietic cells respond to IFN-III. These distinctions illustrate the diverse roles and responses associated with each IFN type.

Despite their distinct pathways, IFNs of different types activate the transcription of overlapping sets of ISGs which complicates the interpretation of their individual roles in im-

mune responses (Cooles and Isaacs, 2022; Hall et al., 2012; Platanias, 2005; El-Sherbiny et al., 2018). While a few ISGs are uniquely stimulated by either IFN-I or IFN-II, many are commonly induced by both. Additionally, within IFN-I subtypes, many reports have shown differing downstream effects, further complicating the identification of specific contributions (Mesev et al., 2019; Garcin et al., 2013; James et al., 2007; Schreiber, 2017). Yet. resolving those differences are critical for understanding IFN biology and its implications for immune responses, disease, and therapy.

1.4 Quantification of gene expression: from microarrays to single-cell sequencing

The challenges in disentangling complex IFN biology emphasizes the importance of genome-wide gene expression profiling, a key approach in biomedical research for analyzing gene expression differences between different conditions such as between healthy and disease states. Different methods have been developed to quantify the level of gene expression, creating the field of transcriptomics. Especially high throughput technologies provide cost-effective and faster analysis of many genes at the same time (Soon et al., 2013). During my thesis, I have utilized transcriptomic datasets produced by different gene expression quantification technologies, chosen based on the specific research question. In this section, I shortly introduce those relevant technologies along with their advantages and disadvantages.

Earlier studies applied microarray-based methods which use the hybridization of labelled nucleic acids probes derived from biological samples to arrayed nucleic acid probes of thousands of genes for expression profiling (Stears et al., 2003; Govindarajan et al., 2012). Even though compared to previous experimental technologies, microarrays serve as cost-effective and quantitative method with well-established protocols and methods, there are some disadvantages. Probe sets on the arrays or chips are fixed and only known transcripts can be detected hindering discovery of novel transcripts (Kratz and Carninci, 2014). Further, binding of multiple probes ('cross-hybridization') might lead to false signals (Okoniewski and Miller, 2006). The detection range of hybridization technology is limited, which affects precision at both ends of the intensity scale. Signals from lowly expressed genes may be masked by background noise, while signals from highly expressed genes may not be detected once they reach the maximum detection limit (Wang et al., 2009). Although microarrays are still applicable for addressing certain biological questions, their limitations required the need for more precise technologies.

RNA sequencing (RNA-seq) emerged as a high throughput solution to address the challenges of microarray technologies, offering detection of a large range of known and un-

known transcripts as well as highly and lowly expressed genes (Wang et al., 2009; Van den Berge et al., 2019). This advancement significantly contributed to the field with major advancements, particularly by allowing for more comprehensive gene expression analysis. However, RNA-seq, while impactful, initially lacked the single-cell resolution to address research questions regarding heterogeneous tissues. RNA-seq analysis provides an average expression for all cell types resulting in highly abundant cells to dominate the overall expression signal and hinder the contributions of less abundant cells (Newberg et al., 2018). Although these limitations exist, RNA-seq has remained the dominant technique for over a decade, leading to the generation of large, valuable datasets such as The Cancer Genome Atlas (TCGA) (Chang et al., 2013), Cancer Cell Line Encyclopedia (Barretina et al., 2012), and Genotype-Tissue Expression project (Lonsdale et al., 2013), which led to further discoveries and techniques.

To address the limitations of bulk tissue RNA-seq techniques, single-cell RNA sequencing (scRNA-seq) has emerged. Since the pioneering work of Tang et al. in 2009 (Tang et al., 2009), diverse scRNA-seq platforms have been established tailored for specific research questions. These methodologies enable detection of each cell within a heterogeneous cell population, allowing the examination of cell-to-cell variability and identification and phenotypic characterization of rare and known cell types (Lim et al., 2023). Especially in the context of disease and therapy, cell-type specific transcriptomic alterations can be identified, enabling more precise disease characterization and enhancing drug discovery and development. The field continues to grow producing large atlases and databases of various tissues and diseases from large collection of organisms such as Human Cell Atlas (Regev et al., 2017), TISCH2 initiative (Han et al., 2023), and tumor microenvironment atlas (Nieto et al., 2021).

scRNA-seq offers several advantages over bulk tissue RNA-seq particularly in examining cellular heterogeneity but still there are technical limitations to be addressed in the field. The main challenges are lack of 'gold standards' and robust methods for cell type classification and downstream analysis of cell type-specific gene expression (Lafzi et al., 2018; Lahnemann et al., 2020). Addressing these limitations is crucial to maximize the potential of scRNA-seq and improve the reliability of biological data interpretation.

1.5 Exploratory analysis of transcriptomics data

Exploratory data analysis examines the structure of data and identifies dominant as well as subtle patterns that may provide insights into the underlying processes. Depending on the research question and the purpose of the analysis, various exploratory data analysis workflows can be employed. Here, I briefly introduce two methods for exploratory data

analysis—dimensionality reduction and clustering—that I used throughout all chapters of my thesis.

1.5.1 Dimensionality reduction

Dimensionality reduction is a key technique in sequencing data analysis to visualize high dimensional data and understand major variations and patterns in the data. There are two types of methods: linear and non-linear. Principal component analysis (PCA) is the most widely used linear method. It identifies orthogonal directions, or principal components, that capture the maximum variance in the data (Pearson, 1901). While PCA is effective for linear structures, it struggles to capture complex, non-linear relationships commonly found in scRNA-seq data (Kiselev et al., 2019; McInnes and Healy, 2018; Choi and Kim, 2019; Linderman, 2021). Additionally, linear methods are sensitive to noise, which can distort the data's true structure. To overcome the limitations of linear methods, non-linear dimensionality reduction techniques have been developed.

Commonly used non-linear dimensionality reduction methods are: t-distributed stochastic neighbor embedding (t-SNE) (Kobak and Berens, 2019) and uniform manifold approximation and projection (UMAP) (McInnes and Healy, 2018). t-SNE preserves local relationships in high-dimensional data by modeling similarities between points as probabilities (Kobak and Berens, 2019; van der Maaten and Hinton, 2008). It models these relationships as probabilities in the original high-dimensional space and seeks to represent them similarly in a reduced-dimensional space. The method adjusts the lower-dimensional representation to minimize the difference between the two sets of probabilities, ensuring that nearby points remain close after dimensionality reduction. While this method effectively captures local patterns, it often distorts the global structure of the data and can be computationally demanding when applied to larger datasets (McInnes and Healy, 2018; Becht et al., 2019). In contrast, UMAP is based on principles of topology to capture both local and global structures. It creates a graph to represent the local relationships between data points and then uses this graph to map the data into a lower-dimensional space. UMAP is computationally efficient and scalable, making it more suitable for analyzing larger datasets compared to t-SNE. Such non-linear dimensionality reduction methods transform complex data into low-dimensional spaces, making it easier to extract biological and dataset-specific insights and relationships in single-cell data.

One important step of dimensionality reduction analysis is the selection of relevant features. This marks the beginning of each analysis and represents an important decision with huge impact on the results, particularly in single-cell data analysis. These features are often referred as highly variable genes (HVGs) (Luecken and Theis, 2019). Each al-

gorithm has its own method for selecting HVGs. For example, Seurat, a commonly used analysis tool in single-cell analysis (Satija, 2016), identifies HVGs based on variance-to-mean ratio, with a default of 2,000 genes. Typically, between 1,000 and 5,000 HVGs are used. Luecken and Theis (2019) recommends selecting more than 2,000 HVGs. Using few HVGs might limit the distinction of fine-grained cell populations (Amezquita et al., 2020, 2021). On the other hand, including a large number of HVGs might introduce noise or capture irrelevant features, hindering detection of true signal. The selection of HVGs depends on the dataset and the specific analysis objectives, but it might significantly influence the accuracy and interpretability of subsequent analyses.

The low-dimensional representation can be further explored to check for potential batch effects. Batch effects may arise from variations in experimental conditions, sample processing, or other technical and biological factors. These effects should be corrected if samples do not cluster by expected conditions or biological properties. However, the correction should not hinder the true biological signal nor impede the downstream analysis (Sprang et al., 2022). Contrast to batch correction, when working with multiple datasets, especially from different sources or experimental conditions, data integration (or harmonization) becomes essential (Luecken et al., 2022). While batch removal corrects for batch within a single dataset, typically from same lab or experiment, data integration addresses nested batch effects, such as those from multiple labs or protocols. The goal of data integration is to combine datasets from different sources into a unified representation while preserving the biological diversity across them.

These dimensionality reduction techniques can be enhanced by using selected feature sets, such as known markers of cell types, which have the capability to stratify data in specific ways. This approach, which is often underused, allows investigation of whether these feature sets still fulfill their purpose on new, unseen data and effectively stratify the data objects into separate clusters. It also enables comparison between smaller, curated feature sets and larger, generic sets of HVGs in terms of their ability to reveal biologically meaningful structures.

1.5.2 Clustering

Clustering is an unsupervised technique used to discover groups of data points with similar features. The goal is to maximize the similarity between data points within clusters to the exclusion of dissimilar data points in other clusters. Clustering serves various tasks across different fields, capturing distinct patterns in the data. For example, in biomedical data, clustering is commonly used to group genes with similar expression profiles, to identify cell types in single-cell datasets, or to detect subpopulations within heterogeneous cell

populations. Clustering methods are useful tools for extracting meaningful biological patterns, enabling further analysis and insights.

Clustering methods can be broadly categorized into partitioning, hierarchical, density-based, and graph-based approaches. Each method is suited to specific tasks, as no single method fits all scenarios (Xu and Wunsch, 2005). Partitioning methods are often used when the number of clusters is predefined (Nies et al., 2019). In contrast, other methods do not require a predefined number of clusters. Hierarchical and partitioning methods are typically applied to smaller, less complex datasets, while density-based and graph-based methods are more efficient for handling larger, complex data. In my thesis, I applied hierarchical clustering to identify temporal gene expression patterns and density-based clustering for grouping similar gene expression profiles in immune cell types. Further, most single-cell methods, that I benchmarked, rely on graph-based approaches for clustering cells. Each method has unique strengths and applications, reflecting the diversity of datasets and clustering goals.

Hierarchical clustering creates tree-like structures called dendrograms by repeatedly merging or splitting data points based on their similarity (Eisen et al., 1998). It is useful for exploring the relationships between data points at different levels of similarity, making it particularly suited for cases where the structure of the clusters is not immediately obvious. Each node represents a single feature, and the branch length between points indicates their degree of similarity or dissimilarity. The tree can be cut at a specific height to define the clusters. This approach not only shows the hierarchical relationships between features but also provides multiple ways to define clusters, making it a valuable tool for exploratory analysis.

The DBSCAN algorithm is a density-based clustering method that groups data points based on local point density (Ester et al., 1996). It defines clusters as regions containing a minimum number of points (*minPts*) within a specified radius ϵ. Core points are points with at least *minPts* neighbors within ϵ. Border points are those within of a core point but with fewer than *minPts* neighbors themselves. Points that are not reachable from any core point are classified as noise. The advantage of DBSCAN include flexibility, a low number of parameters, effectively identifying arbitrary shapes, noise filtering, and no need for predefined cluster numbers.

Graph-based clustering is commonly used in single-cell data to group cells with similar transcriptional profiles into communities that reflect biological features (Zhu et al., 2020). Cells are represented as nodes, and edges represent the similarity of their transcriptional profiles. Similarity measurements, such as Euclidean distance or Pearson correlation, are often used to define links or even weighted links between nodes. However, as scRNA-seq

data dimensionality increases, these metrics struggle to capture relationships, especially non-linear ones, which involve interactions that simple linear models cannot describe. Graph-based clustering can capture such complex relationships by focusing on local neighborhood structures. To address this limitation, primary similarities are first calculated using traditional metrics, then refined by defining secondary similarities as edge weights in a weighted graph. Clustering is then performed based on a graph representation of the data by partitioning the graph into communities or sub-graphs. This approach is essential for studying cellular heterogeneity, particularly in the context of cell type classification.

While established methods exist for clustering single-cell data, one major challenge remains among the grand challenges in single-cell data analysis: the potential biases introduced in cell type classification by prior clustering, which can influence downstream analyses (Aybey et al., 2023; Gibson, 2022; Lahnemann et al., 2020; Pasquini et al., 2021; Zhang et al., 2019a). These biases can arise when the same data points are used both for determining cell types and identifying differentially expressed genes between these cell types. This violates the prerequisite of statistical independence for downstream tests, as the data used to assign class labels are not independent of the statistical tests performed. Overcoming these challenges requires careful methodological approaches to ensure accurate and biologically meaningful analyses.

1.6 Cell type concept: The identity of cells

With the development of single-cell technologies, our understanding of cellular diversity has advanced significantly. Still, challenges remain in defining cell types and classifying cells due to lack of standardized practices and non-comparable results across methods. Historically, the concept of cell type emerged from grouping cells based on phenotypical, functional, and structural similarities, simplifying the organization of cell populations (Zeng, 2022). In scRNA-seq, questions remain about how well unsupervised clusters represent true cell types, the consistency of cell type labels across datasets, the appropriate granularity, and the boundary between cell types and states (Trapnell, 2015). Further, the heterogeneity within the cell types complicates the matter. In the pursuit of categorizing cells, there have been alternative suggestions such as periodic table concept (Xia and Yanai, 2019), reference cell tree (Domcke and Shendure, 2023) or hierarchical trees (Michielsen et al., 2023). These frameworks aim to provide more standardized ways of defining cell types, yet the field remains in its early stages. More advancements in method development and definition of cell types are needed, alongside thorough examinations of the limitations of current approaches. The discrepancies in cell typing across different methods, and the influence of clustering techniques on these definitions, limit the inter-

pretation of the biological data. The field requires more robust and consistent strategies to define and annotate cell types.

1.7 Gene expression signatures and 'how to discover them'

Gene expression signatures (GESs) are sets of genes that exhibit unique expression patterns associated with specific biological pathways, conditions, diseases, or cellular states. These signatures are crucial in biomedical research, particularly in diagnosis, prognosis, and clinical outcome (Itadani et al., 2008). In scRNA-seq, cell type-specific GESs are utilized for classifying cell types and determining cell type abundance in bulk tissue RNA-seq data, providing insights into cellular heterogeneity and biological processes. They are an explicit statement about which genes are important markers for a specific biological phenomenon.

An ideal GSE should be exclusively upregulated under a certain biological or cellular stimulus and demonstrate high coherence within the signature, ensuring that the genes within the signature are biologically relevant to the condition or cell type being studied (Staub, 2012; Kreis et al., 2024). Challenges arise when identifying and applying GESs specific to certain biological conditions or cell types. Validating these signatures across diverse cellular contexts is essential for confirming their robustness and relevance. Using independent datasets ensures their consistency across conditions or tissues, emphasizing their biological significance and clinical potential. These steps ensure that the signature accurately reflects the biological process being studied, not unrelated noise. This is critical for translating findings across different settings, applying them effectively in immune profiling, and understanding complex biologies.

1.8 Cell type specific IFN response

Different cell types respond distinctly to IFNs, and the biological pathways regulated by these cytokines are highly context-dependent (McNab et al., 2015; Lee and Ashkar, 2018; Keskinen et al., 1997; Fenton et al., 2021; Gocher et al., 2022; Sri-Ngern-Ngam et al., 2022; Kosmidis et al., 2018). Notably, immune cell types have different sensitivities to IFN-I and IFN-II. For instance, monocytes are particularly responsive to IFN-II (Waddell et al., 2010). In contrast, IFN-I has broader transcriptional effects across a range of immune cells, including myeloid cells, B cells, T cells, and NK cells (McNab et al., 2015). Despite these insights, there is a lack of studies that comprehensively investigate IFN responsiveness at the single-cell level, particularly with regard to temporal changes and comparisons across different IFN types in immune cell populations. While bulk RNA-

seq or microarray studies reveal broad patterns of IFN-induced gene expression, they do not capture the variability within heterogeneous immune cells (Devlin et al., 2020; Reyes et al., 2019; Waddell et al., 2010). While single-cell studies on IFN responsiveness exist, they often fail to compare the effects of different IFN types or examine the temporal dynamics of these responses (Kartha et al., 2022; de Cevins et al., 2023; Karagiannis et al., 2020; Hartoularos et al., 2023; Goel et al., 2021). These gaps in research highlight the need for more comprehensive studies that can capture the dynamic and diverse nature of IFN signaling in immune cells. Advances in gene expression quantification technologies, combined with the use of GESs and improved bioinformatics methodologies, can provide deeper insights into complex IFN biology.

1.9 Objectives

In the previous sections, I have pointed out the shortcomings of previous studies that tried to disentangle the different types of IFN responses in immune cells, identify robust GESs, and establish unbiased approaches for cell type classification. This led to a number of study objectives of my thesis, building up successively on each other, that are the basis of the results that will be shown in the following three chapters:

i. To identify robust GESs for immune cell types that outperform published ones by leveraging multiple single-cell cancer datasets (Chapter 1).

ii. To develop a clustering-free and statistically unbiased method for cell type classification based on robust immune cell GESs for single-cell datasets, particularly suited for complex experimental setups as discussed in Chapters 2 and 3 (Chapter 1).

iii. To identify GESs that can specifically disentangle transcriptomic signals associated with responses to IFN-I and IFN-II, with higher specificity than published signatures (Chapter 2).

iv. To comprehensively evaluate IFN response GESs across various sequencing platforms, experimental conditions, and disease contexts (Chapter 2).

v. To assess the strength of immune cell type responses to IFN-I and IFN-II in an unbiased and comprehensive way using a newly generated temporal PBMC CITE-seq dataset upon IFN-I and IFN-II stimulation (Chapter 3).

vi. To investigate temporal immune cell type responses to IFN-I and IFN-II more comprehensively than previous studies and GESs by utilizing the tools developed from Chapter 1 and 2 (Chapter 3).

2 Chapter 1: “No gene is an island”

“No man is an island,
Entire of itself.
Each is a piece of the continent,
A part of the main.”
- John Donne, “No Man is an Island”

In this chapter, I present a novel workflow for identifying robust immune cell type GESs. I utilize gene expression similarities across seven scRNA-seq tumor microenvironment (TME) datasets from six different cancer types. I demonstrate the utility of those GESs in cell typing, by establishing and benchmarking a random forest (RF) classifier against five most often used methods. I compare my GESs and other published signatures using two PBMC scRNA-seq datasets. Finally, I evaluate the accuracy of cell type assignments and their impact on statistical downstream analyses using an IFN stimulation scRNA-seq dataset.

(I adapted this chapter based on my publication (Aybey et al., 2023), in which I was the lead author and for which I have conducted all analyses.)

2.1 Introduction

2.1.1 Pitfalls in cell type classification in single-cell datasets

Cell type classification is an important step in single-cell data analysis to examine cell-type specific alterations, which can provide insights into biological processes and disease mechanisms. Despite its importance, there is no standardized approach for this task. Current methods largely fall into two categories: unsupervised and supervised approaches. Unsupervised approaches are the most often used methods for annotating cell types: After clustering the cells based on transcriptional similarity, a cell type is assigned to each cluster based on the top differentially expressed genes (DEGs) or on small sets of canonical marker genes (Butler et al., 2018; Xie et al., 2021). While widely adopted, this process is generally manual, laborious, and error-prone due to the variability in clustering parameters, reproducibility issues, and a missing consensus on cluster definitions (Lahnemann et al., 2020; Zhao et al., 2019; Gibson, 2022).

Supervised methods offer an alternative by mapping reference datasets to the query data, identifying similarities between them (Sun et al., 2022). These approaches utilize various

techniques such as expression profile correlation, machine learning models, and signature scoring (some most commonly used algorithms are explained in Table 2.1). They provide a more systematic approach to cell type annotation, reducing the reliance on manual annotation and addressing some of the reproducibility challenges of unsupervised methods. Additionally, many automated cell type annotation methods have been developed to simplify the annotation process (Pasquini et al., 2021). Since cell type classification is inherently a supervised classification problem, best practices for such tasks (Dupuy and Simon, 2007) recommend avoiding class discovery and thus unsupervised methods to ensure more accurate downstream analyses.

Cell typing significantly impacts downstream analyses. Most supervised and unsupervised methods typically rely on prior clustering and information from multiple HVGs ($> 2{,}000$) (Table 2.1). As they reuse most part of the data (more than 2,000 HVGs) for both cell typing and statistical testing, these methods can introduce biases in downstream analyses, such as differential gene expression (DGE) testing in their estimation of the significance (Aybey et al., 2023; Gibson, 2022; Lahnemann et al., 2020; Pasquini et al., 2021; Zhang et al., 2019a). This may inflate the significance of findings and hide true biological signals by repeatedly relying on overlapping data features. To address this issue, I propose supervised classifiers focused on query data and a smaller set of cell type-specific genes, avoiding cluster-based methods.

Table 2.1: Benchmarked scRNA-seq cell type classification methods.

Method type	Method	Computational approach
Supervised, reference-based	Seurat label transfer (Stuart et al., 2019)	– Correlation of expression profiles between cell clusters from reference and query datasets in PCA space, based on predefined HVGs (default: 2,000)
	CHETAH (de Kanter et al., 2019)	– Internal gene marker selection (default: 200 genes per cell type) based on the highest absolute fold changes between one cell type against others in reference dataset; iterative cell type assignment based on correlation of expression profiles between reference and query datasets followed by hierarchical clustering
	SingleR (Aran et al., 2019)	– Correlation of expression profiles between reference and query datasets, based on internally selected variable genes (top down- or upregulated genes for each cell type; default: 1,000 genes)
	CellTypist (Domínguez Conde et al., 2022)	– Logistic regression classifier; top genes (default: 300) are selected internally for each cell type from the reference dataset
Unsupervised, reference-free	scType (Ianevski et al., 2022)	– Unsupervised clustering based on HVGs (default: 2,000) with cell type assignment for each cluster determined using signature scoring from the internal cell marker database

2.1.2 Importance of gene expression signatures in advancing immune cell typing in transcriptomics

GESs are important tools for understanding complex cell types such as immune cells especially in single-cell data. With the advancements of RNA-based technologies, immune cell type GESs have become essential for quantifying immune cell proportions in blood and immune cell infiltration into tumor through bulk tissue RNA-seq and cell type classification in single-cell datasets (Finotello and Trajanoski, 2018; Sturm et al., 2019). The usage of these sets of genes are especially advantageous over single marker gene strategies. Due to the stochastic expression of genes, most cells might not express canonical markers, but rather large sets of robust gene sets can offer more reliable and robust information (Grabski and Irizarry, 2022; Suvà and Tirosh, 2019).

Many immune cell type GESs have been derived primarily from bulk tissue RNA-seq or microarray datasets (Abbas et al., 2005; Angelova et al., 2015; Bindea et al., 2013;

Charoentong et al., 2017; Rooney et al., 2015). Recently, some GESs from single-cell data have emerged (Magen et al., 2019; Zhang et al., 2019c; Zilionis et al., 2019). However, these gene sets have been derived from single datasets rather than leveraging multiple discovery datasets. Such GESs may capture context-specific biases rather than universally applicable transcriptional patterns, reducing their utility for broad applications. Further, many studies have not validated their signatures across different experimental setups or systematically compared published methods and signatures for tasks like cell type classification in single-cell analysis. These issues further limit their reproducibility across different biological contexts and technical conditions.

To address the issues in immune cell type GES discovery and cell typing in single-cell data, I aimed to identify robust immune cell type GESs using multiple single-cell datasets from the TME. To eliminate the bias in downstream analysis, I opted to build a marker-based supervised cell type classifier that needs as input only the gene expression of genes in my GESs. This classifier would be advantageous over existing methods and enable a largely unbiased analysis of IFN responses, as demonstrated in both internal and external temporal and/or multi-perturbation single-cell datasets throughout the chapters.

2.1.3 Random forest classification

One possible machine learning approach for supervised cell type classification is random forest (RF), an ensemble method based on decision trees. The idea behind the RF is bagging, which leverages many random subsamples of the training data to create decision trees (Hastie et al., 2009). The training data consists of features and samples. For the classification of categorical data, the features serve as predictors of the class of a sample. The samples are randomly subsampled into bootstrap samples and random features are selected for each tree. The best split is chosen for each tree node until the minimum node size is reached. Once trained, each individual tree predicts the class of a new sample and the majority voting across all the trees determines the final prediction. In general, RF shows high prediction performance, is interpretable, requires minimal fine-tuning, and does not rely on clustering.

2.2 Methods

(I have taken the methods sections throughout this thesis directly from my original paper or unpublished manuscripts and presented them in quotation marks. I wrote almost all the texts. I took the following section from my publication (Aybey et al., 2023).)

2.2.1 Single-cell RNA-seq datasets and quality control for genes and cells

"I list all datasets used in this study for expression signature discovery, validation, classifier training and benchmarking purposes in Table 2.2, along with quality control metrics and dataset information. For all discovery datasets, I included only those immune cell types from tumor microenvironments in my analyses which were present in at least three discovery datasets. I obtained log-normalized expression matrices from the TISCH2 database (Han et al., 2023) for the datasets that I used for discovery of signatures. As a validation dataset, I used the tumor immune cell atlas (Nieto et al., 2021). I removed all samples from datasets that I had used for discovery purposes from the Nieto cell atlas that I used for validation." (Aybey et al., 2023)

During the preprocessing of all datasets, I filtered out low-quality cells with fewer than 200 detected genes and removed genes expressed in fewer than three cells. I then applied log-normalization using the LogNormalize method in Seurat (v4.3.0) (Stuart et al., 2019). This normalization method divides each gene's count by the total count per cell, multiplies by a scaling factor of 10,000, and applies a natural logarithm transformation.

"I used the cell type annotations published by the original authors to annotate and validate my expression signatures and to benchmark cell type classification methods. To investigate the statistical bias when cell type classification uses the same genes that are later subjected to statistical testing, I used the dataset of Kartha et al. (2022): I only included IFN-II treatment and control samples for this purpose." (Aybey et al., 2023)

Table 2.2: List of datasets used in this study along with their quality control measures.

Dataset	Source	Cell source	Sequencing technology	Purpose	Number of cells, average number of genes per cell	Portion of mitochondrial genes [<%]	Unique gene count
GSE176078	(Wu et al., 2021)	BRCA	10X	Discovery	43,140 12,661	5	10,000
GSE166555	(Uhlitz et al., 2021)	CRC	10X		13,369 12,681		
GSE140228	(Zhang et al., 2019b)	LIHC	Smart-Seq2		2,351 39,531		
GSE140228	(Zhang et al., 2019b)	LIHC	10X		16,724 13,751		
GSE139555	(Wu et al., 2020)	KIRC	10X		18,120 11,861		
GSE131907	(Kim et al., 2020)	NSCLC	10X		25,915 14,051		
GSE123139	(Li et al., 2020)	SKCM	MARS-Seq		4,817 8,861		
TIC Atlas	(Nieto et al., 2021)	13 cancer types	Various	Validation	229,753 1,265	15	5,000
Hao	(Hao et al., 2021)	PBMC	CITE-seq	Reference	158,783 2,207	15	6,000
Kotliarov	(Kotliarov et al., 2020)	PBMC	CITE-seq	Benchmarking	52,849 748	10	2,500
Zheng	(Zheng et al., 2017)	PBMC	10X		18,000 562	5	1,500
Kartha	(Kartha et al., 2022)	PBMC	SureCell Biorad	Differential gene expression (investigation of bias)	23,754 943	-	200

2.2.2 Gene sets for comparison to my approach

"In addition to my own immune cell signatures, I investigated the following public immune cell signature repertoires: Abbas (Abbas et al., 2005), Charoentong (Charoentong et al., 2017), Angelova (Angelova et al., 2015), Becht (Becht et al., 2016), Bindea (Bindea et al., 2013), Newman (Newman et al., 2015), Nirmal (Nirmal et al., 2018), and Nieto (Nieto et al., 2021). For comparing my gene signature collection with other gene set collections in a random forest approach, I focused on the following studies and cell types: a) Abbas: B cells, dendritic cells (DCs), monocytes, NK, and T cells; b) Charoentong: B cells (general and memory), DCs (immature DCs and plasmacytoid dendritic cells (pDCs)), monocytes, NK, and $CD4^+$ (regulatory, effector memory, central memory, and general) and $CD8^+$ T cells (effector memory, central memory, and general); c) Angelova: B cells (memory and immature), DCs (pDCs, immature, myeloid DCs and general), monocytes, NK, and $CD4^+$ (regulatory, effector memory, and central memory) and $CD8^+$ T cells (effector memory and central memory); d) Nieto: B and plasma cells, DCs (myeloid DCs, conventional DCs

and pDCs), monocytes, NK cells, naïve T cells, $CD4^+$ T (effector memory, transitional memory, memory/naïve and regulatory) and $CD8^+$ T (effector memory and cytotoxic) cells." (Aybey et al., 2023)

2.2.3 Dataset integration

"For the integration of multiple scRNA-seq datasets I used reciprocal principal component analysis (RPCA)-based integration implemented in Seurat (v4.3.0) (Stuart et al., 2019). To find anchors between discovery datasets and to integrate the datasets, I used Seurat standard function (`https://satijalab.org/seurat/articles/integration_rpca.html`)." (Aybey et al., 2023)

2.2.4 Dimension reduction and spatial clustering

"To cluster genes with similar expression profiles in my integrated expression matrix, I used a density-based clustering approach. Prior to clustering, I reduced the dimensionality of the Z-scaled integrated expression matrix using UMAP from uwot (v0.1.14) (Melville et al., 2020) on the gene dimension to the first and second UMAP components. On this spatial representation of the UMAP space -in which each point represents a gene- I performed density-based clustering using dbscan (v1.1-11) (Hahsler et al., 2019), thereby clustering genes into gene clusters. dbscan operated with two parameters: minimum points (minPts) in a gene cluster and maximum distance between two data points (epsilon)." (Aybey et al., 2023)

"To determine two DBSCAN clustering parameters (epsilon and minimum number of points in a cluster minPts), I examined the optimal epsilon after plotting k-nearest neighbor distances in ascending order and analyzing the 'knee' point where maximum curvature was observed for a minimum of ten genes (minPts) in a gene cluster. The optimal epsilon was at 0.3 but since I aimed to obtain more clusters and have a higher resolution, I considered lower epsilon values as my epsilon candidates. For the selection of the epsilon value which captures signatures for all immune cell types, I tried different values ranging from 0.15 and 0.2 in 0.05 interval. To do so, I ran the gene refinement workflow (explained in the results, Figure 2.1) including filtering out genes with negative silhouette scores and taking only top 50 genes with the highest silhouette scores. Then, in the given range, I examined the heatmaps showing the mean signature scores - as calculated using the Average Z-Score method- for each cell type in each discovery dataset. An epsilon of 0.18 resulted in a better resolution capturing signatures for all cell types in the discovery datasets." (Aybey et al., 2023)

2.2.5 Gene cluster refinement using silhouette scores and mean signature scores

"The silhouette scores were used to evaluate the quality of the gene elements and refine the gene clusters by considering the similarity of gene expression profiles within clusters and the dissimilarity between clusters. I calculated silhouette scores for individual genes and clusters using cluster (v2.1.1) (Maechler, 2018). As inputs I used the cluster labels from dbscan and the gene-by-gene correlation distance matrix for genes x and y: $d_{x,y}$ = 1 - r(x,y), where r(x,y) represents the Pearson correlation calculated from Z-scaled integrated expression profiles of genes x and y. The silhouette scores range from -1 to +1, with higher values indicating better clustering results and values closer to negative suggest that the sample is likely to be assigned to the wrong cluster." (Aybey et al., 2023)

"To evaluate the expression strength of each signature in each cell type, I employed the 'Average Z-Score method'. This method allows to measure the relative expression level of a signature in a cell by considering the expression values of all genes associated with that signature. I averaged the Z-scaled expression values (mean-centered and standardized across cells) for each gene within the signature in each cell to obtain mean signature score for a cell. Subsequently, I represented average mean signature scores for each cell type by averaging mean signature scores coming from the cells belonging to a given cell type." (Aybey et al., 2023)

2.2.6 Quantifying gene set similarities

"I measured the similarity of the gene sets (overlap of sets) by calculating the Jaccard index using bayesbio (v1.0.0) (McKenzie, 2016) and the Szymkiewicz–Simpson coefficients (Vijaymeena and Kavitha, 2016) between mine and all published signatures. The Jaccard index calculates the ratio of the intersection of two sets (my gene set and a published gene set) to the union of both sets. It provides a measure of the proportion of shared genes between the sets, indicating the degree of similarity. Similarly, the Szymkiewicz–Simpson coefficient also quantifies the similarity between two sets by dividing the intersection of two sets by the number of elements belonging to the set with minimum number of elements. This coefficient provides an alternative measure to assess the overlap between gene sets considering the differences between set sizes and evaluate the similarity of the genes identified in my study with those reported in the literature." (Aybey et al., 2023)

2.2.7 Cell type classification and performance benchmarking of cell type classification tools

"For my immune cell type classification approach, I applied my immune cell type gene signatures as features in a random forest approach. For building random forest models utilizing randomForest (v4.6-14) (Liaw and Wiener, 2002) I used a ratio of 67:33 for random sampling of training and test data. I used only common signature genes between reference and query datasets as features. Prior to the training, I harmonized original cell type annotations from training datasets at medium-depth level shown in Table 2.3 and only included medium level cell types (monocytes, DCs, B, NK, $CD4^+$ T, and $CD8^+$ T cells). For the assessment of the performance of other published gene signatures, I applied an analogous procedure. Further, I used five different cell type annotation tools with default parameters: Seurat (v4.3.0) (Stuart et al., 2019), singleR (v1.4.1) (Aran et al., 2019), scType (Ianevski et al., 2022), CellTypist (v1.5.0) (Domínguez Conde et al., 2022), and CHETAH (v1.6.0) (de Kanter et al., 2019). Prior to the cell type prediction using Seurat, I applied the standard pipeline to the query and reference dataset including log-normalization, finding and scaling HVGs. The anchors for cell type label transfer were determined between reference and query datasets and cell type labels were then transferred to the query dataset based on the PCA projection. For singleR and CHETAH, predictions were obtained by providing normalized query and reference dataset along with cell type labels from a reference dataset. For CellTypist, I utilized the same reference dataset to train the model and used the default settings with majority voting option. As input expression matrix, I used the raw expression values for the reference and query datasets. In the case of scType, it differs from other algorithms as it does not rely on any reference dataset to label cells. Instead, it utilizes information from cell clusters and specific combinations of cell type markers. I followed the standard workflow of normalization, scaling, and clustering using Seurat. Additionally, I loaded gene sets from the built-in 'Immune system' database provided by scType. To assign cell types to clusters, I followed the steps recommended by scType. In the case of perturbation dataset, I provided RPCA-based integrated matrix as input to Seurat and singleR as suggested by the methods." (Aybey et al., 2023)

"Prior to the predictions, I harmonized original cell type annotations from benchmarking datasets at medium-depth level shown in Table 2.3. To evaluate the performance of the cell type prediction algorithms, I used six statistical metrics: accuracy, specificity, sensitivity, negative predictive value (NPV), positive predictive value (PPV), and F1-score. I reported the mean of each statistical metric for each algorithm." (Aybey et al., 2023)

Table 2.3: Medium-depth level cell type harmonization

"For benchmarking and reference datasets, cell types are summarized into medium-level categories. Larger groups are in bold and specific cell types belonging to those groups in each dataset are listed. 'Other cells' category from the reference dataset are removed from the training." (Aybey et al., 2023)

Groups	Benchmarking datasets		Reference dataset
B	B transitional B switched B unswitched	B	B memory B naive B intermediate Plasma
Monocyte	CD14 monocyte CD16 monocyte	CD16 monocyte	CD14 monocyte CD16 monocyte
DC	DC pDC	-	DC pDC
NK	NK	NK	NK
CD4$^+$ T	T CD4 memory T CD4 naive	T CD4 naive T CD4 memory T CD4 regulatory T CD4 helper	T CD4 naive T CD4 effector memory T CD4 central memory T CD4 activated T CD4 regulatory (Treg) T CD4 cytotoxic activity (CTL) T CD4 proliferating
CD8$^+$ T	T CD8 memory T CD8 naive	T CD8 cytotoxic T CD8 naive	T CD8 naive T CD8 effector memory T CD8 central memory T CD8 activated
T unconventional	Double negative T cells Unconventional CD161^{hi}/CD3$^+$/CD8$^+$ T cells	-	**Other cells:** Mucosal-associated invariant T cells (MAIT), gamma delta T cells (gdT), double negative T cells, HSC, innate lymphoid cells, erythrocytes, platelets
HSC	Hematopoietic stem cells (HSC)	-	

I calculated prediction metrics based on the concordance between predicted (p) and real (r) cell types. True positives (TP) represent the number of cases where p correctly matches r. False positives (FP) refer to instances where p is incorrectly predicted as r even though they belong to other cell types. False negatives (FN) count the cases where cells belonging to r are incorrectly predicted as another cell type. True negatives (TN) include all other correct classifications that do not belong to type r and were not predicted as r. Subsequently, I utilized these four metrics to calculate six statistical metrics for benchmarking, based on the following formulas:

$$\text{Accuracy} = \frac{TP + TN}{TP + TN + FP + FN} \tag{1}$$

$$\text{Sensitivity} = \frac{TP}{TP + FN} \tag{2}$$

$$\text{Specificity} = \frac{TN}{TN + FP} \tag{3}$$

$$\text{PPV} = \frac{TP}{TP + FP} \tag{4}$$

$$\text{NPV} = \frac{TN}{TN + FN} \tag{5}$$

$$\text{F1-score} = 2 \times \frac{PPV \times \text{Sensitivity}}{PPV + \text{Sensitivity}} \tag{6}$$

2.3 Results

2.3.1 Successful integration of multiple TME scRNA-seq datasets

To leverage multiple scRNA-seq datasets for immune cell GES discovery, I developed a workflow based on gene-by-gene expression similarities (Figure 2.1). First, I obtained seven published TME datasets which included only treatment-naïve samples of immune cells coming from six different cancer types: skin cutaneous melanoma (SKCM), liver hepatocellular carcinoma (LIHC), breast cancer (BRCA), kidney renal clear cell carcinoma (KIRC), non-small cell lung cancer (NSCLC), and colorectal cancer (CRC) (Table 2.2). For each cell type relevant for my GES discovery, I ensured its presence in at least three datasets, based on cell type annotations available from the results of original studies. Each dataset contained various cell types, with differences in cell type distribution and the extent to which each dataset contributed to specific cell populations across different cancer types (Figure 2.2A). This variability demonstrates the context-specific nature of cell type abundance. It also emphasizes the importance of integrating multiple datasets to ensure comprehensive immune cell representation. This variety and additive information coming from multiple datasets provided the basis for my GES discovery.

To harmonize the datasets, I performed data integration as explained in Section 1.5.1, addressing batch effects that stem from differences in experimental protocols, platforms, and processing across studies. Integration in this context is a multi-nested batch correction and refers to aligning the datasets in a shared low-dimensional space, ensuring that biological signals—specifically immune cell type information—are preserved while removing variations caused by dataset-specific biases.

To achieve this, I utilized the 3,000 HVGs to construct an integrated gene expression matrix (3,000 genes x 123,509 cells) (see Methods). Before integration, the UMAP of unharmonized data showed clear separation of cells based on their dataset of origin, indicating batch effects and technical artifacts that mask meaningful immune cell type information (Figure 2.2B). After integration, UMAP plots based on the harmonized matrix demonstrated that cells clustered by cell type rather than by dataset. Similar cell types from different datasets grouped together, confirming successful alignment of the datasets (Figure 2.2C). Thus, this process identified shared features across datasets, represented them in a common framework, and harmonized expression values to reduce technical variability while preserving biologically meaningful differences.

This successful integration enables a unified examination of gene-by-gene similarities across datasets, ensuring that downstream analyses can capture biological variation rather than technical differences. The before-and-after UMAP visualizations illustrate this tran-

sition, showing that integration effectively preserved immune cell type signals while eliminating dataset-specific biases. Therefore, the integrated expression matrix provide a robust foundation for subsequent GES discovery.

2.3.2 Density-based clustering and sequential filtering yielded 14 refined GESs

I aimed to cluster gene sets with similar expression patterns across cells to identify distinct gene modules that characterize immune cell subsets. To achieve this, I reduced the dimensions of the Z-scaled integrated expression matrix by genes and not by cells (which is usually done in the single-cell analysis). This means that, instead of examining how each cell expresses various genes (cell-centric), I examined how each gene is expressed across different cells (gene-centric). I represented each gene by its first and second UMAP dimensions to remove the effect that more abundant cell types have more impact on the clustering of genes than less abundant cell types (Figure 2.2D). Distinct clusters were visually detectable. Using the UMAP coordinates, I grouped genes into clusters of at least ten genes, employing density-based clustering algorithm, DBSCAN (see Methods). This approach yielded in 57 gene clusters that are showing closely similar expression patterns and are used as seeds for subsequent steps of my GES discovery workflow.

To refine 57 initial gene clusters, I applied additional steps to filter and polish the gene sets at both the gene and cluster levels (Figure 2.1B). First, I excluded low-congruent genes with negative silhouette scores. Silhouette scores measure how similar each gene is to its own cluster compared to other clusters. Negative scores indicate poor alignment, suggesting that these genes did not fit well within their clusters. Next, I ensured that each cluster was of appropriate size. I removed any clusters containing fewer than ten genes, as small clusters may lack statistical power and may not reflect robust biological signals. For larger clusters, I kept the top 50 genes based on their silhouette scores, ensuring that the most representative genes were included in each cluster and excluding less relevant ones. Further, I removed clusters with poor discriminative power as they they lacked cell-type specificity. Such signatures were mostly related to general biological processes, such as the cell cycle, rather than cell-type-related signals. To do so, I applied a maximum-median filter which used mean signature scores for each cell type (using the annotations by the authors), calculated across datasets ('Average Z-score Method'). I kept clusters with a minimum difference of 0.6 between the maximum and median signature scores, measured across at least three datasets. This extensive statistical filtering process reduced the initial 57 clusters to 14 refined GESs. The original gene-level UMAP based on 3,000 HVGs (Figure 2.2D) and the new UMAP based on all genes of the 14 GESs (Figure 2.2E) separated each gene cluster, confirming that the GES genes

appropriately represent the major gene clusters in this dataset.

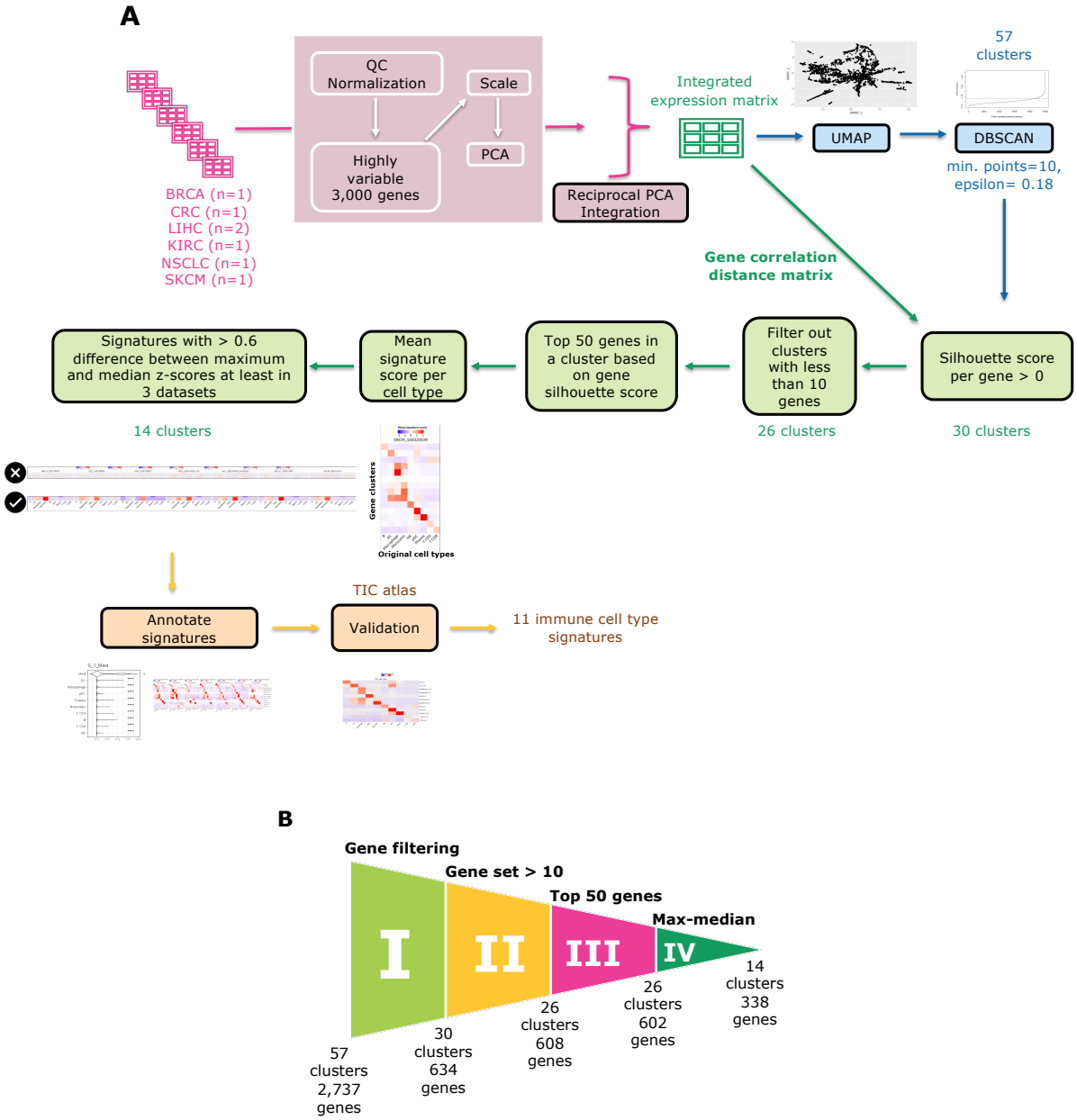

Figure 2.1: Immune cell type gene signature discovery workflow.
(A) The workflow comprises the following steps: dataset integration, density-based clustering using DBSCAN, refinement of gene sets using filtering approaches based on silhouette scores and mean signature expression score and annotating and validating the signatures. **(B)** Funnel plot showing the refinement process in each step. The refinement process consists of five filtering steps: gene filtering based on silhouette scores, selection of gene sets with minimum ten genes, selection of top 50 genes based on silhouette scores and max-median filter based on mean signature expression scores. Each step is labeled from I to IV. The final number of clusters and genes is shown after each filtering step. (Reprinted from Aybey et al. (2023))

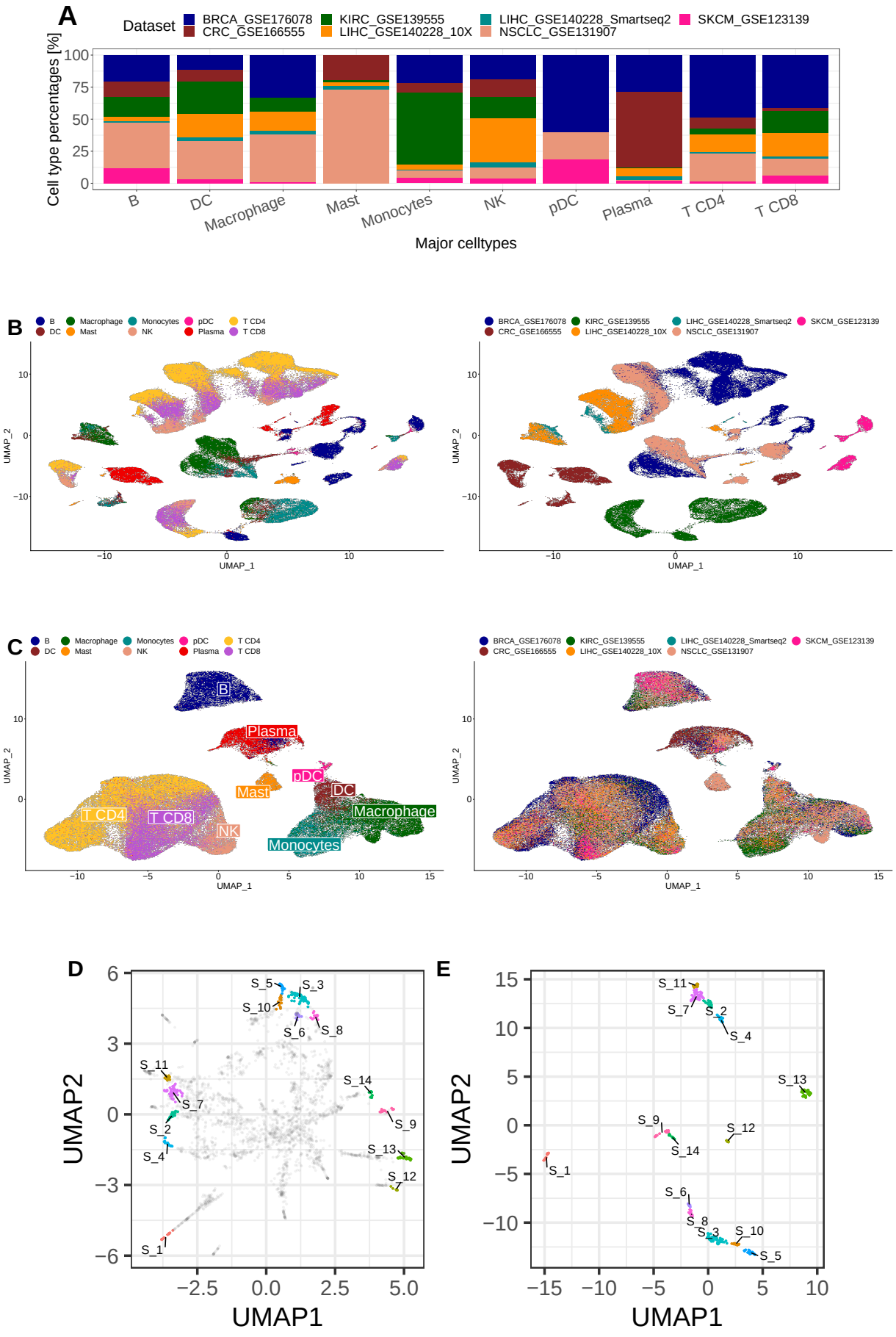
A
Dataset
BRCA_GSE176078
CRC_GSE166555
KIRC_GSE139555
LIHC_GSE140228_10X
LIHC_GSE140228_Smartseq2
NSCLC_GSE131907
SKCM_GSE123139
Cell type percentages [%]
100
75
50
25
0
B
DC
Macrophage
Mast
Monocytes
NK
pDC
Plasma
T CD4
T CD8
Major celltypes
B
Macrophage
Monocytes
pDC
T CD4
DC
Mast
NK
Plasma
T CD8
UMAP_1
UMAP_2
C
D
E
UMAP1
UMAP2
S_1
S_2
S_3
S_4
S_5
S_6
S_7
S_8
S_9
S_10
S_11
S_12
S_13
S_14

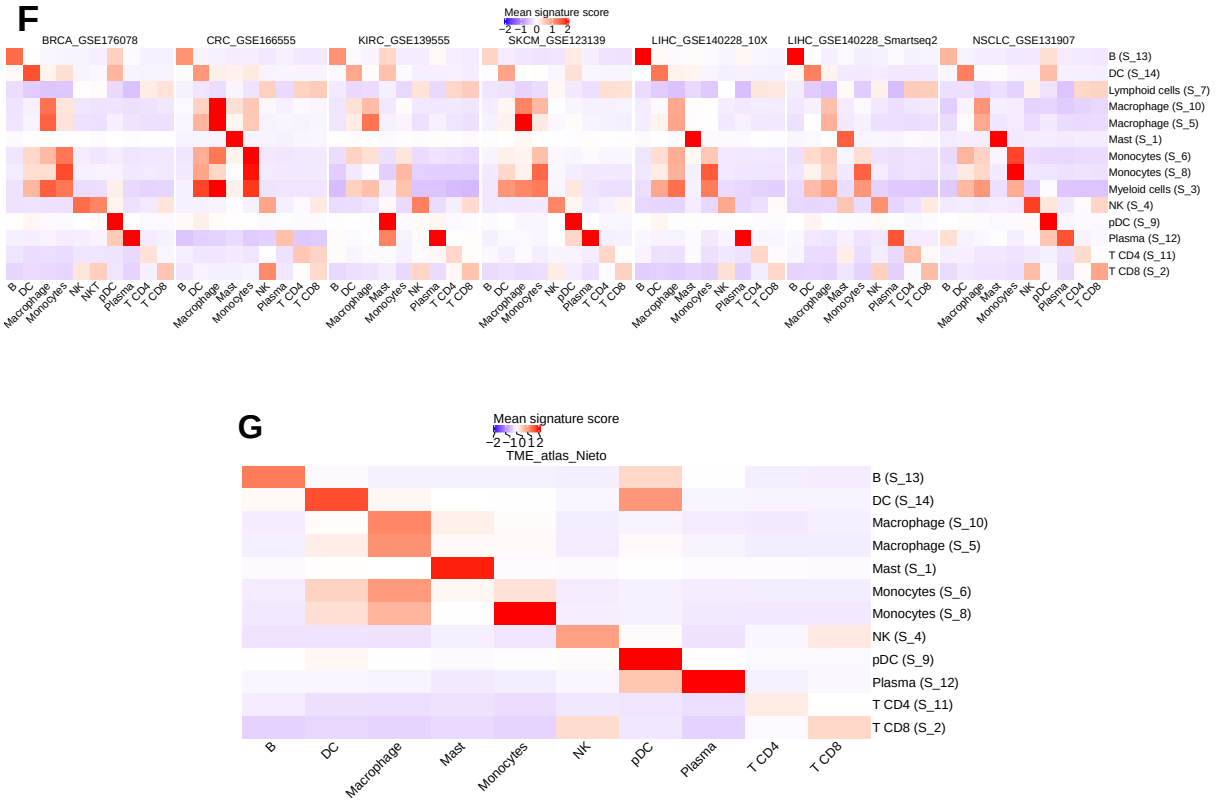

Figure 2.2: Data characteristics and results of the gene signature discovery.

(A) Contribution of discovery datasets to each immune cell type. **(B-C)** UMAP plots of before (B) and after (C) integration. Each point represents a single-cell, and each cell is colored by cell type or dataset. The cell type labels are taken from the original publications. Cell type labels are placed in the center of the cell type clusters. Note the successful integration and harmonization of the datasets. Abbreviations: DC, dendritic cell; NK, natural killer; pDCs, plasmacytoid dendritic cell. **(D-E)** UMAP plots based on 3,000 HVGs or final genes from the gene signatures. The dimensionality of the gene space of expression data is reduced in each step, starting from 3,000 common HVGs in the integration step to finally 338 genes of my gene sets. Each point represents a gene. UMAP1 and UMAP2 are plotted for each gene in x and y axis, respectively. In D and E genes in my gene signatures are annotated in different colors. In D other genes are colored gray. Cluster numbers are placed in the center of the clusters. Genes from each refined gene set cluster together to the exclusion of other gene sets. **(F-G)** Mean signature expression scores per cell type of refined gene signatures shown in the discovery and validation datasets. Red and blue represent high and low mean signature expression scores, respectively. Rows represent the gene signature cluster numbers along with the manual annotations while columns represent the cell types defined by the original authors in the datasets. The signature annotation names contain cell type which the signature can detect. Discovery and validation datasets are shown in F and G, respectively. (Adapted from Aybey et al. (2023))

2.3.3 Validation of refined gene clusters identified eleven robust immune cell type GESs

I assessed the relevance and validity of the refined 14 GESs in the discovery and validation datasets. First, I manually annotated cell types by assigning each GES to the cell type in which it had the highest expression score in at least three discovery datasets. The result is shown in the heatmap in Figure 2.2F. I used a medium level of granularity with regard to the cell types: B cells, DCs, macrophages, mast cells, monocytes, NK cells, pDCs, plasma, $CD4^+$ T cells, and $CD8^+$ T cells. In addition to the distinct immune cell type GESs, I obtained two lineage specific GESs for myeloid and lymphoid lineages. Then, I statistically tested the cell type specificity of each manually annotated GES within the discovery datasets. I compared the mean signature score of each GES in its designated cell type against all other cell types. All 14 GESs showed significantly higher scores (two-sided Wilcoxon test, raw $p < 0.01$) in at least three discovery datasets (Appendix Figure A.1). Since my goal was to retrieve GESs for distinct immune cell type populations, I excluded the lineage GESs from further analysis and ended up with twelve immune cell type GESs. Finally, to validate these twelve GESs in independent data, I used a single-cell TME atlas (Nieto et al., 2021) comprising 13 cancer types. The validation included comparing mean signature scores between groups (cell types) in a heatmap (Figure 2.2G) and performing statistical tests (two-sided Wilcoxon test, Appendix Figure A.1). Except for S_6 (monocyte), all immune cell type GESs showed significantly higher scores (two-sided Wilcoxon test, raw $p < 0.01$). These resulted in eleven robust, refined, and validated immune cell type GESs which constitute my final immune cell type GES repertoire (Table 2.4).

Table 2.4: Summary of my refined immune cell type signatures.

Cluster number	Cluster annotation	Genes	Number of genes
S_13	B	TCL1A, VPREB3, CD22, EBF1, FCER2, STAG3, MS4A1, PARP15, CD79B, KHDRBS2, BANK1, FAM129C, CD79A, CXCR5, LINC00926, BACH2, AFF3, LY9, RALGPS2, SMIM14, FCRLA, CD37, SPIB, FCRL1, IRF8, CD19, CNR2, TNFRSF13B, ADAM28, COL19A1, PAX5, ARHGAP24, TCF4, BLK, PKIG, RIC3, IFT57, TNFRSF13C	38
S_14	DC	CD1E, HLA-DQB2, CD1B, PKIB, CALCRL, CD1A, FCER1A, S100B, PLD4, CD1C, PPP1R14A, NAPSA, CD207	13
S_10	Macrophage	APOE, CTSL, GPNMB, CD9, TREM2, CTSD, APOC1, ADAMDEC1, SPP1, MMP9, PLA2G7, LIPA, ACP5, NUPR1, FN1	15
S_5	Macrophage	CCL13, MS4A4A, SLC40A1, LYVE1, RNASE1, SIGLEC1, C1QA, STAB1, CXCL12, ABCA1, IGF1, GPR34, PLTP, C1QB, PMP22, A2M, LGMN, FOLR2, SLCO2B1, MRC1, DAB2, NRP1, LILRB5, C1QC, F13A1, PLAU	26
S_1	Mast	TPSAB1, HPGDS, ADCYAP1, CPA3, PLAT, GATA2, CTSG, HPGD, KIT, CLU, IL1RL1, KIAA1549, RSPH9, SYTL4, HDC, VWA5A, RGS13, TPSB2, LIPC, SLC18A2	20
S_8	Monocytes	LILRA5, SLC25A37, CFP, S100A12, CD300E, TIMP1, APOBEC3A, FCN1, TREM1, SLC11A1, VCAN, S100A9, S100A8, CDA, THBS1, FGR	16
S_4	NK	GZMB, CD160, TXK, KIR2DL4, TMIGD2, CTSW, KRT86, KLRF1, SH2D1B, GNLY, PRF1, KLRD1, XCL2, CLIC3, XCL1, HOPX, MATK, PTGDR, KRT81, KLRC1	20
S_9	pDCs	SCT, RGS7, IRF4, VASH2, GPM6B, MAP1A, NME8, PTCRA, PTGDS, AEBP1, CLEC4C, SMPD3, TTC39A, PHEX, MMP23B, PLVAP, PLAC8, RASD1, LILRA4, PTPRS, DNASE1L3, LRRC26, SLC35F3, TPM2, KRT5, TSPAN13	26
S_12	Plasma	IGLL5, FKBP11, ITM2C, XBP1, DPEP1, SEC11C, HSP90B1, TNFRSF17, SDC1, CAV1, SSR4, DERL3, MZB1, JSRP1, CERCAM	15
S_11	T CD4	FAS, TNFRSF25, PBX4, FAAH2, ICOS, CD28, CCR4, TMEM173, MAL, LTB, ARID5B, PBXIP1, TNIK, NPDC1, LEF1, FBLN7	16
S_2	T CD8	FASLG, CCL5, RAB27A, CD8B, CPNE7, CST7, OASL, GZMH, GZMA, CHST12, SAMD3, CLEC2B, CD8A, APOBEC3G, GZMM, SLA2, TNIP3, IFNG, TSEN54, CRTAM, C12orf75, LAG3, GZMK	23

2.3.4 My gene set collection is novel and smaller compared to published immune cell type GESs

Lastly, I evaluated the novelty and relevance of my immune cell type GESs by comparing their gene content with seven published gene lists. I used two similarity metrics—the Jaccard index and the Szymkiewicz-Simpson index—to quantify overlaps between my GESs and previously published GESs. The results are visualized in heatmaps (Figure 2.3). The Jaccard index, which measures the proportion of shared genes relative to the union of two sets, ranged from 0 to 0.32. In contrast, the Szymkiewicz-Simpson index, which considers the shared genes relative to the smaller of the two sets, ranged from 0.08 to 0.67. The generally higher values for the Szymkiewicz-Simpson index reflect that my GESs tend to be generally smaller and more refined compared to published ones.

None of my gene sets yielded indices of one, meaning that none of them have been completely described in the literature before, either as full sets or as subsets of other signatures. The degree of overlap of the GESs varied across different cell types. For some cell type populations, such as plasma cells, pDCs, monocytes, and macrophages, the maximum Jaccard indices were relatively low (<0.1), indicating that these GESs are more distinct and novel and share fewer genes with those from published datasets. In contrast, the highest Jaccard indices were observed for Bindea-mast cells (0.32) and Nirmal- or Newman-B cells (0.31 and 0.21, respectively), suggesting moderate overlap in gene content. Similarly, the highest Szymkiewicz-Simpson scores were found for Becht-B cells (0.67), Bindea-mast cells (0.6), and Nirmal-B cells (0.5). These results demonstrate that while some overlap exists with previously published GESs, particularly for certain cell types, my GESs are novel in their overall composition and refined size compared to existing GESs.

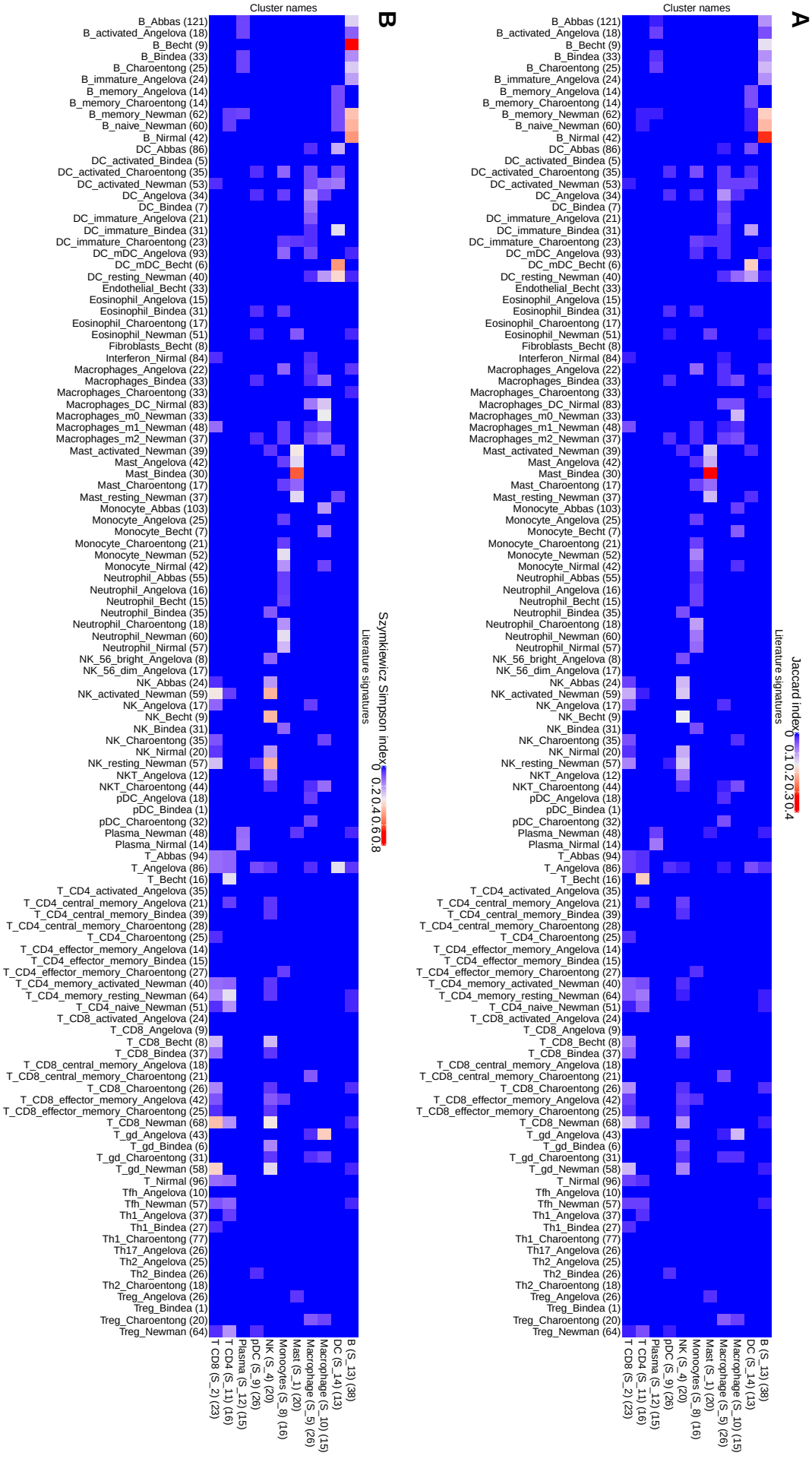
A
Cluster names
B_Abbas (121)
B_activated_Angelova (18)
B_Becht (9)
B_Bindea (33)
B_Charoentong (25)
B_immature_Angelova (24)
B_memory_Angelova (14)
B_memory_Charoentong (14)
B_memory_Newman (62)
B_naive_Newman (60)
B_Nirmal (42)
DC_Abbas (86)
DC_activated_Bindea (5)
DC_activated_Charoentong (35)
DC_activated_Newman (53)
DC_Angelova (34)
DC_Bindea (7)
DC_immature_Angelova (21)
DC_immature_Bindea (31)
DC_immature_Charoentong (23)
DC_mDC_Angelova (93)
DC_mDC_Becht (6)
DC_resting_Newman (40)
Endothelial_Becht (33)
Eosinophil_Angelova (15)
Eosinophil_Bindea (31)
Eosinophil_Charoentong (17)
Eosinophil_Newman (51)
Fibroblasts_Becht (8)
Interferon_Nirmal (84)
Macrophages_Angelova (22)
Macrophages_Bindea (33)
Macrophages_Charoentong (33)
Macrophages_DC_Nirmal (83)
Macrophages_m0_Newman (33)
Macrophages_m1_Newman (48)
Macrophages_m2_Newman (37)
Mast_activated_Newman (39)
Mast_Angelova (42)
Mast_Bindea (30)
Mast_Charoentong (17)
Mast_resting_Newman (37)
Monocyte_Abbas (103)
Monocyte_Angelova (25)
Monocyte_Becht (7)
Monocyte_Charoentong (21)
Monocyte_Newman (52)
Monocyte_Nirmal (42)
Neutrophil_Abbas (55)
Neutrophil_Angelova (16)
Neutrophil_Becht (15)
Neutrophil_Bindea (35)
Neutrophil_Charoentong (18)
Neutrophil_Newman (60)
Neutrophil_Nirmal (57)
NK_56_bright_Angelova (8)
NK_56_dim_Angelova (17)
NK_Abbas (24)
NK_activated_Newman (59)
NK_Angelova (17)
NK_Becht (9)
NK_Bindea (31)
NK_Charoentong (35)
NK_Nirmal (20)
NK_resting_Newman (57)
NKT_Angelova (12)
NKT_Charoentong (44)
pDC_Angelova (18)
pDC_Bindea (1)
pDC_Charoentong (32)
Plasma_Newman (48)
Plasma_Nirmal (14)
T_Abbas (94)
T_Angelova (86)
T_Becht (16)
T_CD4_activated_Angelova (35)
T_CD4_central_memory_Angelova (21)
T_CD4_central_memory_Bindea (39)
T_CD4_central_memory_Charoentong (28)
T_CD4_Charoentong (25)
T_CD4_effector_memory_Angelova (14)
T_CD4_effector_memory_Bindea (15)
T_CD4_effector_memory_Charoentong (27)
T_CD4_memory_activated_Newman (40)
T_CD4_memory_resting_Newman (64)
T_CD4_naive_Newman (51)
T_CD8_activated_Angelova (24)
T_CD8_Angelova (9)
T_CD8_Becht (8)
T_CD8_Bindea (37)
T_CD8_central_memory_Angelova (18)
T_CD8_central_memory_Charoentong (21)
T_CD8_Charoentong (26)
T_CD8_effector_memory_Angelova (42)
T_CD8_effector_memory_Charoentong (25)
T_CD8_Newman (68)
T_gd_Angelova (43)
T_gd_Bindea (6)
T_gd_Charoentong (31)
T_gd_Newman (58)
T_Nirmal (96)
Tfh_Angelova (10)
Tfh_Newman (57)
Th1_Angelova (37)
Th1_Bindea (27)
Th1_Charoentong (77)
Th17_Angelova (26)
Th2_Angelova (25)
Th2_Bindea (26)
Th2_Charoentong (18)
Treg_Angelova (26)
Treg_Bindea (1)
Treg_Charoentong (20)
Treg_Newman (64)
T CD8 (S_2) (23)
T CD4 (S_11) (16)
Plasma (S_12) (15)
pDC (S_9) (26)
NK (S_4) (20)
Monocytes (S_8) (16)
Mast (S_1) (20)
Macrophage (S_5) (26)
Macrophage (S_10) (15)
DC (S_14) (13)
B (S_13) (38)
Literature signatures
Jaccard index
0
0.1
0.2
0.3
0.4
B
Cluster names
Literature signatures
Szymkiewicz Simpson index
0
0.2
0.4
0.6
0.8

Figure 2.3: Heatmap of Jaccard index scores (A) and Szymkiewicz–Simpson coefficients (B) between my immune cell type signatures and seven other published immune cell type signatures.

Jaccard index scores and Szymkiewicz–Simpson coefficients are calculated between my eleven refined gene signatures (rows) and seven published cell signatures (columns). The number of genes in each gene set has been indicated inside brackets. (Reprinted from Aybey et al. (2023))

2.3.5 Random forest classification using my immune cell type genes outperformed or matched commonly used methods

One application of immune cell GESs is cell type classification in single-cell datasets. Currently, there is no consensus on how to best assign cell types to cells in a single-cell data. The most common practice is manual annotation or automated clustering-based methods using large number of HVGs (>2,000). These methods often introduce statistical bias in the downstream analyses (Gibson, 2022; Lahnemann et al., 2020; Pasquini et al., 2021; Zhang et al., 2019a). To address these challenges, I hypothesized that a simple, clustering-free random forest (RF) approach, utilizing small, robust immune cell type GESs, could achieve comparable or better classification performance.

To test my hypothesis, I trained an RF classifier using the Hao PBMC dataset (Hao et al., 2021) and Z-scaled expression of 167 genes from my GESs as features. These GESs represent eight different immune cell populations found in PBMC: plasma, monocytes, DCs, pDCs, B, NK, $CD4^+$, and $CD8^+$ T cells. I excluded macrophage and mast cell GESs because they are not relevant to PBMC datasets. Further, I ensured that the cell type context from published GESs aligned with those in my signature repertoire as I later compare the utility of my signatures with published ones. This setup provided the basis for robust comparison of different methods and GESs in the PBMC context.

In two independent PBMC datasets, I benchmarked the RF method against commonly used methods: Seurat, singleR, CHETAH, scType, and CellTypist (see Methods and Table 2.1). These methods differ in their approaches to cell annotation. The RF method, Seurat, singleR, CHETAH, and CellTypist are reference-based methods, whereas scType relies on clustering and marker-based annotation. Seurat and scType use the top 2,000 HVGs as features, while CHETAH, singleR, and CellTypist process the entire gene expression matrix and internally select relevant genes. I trained all reference-based methods on the Hao PBMC dataset, except for scType, which operates without a reference. To compare performance, I utilized six metrics commonly used in classification tasks: accuracy, specificity, sensitivity, negative predictive value (NPV), positive predictive value (PPV), and F1-score. Subsequently, I averaged these metrics for each method across cell types in

the benchmarking datasets to provide a summarized performance metric for comparison.

The first benchmarking dataset was the Kotliarov PBMC CITE-seq dataset (Kotliarov et al., 2020), in which cell types were defined based on protein expression. This is considered one of the most informative data in the cell type classification. Among the methods tested, scType achieved the highest scores (69–83%), followed by Seurat (68–74%), CellTypist (67–74 %), and the RF approach (67–74%) (Figure 2.4A). In contrast, CHETAH and singleR had the lowest scores, 59–72% and 64–73%, respectively. The RF approach outperformed singleR and CHETAH in every metric except for the sensitivity of singleR. Overall, RF had medium to high prediction scores and showed similar results to CellTypist, Seurat, and scType.

Another benchmarking dataset, the Zheng PBMC dataset (Zheng et al., 2017), was based on the FACS-sorted cells, which is a frequently used standard data for classifying cell types in experiments and serving as the 'ground truth'. This dataset includes nine immune cell populations: B cells, CD14 monocytes, naïve $CD8^+$ T cells, cytotoxic $CD8^+$ T cells, NK cells, memory $CD4^+$ T cells, naïve $CD4^+$ T cells, regulatory $CD4^+$ T cells, and helper $CD4^+$ T cells. For benchmarking, I randomly down-sampled the dataset to 2,000 cells per cell type (18,000 cells in total). The top-performing models were the RF model (94–99%), Seurat (95–98%), scType (92–99%), and CellTypist (95–98%) (Figure 2.4A). In contrast, singleR (87–97%) and CHETAH (68–93%) had lower scores than the RF method in nearly every metric, as they also yielded lower scores for the Kotliarov dataset. Overall, my RF approach using my immune cell type GESs classified immune cells in PBMC with high performance, equal to or better than widely used algorithms, but using information from a small set of genes.

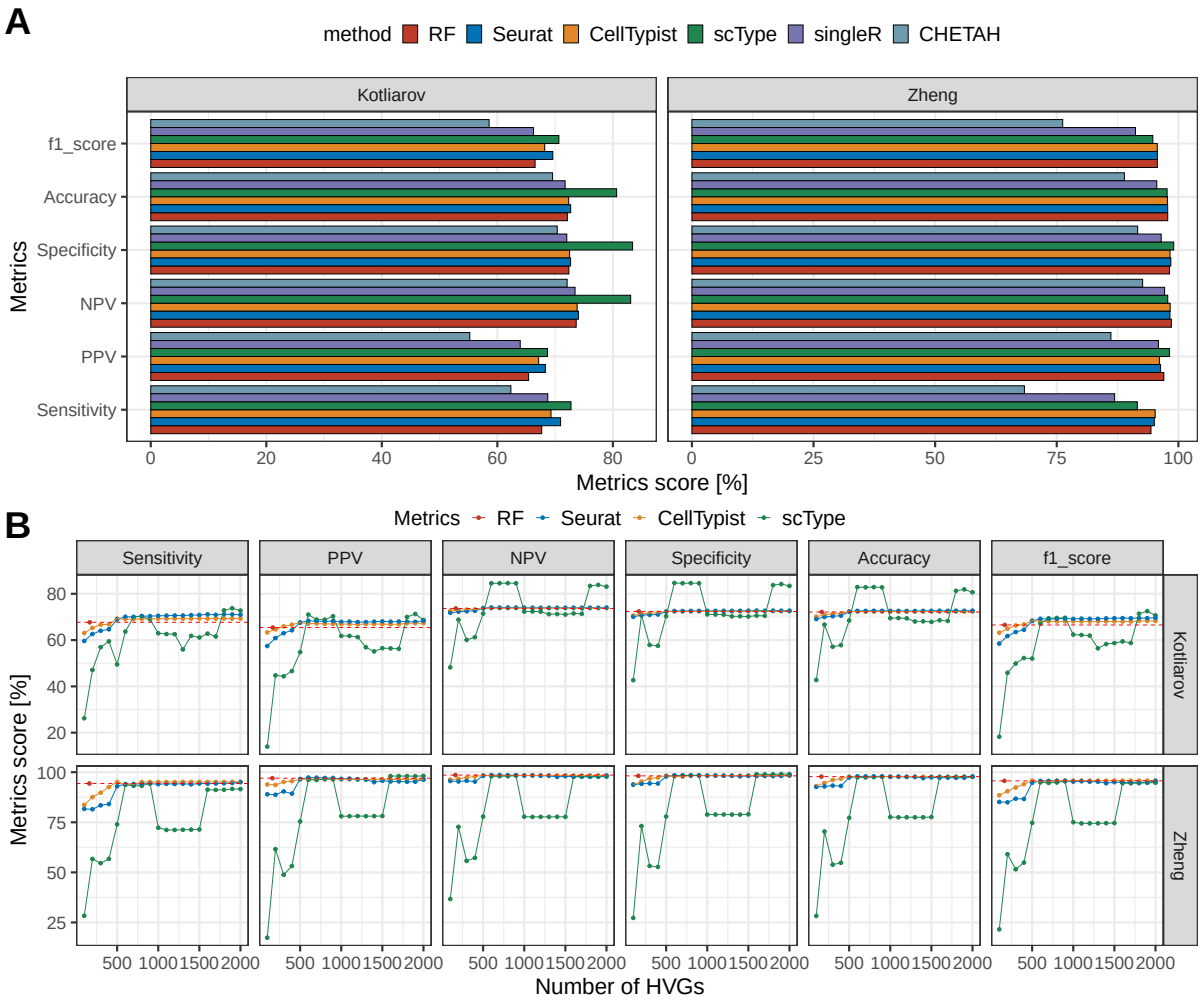

Figure 2.4: Benchmarking of the random forest model against most used cell type annotation algorithms.

(A) The random forest model shows higher or comparable prediction statistics compared to five commonly used tools in benchmarking datasets. Mean statistic metrics are displayed for each method. The Hao dataset is used as a reference dataset. The Kotliarov and Zheng datasets are used for benchmarking. **(B)** Prediction metrics change with increasing number of HVGs. In an interval of 100 HVGs, I predicted the cell type labels executing Seurat, CellTypist and scType using Hao reference data on Kotliarov or Zheng benchmarking datasets. I report the mean scores for six statistical metrics for each HVGs set. The prediction scores for the RF approach are shown in red points and dashed lines. (Reprinted from Aybey et al. (2023))

2.3.6 RF approach outperformed other methods with fewer genes

I assessed how the number of features used for cell type classification influences prediction performance. I examined the methods that previously showed comparable or better performance relative to my RF model: CellTypist, Seurat, and scType. For these methods, I calculated the statistical metrics across a range of HVGs (100 to 2,000 HVGs in 100 intervals) using the Kotliarov and Zheng benchmarking datasets (Figure 2.4B). Interestingly, the clustering-based, reference-free, marker-based approach, scType, showed significant performance variation depending on the number of HVGs. At lower HVG counts, its performance was notably poor (10–30%), and even within the 1,000-1,500 HVGs range, it deviated by about 20% from its maximum performance. This suggests that clustering-based approaches might not be ideal for cell type classification problem. Seurat and CellTypist demonstrated higher stability than scType. Still they were sensitive to the number of HVGs below 500, with performance differing by approximately 10% from their maximum performance, but achieved stable classification performance above 500 HVGs. When less than 500 HVGs were used, Seurat, CellTypist, and scType underperformed compared to RF, showing that these methods are more sensitive to the number of features when the gene set is small. This analysis demonstrated that using a limited number of gene sets ($\approx$ 170 genes) combined with a clustering-free RF classification approach, obtains superior classification results compared to other methods operating on the same number of genes.

2.3.7 Other top-performing cell type classification methods except RF classifier misclassified myeloid cells

I examined the impact of using small, robust GESs instead of multiple HVGs on the downstream analysis, which will be critical in later chapters for exploring complex IFN biology. Commonly used methods generally operate either on unsupervised clustering methods or on multiple HVGs, which introduce bias in statistical analyses, such as in DGE between perturbations. In the following, I describe one example how such bias might arise in a typical experimental setup in which stimulated and unstimulated cells are investigated by scRNA-seq as shown schematically in Figure 2.5. The strongest response from a specific cell population (e.g., B) to a stimulus could cause misclassification of cells from other populations (e.g., A and C) as B, leading to higher number of cell population B and inflated p-values in DGE testing. To minimize bias and ensure reliable downstream analyses, the selection of genes is critical.

To demonstrate the bias caused by utilizing many HVGs—employed in both clustering and cell typing—, I focused on IFN biology, where IFN-g strongly affects monocytes

and DCs (Schroder et al., 2003; Waddell et al., 2010). I used a scRNA-seq dataset of IFN-g-stimulated PBMCs from Kartha et al. (2022), with samples collected after 1 h and 6 h post-stimulation. I classified immune cell types using RF and other three top-ranking methods from my earlier analysis: Seurat, scType, and CellTypist.

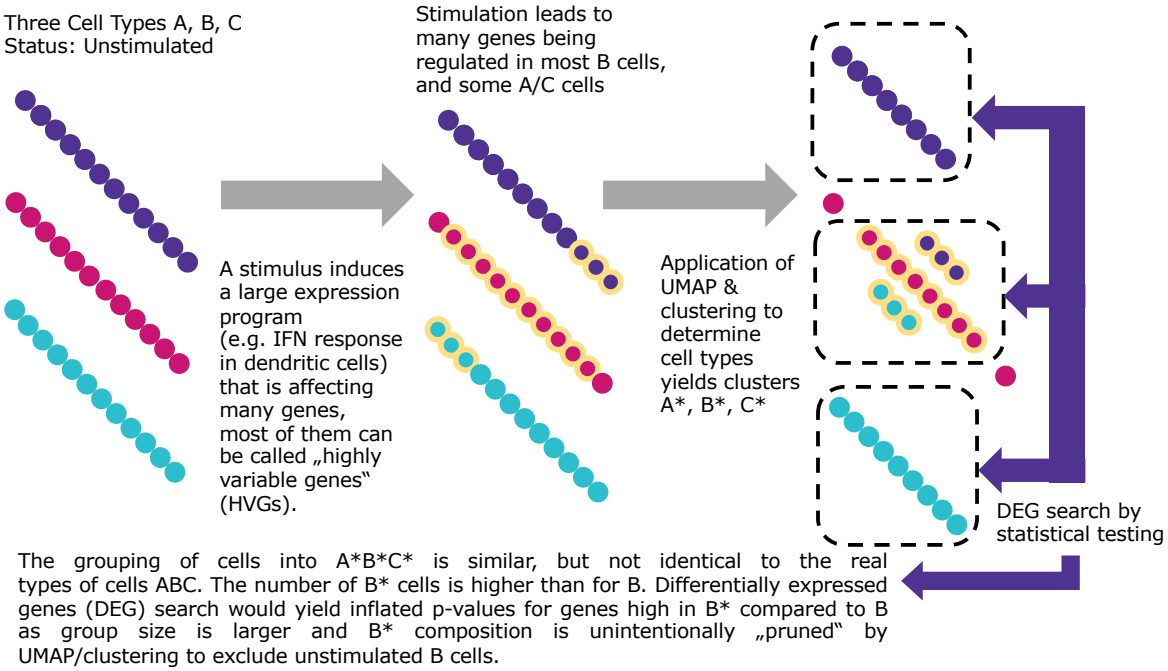

Figure 2.5: Explanation schema for the possible downstream analysis bias.

(Created by Dr. Eike Staub, reprinted from Aybey et al. (2023))

Based on the initial examination of the number of cells assigned to the myeloid cells, the RF method classified about 50% fewer DCs (n = 66) compared to other methods (Seurat: n = 126, scType: n = 105, and CellTypist: n = 115). Interestingly, most of the differently annotated DCs in other methods were classified as monocytes in RF (Figure 2.6A). Next, I compared the cells assigned as DCs in RF (DC_RF) with those classified as monocytes in RF but as DCs in other methods (Mono_RF). I examined the differences between those populations based on DC markers (FCER1A, CD1C, FLT3, and CD1E) and monocyte markers (CD14, FCGR3A, CTSS, FCN1, S100A9, LYZ, VCAN, TLR2, ITGB2, ITGAM, CTSD, CTSA, and NLRP3) (Figure 2.6B). Confirming the RF cell type annotations, DC_RF had higher expression of DC markers but not monocyte markers compared to Mono_RF. This suggested the misclassification of Mono_RF cells as DCs upon IFN-g stimulation in the other three methods. These major differences in cell type classification numbers might have consequences in statistical testing during DGE analysis, which I will further assess.

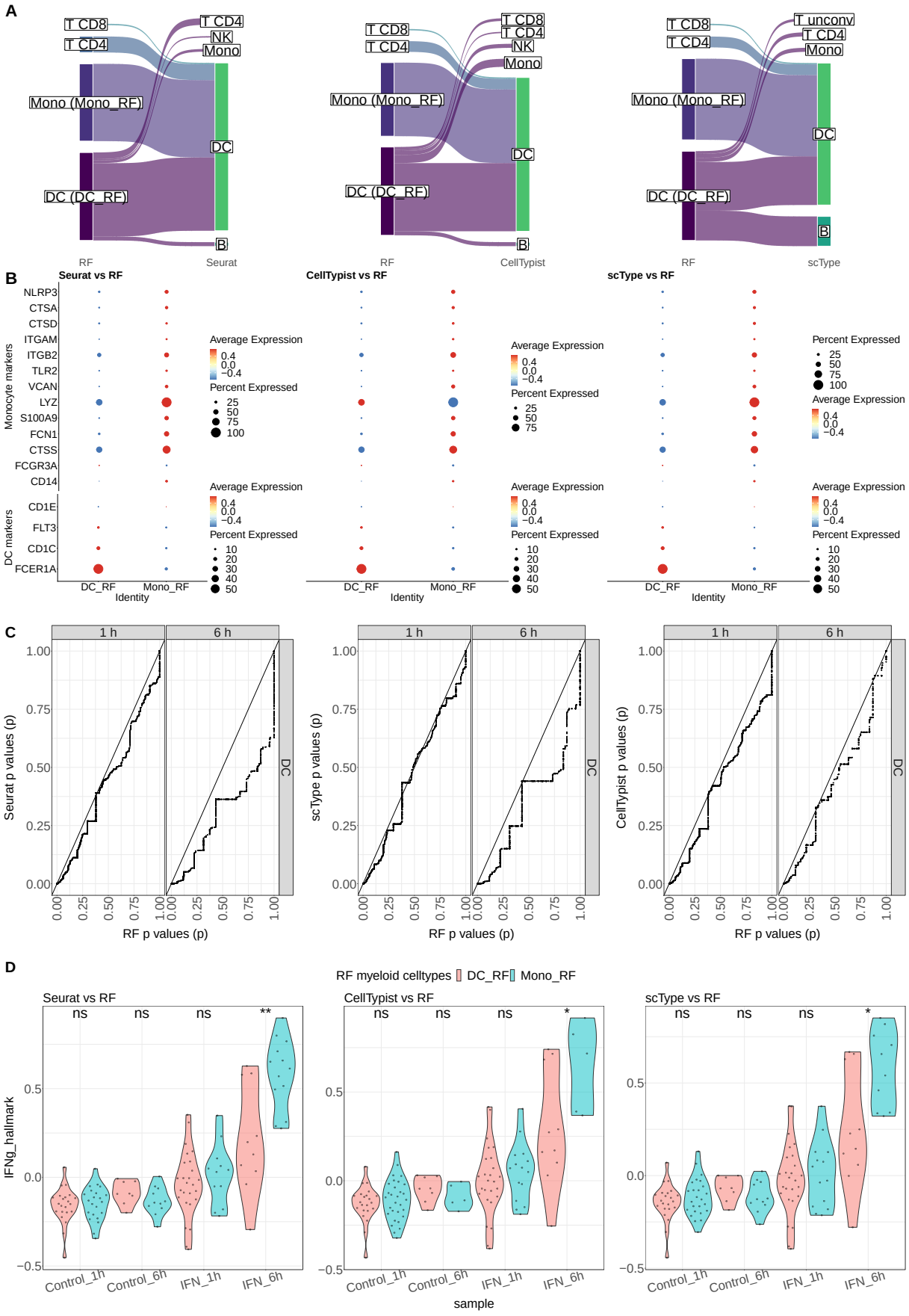
A
T CD8
T CD4
Mono (Mono_RF)
DC (DC_RF)
T CD4
NK
Mono
DC
B
RF
Seurat
T CD8
T CD4
Mono (Mono_RF)
DC (DC_RF)
T CD8
T CD4
NK
Mono
DC
B
RF
CellTypist
T CD8
T CD4
Mono (Mono_RF)
DC (DC_RF)
T_unconv
T CD4
Mono
DC
B
RF
scType
B
Seurat vs RF
CellTypist vs RF
scType vs RF
Monocyte markers
NLRP3
CTSA
CTSD
ITGAM
ITGB2
TLR2
VCAN
LYZ
S100A9
FCN1
CTSS
FCGR3A
CD14
DC markers
CD1E
FLT3
CD1C
FCER1A
DC_RF
Mono_RF
Identity
Average Expression
Percent Expressed
C
1 h
6 h
DC
Seurat p values (p)
scType p values (p)
CellTypist p values (p)
RF p values (p)
D
RF myeloid celltypes DC_RF Mono_RF
Seurat vs RF
CellTypist vs RF
scType vs RF
IFNg_hallmark
ns
*
**
Control_1h
Control_6h
IFN_1h
IFN_6h
sample

Figure 2.6: Possible downstream statistical analysis bias demonstrated in interferon gamma stimulated PBMC Kartha scRNA-seq dataset.

Cell types are labeled using the random forest (RF) model utilizing the immune cell type genes, or using Seurat, scType and CellTypist. Mono_RF cells are cells labeled as monocytes in RF but as dendritic cells (DCs) in other methods while DC_RF cells are DCs labeled as DCs in RF. **(A)** Sankey plot showing different cell type assignments in RF and other methods for cells classified as DCs either by RF or other methods. **(B)** Dot plots showing expression of monocyte or DC gene markers in Mono_RF and DC_RF cells. The size of the dots represents the percentage of expression while Z-scaled average expressions are shown from blue (low) to red (high). **(C)** P-value-to-p-value scatter plots showing over-optimistic p values for Seurat, scType and CellTypist compared to RF. I perform differential gene expression analyses for 2,000 HVGs using the cell types defined as DCs in different cell typing methods, for each sampling time point separately. P values generated for RF-generated DC cell groups are displayed on the x-axis while DC groups from other cell typing methods are shown on the y-axis. In each comparison, the comparison line falls below the trend line pointing out over-optimistic results from other methods compared to RF. **(D)** IFNg Hallmark scores for DCs annotated by RF DC_RF or misclassified monocytes Mono_RF. For each condition, mean signature scores for IFNg-Hallmark genes are calculated. DCs annotated by RF are compared with those cells classified as monocytes by RF but as DCs by other approaches. I apply Wilcoxon rank sum tests to compare IFNg-Hallmark scores between those two cell type groups at each time point separately (ns = non-significant ($p > 0.05$); * = $p < 0.05$, ** = $p < 0.01$). (Adapted from Aybey et al. (2023))

2.3.8 RF approach using fewer genes reduced bias in downstream analysis compared to commonly used methods

To investigate the impact of misclassification on downstream analysis, I performed DGE analysis (Wilcoxon rank sum test) between IFN-g stimulated and unstimulated cells classified as DCs by each cell type classification approach at each time point. Then, I compared the raw p-value distributions of 2,000 HVGs from the RF method against the other three approaches using a p-value-to-p-value scatter plot (Figure 2.6C). In all comparisons, the p-values from the RF method were generally higher than those from the other methods, as indicated by the curve being below the diagonal. This suggests that the RF method yielded more conservative results. This gap was particularly more pronounced at 6 h, when general IFN-g responses are expected to peak [Note: In Chapter 3, I will show that general IFN-g responses, particularly in myeloid cells, are strongest at later time points.]. The observed pattern suggests that the other methods may have produced "overly optimistic p-values", which could be due to the misclassification of cell types. This inflated statistical significance can lead to incorrect conclusions in the DGE analysis and showcases again the importance of accurate cell type classification for reliable downstream statistical analysis.

The bias might stem from the mixing of information related to treatment response and

cell typing, as previously shown in Figure 2.5. To test this hypothesis and investigate the biological differences between misclassified DCs (Mono_RF) by other approaches and 'true DCs' classified by RF (DC_RF), I compared their IFN-g responsiveness using the mean signature score of the IFNg-Hallmark signature (Liberzon et al., 2015) (Figure 2.6D). At 6 h, Mono_RF had a significantly higher score compared to DC_RF (Wilcoxon rank sum test, raw $p < 0.05$), while at 1 h, the IFNg score was higher but not significantly. This analysis suggests that, at 6 h, the misclassified Mono_RF cells have a stronger IFN-g response compared to DC_RF cells. This comprehensive analysis showed that, in a complex experimental setup upon IFN-g stimulation, the other three methods misclassified myeloid cells, not due to inherent cell type-specific differences, but because of differences in IFN-g response levels.

2.3.9 My immune cell type GES repertoire outperformed published ones in RF-based cell type classifier

To demonstrate the utility of my immune cell type GES compared to other published GES repertoires, I evaluated their applicability in RF-based cell type classification using Kotliarov and Zheng benchmarking datasets. Notably, all published GESs were derived or utilized in the TME context, providing a similar cellular context for analysis and interpretation. I trained RF models using the Hao PBMC reference dataset and genes from each GES repertoire as features and calculated average statistics metrics (Figure 2.7). As a baseline control, I included a random gene set matching the size of features used for the RF classifier (167 and 163 genes for Kotliarov and Zheng datasets, respectively). As expected, random genes yielded the lowest scores in every metric, showing that selecting genes without any biological relevance or specific association with immune cell types leads to ineffective classification. RF trained with my immune cell GESs achieved the highest overall performance across all metrics, followed by the Charoentong gene set. The largest differences between my GESs and those of Charoentong were observed in sensitivity, PPV, and F1 scores for the Kotliarov (2.4%) dataset and in sensitivity for the Zheng (8%) dataset. This indicates that my GESs were better at identifying true positive immune cells, minimizing false positives, and achieving a better balance between precision and PPV. The smallest differences were in NPV scores (0.6% and 2.1%, respectively), suggesting that while my GESs still performed better, both my immune cell type GESs and Charoentong gene set performed similarly in correctly identifying non-immune cells. Overall, my immune cell type GESs demonstrated superior performance and robustness in cell type classification tasks compared to widely used published GESs.

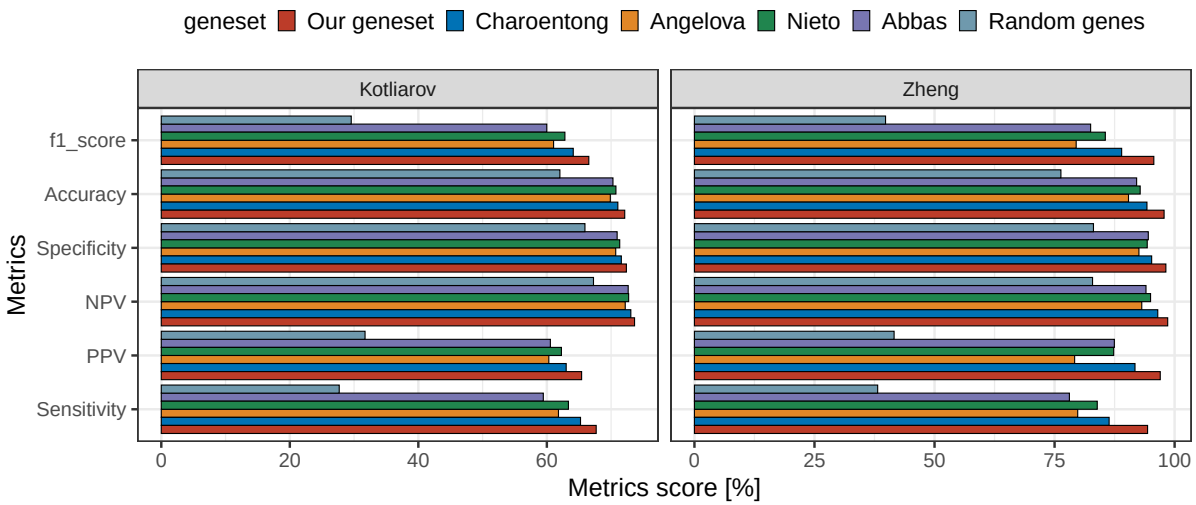

Figure 2.7: Comparison of my immune cell type signature repertoire with other published signatures on random forest approach in benchmarking datasets.

Mean statistic metrics are shown for random forest models trained using my immune cell gene set and different published immune cell type repertoires (Abbas, Angelova, Charoentong, and Nieto). I also include results from random forest models trained on random genes (with the same number of random genes as I have used for the RF classifier). Using my gene signatures yields better prediction performance in the benchmarking data from Kotliarov and Zheng than all other published GES repertoires. (Reprinted from Aybey et al. (2023))

2.4 Discussion

In this part of my study, my primary goal was to address one of the grand challenges (Lahnemann et al., 2020) in the single-cell field by developing a toolbox for classifying immune cell types, particularly in complex single-cell datasets. I tackled this challenge by identifying robust immune cell type GESs that help avoid usage of large number of genes, implementing a supervised, clustering-free RF classifier and benchmarking it against most commonly used methods. Here, I provided a method for cell typing that has strong performance for PBMC. My RF classifier offers a framework for characterizing complex IFN biology in my single-cell, temporal, and multi-perturbation experiment that I will describe in Chapter 3.

Through this process, I identified eleven novel and robust immune cell type GESs from ten distinct immune cell populations by leveraging multiple TME scRNA-seq datasets. These gene sets especially for plasma cells, pDCs, monocytes, and macrophages exhibited minimal overlap with other published immune cell type GES repertoires (Figure 2.3). Such low concordance was partially expected, as observed in previous study by Nirmal et al. (2018). This lack of overlap not only show the novelty of my GESs but can also

be attributed to several study-intrinsic factors, such as differences in study protocols, sequencing techniques, and signature discovery methodologies. Despite this, in cell type classification tasks, my signature set outperformed other published GESs of the same cell type content, demonstrating its superior performance (Figure 2.7). Such meta-analysis and comprehensive evaluation and validation in the context of immune cell type GES discovery has not been conducted yet in other studies. These emphasize the robustness and applicability of the immune cell type GESs I developed, showcasing that they are a valuable tool for cell type classification.

Immune cell typing has long been challenged by the variability in gene expression profiles observed between different cellular environments, such as those present in tissue versus blood (Nirmal et al., 2018; Pallotta et al., 2022; Schelker et al., 2017). These tissue-specific factors influence gene expression patterns and lead to substantial differences in immune cell phenotypes. These differences often limit the utility of GESs derived in one context, such as the TME, when applied to another, such PBMC. In my study, however, TME-derived GESs showed high performance on PBMC data (performance scores in the range 94–99% and 65–75% in Kotliarov and Zheng datasets, respectively). These results demonstrate the versatility of my GES repertoire and its broad applicability, as it expands the potential for cross-context analyses while maintaining high classification accuracy.

To develop a machine learning approach for the classification of immune cell types, I employed a decision tree-based method, the RF classifier. RF models are widely and successfully used in bioinformatics due to their robustness, ability to handle high-dimensional data, efficiency, high prediction accuracy, and interpretability (Qi, 2012). In my study, the RF classifier outperformed SingleR and CHETAH on two independent PBMC benchmarking datasets, while yielding comparable or superior results to Seurat, scType, and CellTypist (Figure 2.4A). A key advantage of the RF classifier is its ability to classify cell types using fewer genes, leaving more genes available for unbiased DGE analysis ($\approx$ 170 genes versus $>$ 2,000 HVGs in other approaches). The RF classifier excelled when other top-performing methods operated on less than 300—500 HVGs (Figure 2.4B). Notably, scType, an unsupervised method that relies heavily on clustering results and internal marker gene scoring, exhibited high sensitivity to HVG selection, further affirming the robustness of the RF classifier. These findings demonstrate the significant advantages of using my immune cell type gene sets in combination with an RF approach for immune cell type classification.

Many publications (Gibson, 2022; Lahnemann et al., 2020; Pasquini et al., 2021; Zhang et al., 2019a) point out the bias in the downstream analysis when the same gene expression data is used, for both cell typing and downstream statistical analyses of differential expression between the very same cell types. No study has demonstrated how this bias manifests

itself in a concrete experimental context. Using a temporal IFN-g stimulation experiment as an example, I quantitatively showed this bias (Figure 2.6). Three top-performing methods from my previous analysis, Seurat, CellTypist, and scType, misclassified monocytes as DCs due to the upregulation of IFN-g response in these misclassified cells. Compared to the RF model, these methods showed inflated p-values, highlighting the impact of the misclassification and the bias in the downstream analysis. These results clearly illustrate how cell type misclassification can impact the outcomes of downstream analyses, emphasizing the importance of using a robust and accurate cell typing method to avoid such biases.

In summary, I developed robust, novel, and conservative immune cell type GESs through a comprehensive discovery and validation process. These GESs were highly effective in cell type classification tasks, a key scRNA-seq application. The simple RF approach using these small gene sets outperformed most used methods, which rely on large sets of HVGs. Beyond its performance, the RF method was robust to perturbations and batch effects, allowing unbiased downstream analysis. Encouraged by these promising results, I applied the RF method to further IFN-stimulation PBMC scRNA-seq datasets in the subsequent chapters. Overall, my gene similarity-based discovery workflow can be applied to identify cell type-specific GESs in other environments, and the marker-based RF classifier can be adapted for cell typing in diverse cellular contexts.

3 Chapter 2: Diverging routes of IFN-I and IFN-II signaling: “the road less taken”

“Somewhere ages and ages hence:
Two roads diverged in a wood, and I—
I took the one less traveled by,
And that has made all the difference.”
Robert Frost, “The Road Not Taken”

In this chapter, I aim to disentangle gene expression signals specific to IFN-I and IFN-II responses using five IFN-stimulated healthy bulk tissue RNA-seq datasets across four different cell types. I apply a meta-analysis workflow to derive IFN-I and IFN-II specific response GESs. I validate these GESs in three external bulk tissue RNA-seq datasets from three distinct cellular contexts and assess cell type-specific IFN responses in a PBMC scRNA-seq dataset. I compare my IFN GESs to published IFN GESs throughout the discovery, validation, and assessment steps, assessing signal specificity and coherence at both general and cell type-specific levels. I also explore the association between IFN signatures and disease severity in three independent SLE microarray datasets. Additionally, I evaluate the separability of my IFN-I and IFN-II GESs in TCGA bulk tissue RNA-seq datasets from 32 different indications. Finally, I investigate the relationship between IFN-I and IFN-II scores and immune checkpoint inhibitor (ICI) therapy response in three RNA-seq datasets from different cancer indications with biospecimen collected at baseline of therapy.

(I adapted this chapter based on my unpublished manuscript (Aybey et al., 2025a), in which I was the lead author and for which I have conducted all analyses. I will submit the manuscript to a peer-reviewed journal as soon as I submit my thesis for assessment.)

3.1 Introduction

3.1.1 Defining and assessing IFN activity: challenges and needs

Understanding IFN activity is crucial for studying disease mechanisms, monitoring therapeutic responses, and predicting clinical outcomes. However, measuring IFN signaling in clinical settings is challenging due to inconsistencies in current biomarkers, which often lack relevance to specific diseases and treatments. Direct measurement of IFN proteins in serum is often unreliable because of poor sensitivity and variability in detection methods

(El-Sherbiny et al., 2018; Jabs et al., 1999). As a result, IFN activity is typically determined using the mRNA expression of ISGs, which represent downstream targets of IFN signaling. These ISGs are grouped into GESs or curated ISG lists that are upregulated upon IFN stimulation.

Several IFN GESs have been published, with some claiming specificity for distinct IFN types, particularly for IFN-I and IFN-II (Ayers et al., 2017; Bennett et al., 2003; Chaussabel et al., 2008; Dummer et al., 2020; Staub, 2012). Nevertheless, these approaches have limitations. Most signatures represent general IFN responses and often overrepresent IFN-I ISGs, failing to differentiate between IFN-I and IFN-II or among IFN-I subtypes like IFN-a and IFN-β (IFN-beta, IFN-b) (Cooles and Isaacs, 2022; El-Sherbiny et al., 2018; Hall et al., 2012). This is partially due to the overlap of ISGs activated by specific IFNs with those of other IFNs or unrelated pathways, complicating the interpretation of IFN-specific activity. There is a clear need for more refined GESs that can reliably distinguish between IFN types, as well as for comprehensive evaluation of the specificity of IFN GESs.

Another limitation of these GESs is their lack of generalizability, often due to an insufficient number of different data sets being used during discovery and validation. Many signatures are highly specific to disease, treatment, cell type, or dataset. They are often derived from single datasets under similar experimental conditions without rigorous external validation. An example of the discovery and validation processes of several published IFN-II GESs illustrates the current state of GES discovery in IFN biology (Table 3.1). The signatures presented by Ayers et al. (2017), for instance, are based on RNA-seq data from melanoma and confirmatory datasets, but they have not been rigorously validated in other contexts. Similarly, the GESs presented by Azizi et al. (2018); Platanias (2005) and Sharma et al. (2017) rely on manual curation, which may introduce bias and limit the reproducibility. The limited validation across external datasets reduces the broader applicability of these GESs. Expanding the discovery of universally applicable IFN GESs, using multiple datasets and evaluating their performance across various cellular environments, sequencing platforms, and disease contexts, is essential for improving their accuracy and generalizability in clinical and experimental settings.

Assessing IFN activity in bulk tissue also poses challenges due to variations in cell population sizes, which can influence ISG expression levels and mask subtle differences in IFN activity between distinct cell types. This limits the ability to interpret IFN signaling dynamics accurately in complex tissues and fails to capture the resolution needed to evaluate cell-type-specific IFN responses. To address this, single-cell analysis is critical, but no comprehensive evaluation of IFN GESs has yet been conducted in single-cell data. Incorporating single-cell IFN stimulation data is necessary to assess the specificity of IFN

GESs and to better understand cell-type-specific IFN responses.

While advancements in the IFN field continue, several technical, biological, and clinical challenges remain. Addressing these requires the development of robust and systematic IFN GESs capable of distinguishing IFN types, along with comprehensive discovery and validation steps. These signatures must be validated across various datasets, biological setups, and technical platforms to ensure their broad applicability. Furthermore, these must be evaluated at the single-cell level to accurately assess fine-grained cell-type-specific responses. By addressing these limitations, it will be possible to increase the reliability and generalizability of IFN GESs in diverse contexts.

Table 3.1: Overview of the published IFN-II signatures.

IFN-II signatures	Method	Discovery datasets	Validation datasets
Ayers (Ayers et al., 2017)	– Top genes among 680 tumor and immune-related genes are selected. – Genes not associated with survival response in confirmatory melanoma dataset are removed.	– KEYNOTE-001 metastatic melanoma RNA-seq dataset – KEYNOTE-001 confirmatory melanoma RNA-seq dataset	– KEYNOTE-002 Pembrolizumab treated patients with head and neck squamous cell carcinoma or gastric cancer RNA-seq dataset
Azizi-Platanias (Azizi et al., 2018; Platanias, 2005)	Manual curation from Platanias (2005)		
Sharma (Sharma et al., 2017)	Manual curation		
Waddell (Waddell et al., 2010)	– DGE	– Microarray dataset from PBMCs or isolated immune cells from one healthy donor treated with IFN-I and IFN-II – Temporal data	-
Hallmark (Liberzon et al., 2015)	– Meta-analysis, consensus clustering, and manual assessment	– IFN-g stimulated macrophages (three microarray datasets)	– IFN-g stimulated primary keratinocytes (one microarray dataset) – IFN-g stimulated STAT1 wild type macrophages (one microarray dataset)
Dummer (Dummer et al., 2020)	Manual curation		

3.1.2 Disease relevance of IFN signaling in autoimmune diseases and cancer

IFNs are key mediators in various diseases, including cancer (Pinto and Andrade, 2016) and autoimmune diseases such as systemic lupus erythematosus (SLE) (Bengtsson and Ronnblom, 2017). They regulate key signaling pathways involved in pathogen recognition, disease progression, and treatment. Through their involvement in immune responses and inflammation, IFNs can either worsen or improve symptoms, depending on the disease context. Their role in both the initiation and progression of disease makes them important targets for therapeutic interventions.

SLE is an autoimmune disease caused by a dysregulated immune system, leading to organ damage over time (Caielli et al., 2023). The accumulation of dead cells, due to impaired clearance of apoptotic debris and exposure of nuclear components into the extracellular environment, triggers a constant immune response and excessive IFN-I signaling (Ardoin and Pisetsky, 2008), rather than IFN-II signaling (Chasset et al., 2022; Gómez-Bañuelos et al., 2024). The disease outcome is measured by the SLE Disease Activity Index (SLEDAI), which reflects disease activity, organ damage, and overall health status (Bombardier et al., 1992). Studies have shown a positive correlation between SLEDAI and IFN-I GESs (Bengtsson et al., 2000). Additionally, some SLE-related IFN GESs have been identified by studying the relationship between IFN-I signaling and various disease parameters, patient populations, and immune compositions (Bennett et al., 2003; Chaussabel et al., 2008). These reports illustrate the critical role of IFN signaling, particularly IFN-I, in the progression and treatment of SLE.

In oncology, IFNs exhibit complex biology due to their dualistic and context-dependent nature (Boukhaled et al., 2021; Jorgovanovic et al., 2020). They can have antitumorigenic effects in acute inflammation but contribute to tumor progression in chronic inflammation. Despite initial interest, the clinical use of IFNs, especially IFN-I therapy in oncology, has declined due to severe side effects (Borden, 2019). But clinical trials show varying results of IFN-I therapy across different cancer types (Aricò et al., 2019; Boukhaled et al., 2021; Jorgovanovic et al., 2020). New insights into cell-type specific IFN mechanisms in oncology could lead to novel treatments, including improved standard care, combination therapies, and cancer vaccines, such as *ex vivo* IFN-stimulated DC therapy.

IFNs are key signals in determining prognosis, disease characteristics, and treatment response in clinical cancer samples. A recent comprehensive analysis of multiple immuno-oncology-related GESs found that most IFN GESs clustered together in real-world cancer samples from TCGA (Kreis et al., 2021). This indicates that IFN signaling is a common and conserved feature across various cancer types and can be utilized to characterize patient populations, particularly in the context of immune modulation and the TME.

Moreover, studies have associated upregulated IFN-II signaling in baseline cancer samples to better responses to ICI therapy (Grasso et al., 2020; Karachaliou et al., 2018; Mo et al., 2018). Specifically, an IFN-II signature (Ayers et al., 2017) (the Ayers signature, mentioned in Section 3.1) was identified from baseline tumor samples of pembrolizumab-treated melanoma patients, correlating with clinical benefit. This association suggested that IFN-II activity may prime tumors for a stronger immune response and could serve as a predictive biomarker to evaluate IFN signaling profiles in cancer patients, aiding in the selection of those more likely to respond to ICI therapies (Bai et al., 2020). Given the relevance of IFN-II signaling in cancer, its associated GESs and cell-type specific IFN-regulated mechanisms have the potential to serve as valuable tools for developing more effective immuno-oncology treatments.

To enable more thorough and reliable analysis of IFN signaling, I aim to discover and validate IFN-type specific response GESs that are applicable across a range of cellular environments, sequencing technologies, and disease contexts. Given the critical role of IFN signaling in diseases such as SLE and cancer, I explore the effects and relationships of my IFN GESs in these disease contexts and disease parameters. This approach is expected to demonstrate the broad applicability and generalizability of my IFN-type specific GESs.

3.2 Methods

(I have taken the methods section of this chapter from my unpublished manuscript (Aybey et al., 2025a).)

3.2.1 Datasets and processing

"I downloaded raw expression matrices for bulk tissue IFN stimulation RNA-seq datasets from public repositories: 1st donor and BEAS-2B cell line from Ziegler dataset (Ziegler et al., 2020) (via contact with the authors), Jankowski dataset (Jankowski et al., 2021) (Gene Expression Omnibus (GEO) (Edgar et al., 2002) accession number GSE161916), Rai dataset (Rai et al., 2017) (`http://www.ilincs.org/apps/grein/?gse=GSE74863`) and Lee dataset (Lee et al., 2020) (GEO accession number GSE161664). I normalized raw counts using DESeq2 (v1.30.1) (Love et al., 2014). I obtained processed Transcripts Per Million (TPM) matrices for Colli dataset (Colli et al., 2020) (cmdga.org with GEO accession code GSE148058 and GSE133218) and 2nd donor from Ziegler dataset (Ziegler et al., 2020) (GEO accession number GSE148829). I obtained Fragments Per Kilobase of transcript per Million mapped reads (FPKM) matrix for Fujiwara dataset

(Fujiwara et al., 2018) (GEO accession number GSE120844). I downloaded DESeq2 normalized count matrix for Devlin dataset (Devlin et al., 2020) (GEO accession number GSE145647). I filtered out lowly expressed genes (genes with overall expression < 10 for raw counts and < 1 for normalized counts). I list the details of these datasets, separated by their use for signature discovery or validation, in Table 3.2." (Aybey et al., 2025a)

Table 3.2: Datasets used in the discovery and validation steps.

Purpose	Dataset	Cell Source	Stimulation	Dose [ng/ml]	Time [h]
Discovery	(Ziegler et al., 2020) Donor 1	Lung-Basal cells	IFN-a, IFN-g	0.1, 0.5, 1, 2, 5, 10	12
	(Jankowski et al., 2021)	Kidney-HPPT cell line	IFN-a, IFN-b, IFN-g	10	12
	(Fujiwara et al., 2018)	Skin-SK-MEL-624 cells	IFN-g	10	24
	(Colli et al., 2020)	Pancreas-EndoC-BH1 cell line	IFN-a	11 pg/ml	2, 8, 18
	(Rai et al., 2017)	Lung-IMR90 cell line	IFN-b	10	24
Validation	(Ziegler et al., 2020) Donor 2	Lung-Basal cells	IFN-g, IFN-a	0, 0.1, 0.5, 1, 2, 5, 10	12
	(Ziegler et al., 2020)	Lung-Bronchial cell line BEAS-2B	IFN-g, IFN-a	0, 0.1, 0.5, 1, 2, 5, 10	12
	(Devlin et al., 2020)	Whole Blood	IFN-b, IFN-g, IFN-λ	2 (IFN-a), 10 (IFN-g, IFN-λ)	4
	(Lee et al., 2020)	Lung-Small airway epithelial cells SAEC	IFN-a, IFN-b, IFN-g, IFN-λ	10	12

"For SLE microarray datasets, I obtained Robust Multi-Array Average (GEO accession numbers GSE121239 and GSE121239) (Toro-Domínguez et al., 2018) or batch normalized gene expression matrices (GEO accession number GSE65391) (Banchereau et al., 2016) only from baseline samples. I included SLEDAI values from each publication for each patient in my analysis." (Aybey et al., 2025a)

"I used TPM-normalized values for TCGA bulk tissue RNA-seq expression data from the Xena database (Goldman et al., 2020). For ICI trial bulk tissue RNA-seq datasets of gastric cancer-pembrolizumab (Kim et al., 2018) and melanoma-ipilimumab (Van Allen et al., 2015), I obtained FPKM processed datasets from Cui et al. (Cui et al., 2021). For

IMvigor210 bladder trial with atezolizumab treatment, I used TPM normalized values processed internally using raw gene expression data from `http://research-pub.gene.com/IMvigor210CoreBiologies` (Mariathasan et al., 2018). I also included response data (responders and non-responders according to RECIST) from the given sources in the analysis." (Aybey et al., 2025a)

"I assessed a scRNA-seq dataset of PBMCs stimulated with IFN-b, IFN-g, and TNF-alpha (TNF-a) in my study. I downloaded raw counts of scRNA-seq GSE181897 dataset (Hartoularos et al., 2023) from GEO (GEO accession number GSE181897). I analyzed the data using Seurat (v4.3.0) (Stuart et al., 2019). I removed cells expressing less than 200 genes or more than 4,000 unique gene counts and genes expressed in less than three cells. I filtered out cells having mitochondrial gene portion more than five percent. For downstream analyses, I normalized the raw expression values of each single-cell dataset using LogNormalize method from Seurat. I classified immune cell types based on my RF from Chapter 1 utilizing my immune cell type GESs (Aybey et al., 2023). As my gene features, I utilized 167 genes from my signatures for eight different cell type populations (plasma, monocytes, DCs, pDCs, B, NK, $CD4^+$, and $CD8^+$ T cells). As a reference PBMC dataset for the cell type classification, I used fine grained cell type annotations from Hao PBMC reference dataset (Hao et al., 2021). For further analyses, I filtered out cell types (plasma, innate lymphoid cells and double-negative T cells) with less than ten cells in each condition." (Aybey et al., 2025a)

3.2.2 Network meta-analysis workflow

"I analyzed individual discovery datasets to identify DEGs following different IFN treatments. Prior to statistical analyses for DEG identification, I selected common top 5,000 HVGs across all discovery datasets by summing up their ranks based on variance and prioritizing those 5,000 genes with the highest additive rankings for further analysis. Then, I performed statistical analyses for DGE on these 5,000 HVGs for each discovery dataset, separately. I used $\log_2$-transformed normalized expression values as input to linear models using limma (v3.46.0) (Ritchie et al., 2015). The models were fitted to the data using lmFit function with different dose or time points as co-variates and the analysis was performed using the eBayes function (setting trend=T). I obtained estimated regression coefficients (interpreted as log-fold change (logFC)) and its standard errors from each comparison for each gene and discovery dataset for the subsequent analysis of discovering IFN type specific GESs." (Aybey et al., 2025a)

"Utilizing network meta-analysis (NMA), I compared multiple treatments across various studies, extending traditional meta-analysis approaches as detailed in Rucker (2012) and

Winter et al. (2019). Within this framework, treatments are represented as nodes within a network, and direct effects are computed akin to traditional meta-analysis methods using variance-weighted effect size averages. Given that not all treatments were uniformly represented across five datasets in my analysis, NMA allowed for the assessment of indirect comparisons that might not have been possible with traditional methods. By aggregating direct estimates along possible paths between treatments, indirect effect sizes complement direct estimates, increasing the reliability of comparisons across studies. For comparisons involving only one or two studies, effect estimates are supported by multiple other studies. Conversely, comparisons supported by multiple studies tend to yield effect estimates like those obtained through traditional meta-analysis techniques. Indirect and direct effect sizes are summed up for the calculation of overall effect estimates of individual comparisons and random effect model is applied to account for heterogeneity in different studies. For the implementation, I provided limma results as input to netmeta (v2.9-0) (Balduzzi et al., 2023). I used logFC between control and treatments along with standard errors as input. The output for each gene includes a 4x4 FC matrix along with p-values for each comparison. This matrix contains estimated FC values derived from comparisons among all conditions such as IFN-a vs. IFN-b, IFN-b vs. IFN-g, IFN-a vs. IFN-g, and the control against all three treatments (control vs. IFN-a, control vs. IFN-b, and control vs. IFN-g). The summary p-values accompanying the matrix address the null hypothesis that there is no significant difference in treatment effectiveness among the compared groups. To account for multiple correction errors and control the false discovery rate (FDR), I applied Benjamini-Hochberg correction to the raw p-values coming from each treatment comparison separately." (Aybey et al., 2025a)

3.2.3 Comparisons with published signatures: focus on type I/II IFN gene signatures

"I compared my own type I/II IFN GESs to various published signatures. To this end, I obtained a curated list of published, coherent high quality signatures for IFN signaling from RosettaSX platform for signature evaluation (Kreis et al., 2021): IFNa-Hallmark (Liberzon et al., 2015), IFNg-Hallmark (Liberzon et al., 2015), IFN-Bilgic (Bilgic et al., 2009), IFN-Feng (Feng et al., 2006), IFN-MB-Staub (Staub, 2012), IFN-Rice (Rice et al., 2013), IFN-SLE-Bennett (Bennett et al., 2003), IFN-Walsh (Walsh et al., 2007), IFNg-Dummer (Dummer et al., 2020), IFN-Chaussabel M1-2 (Chaussabel et al., 2008), IFN-Chaussabel M3-4 (Chaussabel et al., 2008) and IFN-Chaussabel M5-12 (Chaussabel et al., 2008). I also included further published IFN-II signatures in my comparative analysis: IFNg-Ayers (Ayers et al., 2017), IFNg-Azizi-Platanias (Azizi et al., 2018; Platanias, 2005), IFNg-Sharma (Sharma et al., 2017), and IFNg-Waddell (Waddell et al., 2010)." (Aybey

et al., 2025a)

"To determine the relevance of the signatures in an expression dataset, I calculated Coherence Score (CS) (Staub, 2012). CS is based on the mean of Pearson correlation of all gene pairs in the gene signature in a specific dataset. It varies between -1 and +1 defining weak and strong correlation between the genes in the signature, respectively. CS > 0.2 generally identifies signatures that are coordinately regulated transcriptional modules in a data set, and therefore point to good translatability into and relevance in a new data set (Kreis et al., 2021)." (Aybey et al., 2025a)

"To examine the separability of my IFN type genes, I reduced the dimensionality of GSE181897 scRNA-seq dataset of control, IFN-b, and IFN-g stimulated samples using UMAP from uwot (v0.1.8) (Melville et al., 2020) (2 principal components) based on either my own or published IFN signature genes." (Aybey et al., 2025a)

3.2.4 Evaluation and comparison of my signatures and their relationship to disease parameters

"To examine the relevance of the GESs to the SLE disease parameters, I calculated Spearman correlation between mean signature expression scores and SLEDAI. For each TCGA cohort, I calculated Pearson correlation between each published IFN-I or $CD8^+$ T cell signatures (Charoentong (Charoentong et al., 2017), Angelova (Angelova et al., 2015), Becht (Becht et al., 2016), Bindea (Bindea et al., 2013), Nieto (Nieto et al., 2021), Newman (Newman et al., 2015), and Aybey (Aybey et al., 2023)) with each other separately or with my IFN GESs. I transformed correlation coefficients into Z-scores using Fisher's transformation, with the advantage that these are normally distributed and better suited for statistical testing." (Aybey et al., 2025a)

"For hypothesis testing of the differences between distributions of Z-transformed correlation scores or differences between mean signature expression scores in responders and non-responders or of my IFN signatures I used two-sided Student's t-test." (Aybey et al., 2025a)

3.3 Results

3.3.1 Network meta-analysis-based GES discovery identified IFN-I and IFN-II specific response GESs

To distill GESs specific to IFN-a, IFN-b, and IFN-g, I utilized five RNA-seq datasets of healthy bulk tissue stimulated with these IFNs, derived from diverse tissues and experimental setups (Table 3.2). This diversity enables the discovery of response genes applicable across broader contexts, but also introduces challenges, such as variability in IFN stimulation conditions, time points, concentrations, tissue types, and normalization methods. To address these complexities and obtain gene-wise results on DGE from pairwise comparison of each IFN type, I applied a network meta-analysis (NMA)-based workflow adapted from Winter et al. (2019) (see Methods, Figure 3.1). NMA extends traditional meta-analysis, which relies on direct comparisons from each study that test the same treatments, by incorporating indirect comparisons. This means that even if two treatments were not directly compared in the same study, NMA can still compare their effects by linking them through other studies. This approach allowed me to compare each IFN treatment pairwise while leveraging available data in the public domain, rather than relying solely on the comparisons coming from individual studies.

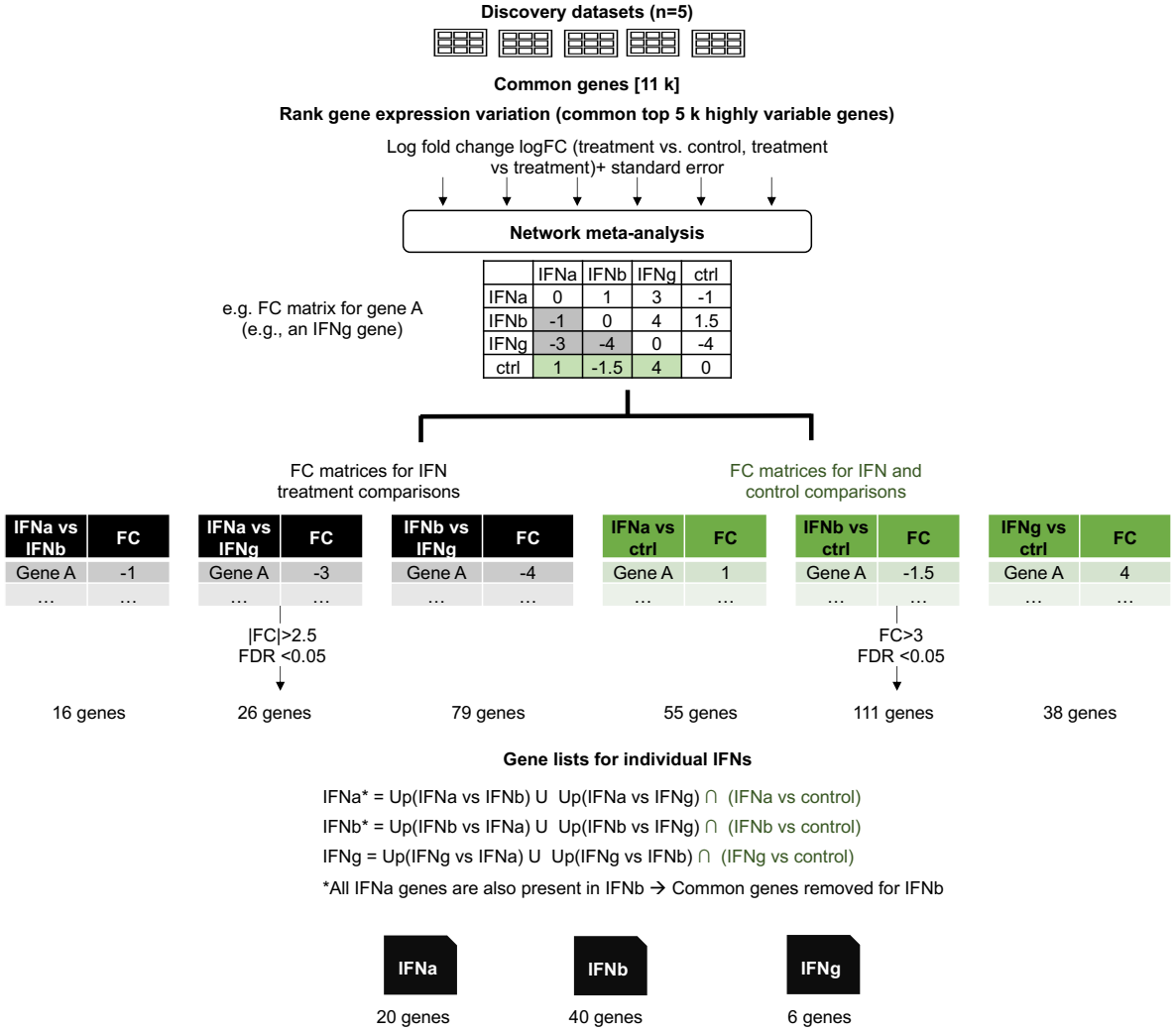

Figure 3.1: Network meta-analysis workflow for obtaining IFN signatures.

For the workflow, five bulk tissue RNA-seq IFN stimulation discovery datasets are used and $\approx 11,000$ common genes are ranked based on variance in each dataset. The common top 5,000 highly variable genes are selected for downstream analysis. Log fold changes (logFC) are calculated between stimulation and control, and between each available treatment for each dataset, along standard errors. Network meta-analysis is applied on these results to obtain FC values and FDR-adjusted p-values between each IFN treatment for each gene along with comparison between each IFN treatment and control (ctrl). Three lists of FC are compiled for IFN treatment comparisons and genes for |FC| less than 2.5 and more than 0.05 for FDR are filtered out. Additionally, three lists of FC are compiled for IFN treatment and control comparison. Only genes with more than FC of 3 and less than FDR of 0.05 are taken into consideration. Finally, gene list for each individual type of IFN are constructed by taking only upregulated genes in each IFN type compared to other treatments or control.

Initially, I aimed to systematically investigate the distinct transcriptional effects of different IFNs in comparison to one another. For each IFN treatment, I performed DGE analysis on top common 5,000 genes versus controls across all datasets (see Methods, Figure 3.1). The p-value distributions indicated a high number of genes ($> 500 - 1000$) with low raw p-values, showing an overabundance of significant genes compared to those with higher p-values (Figure 3.2). This indicated a strong differential expression signal and the suitability of these datasets for further analysis, as they provided robust evidence for genes affected by different IFN stimulations (Breheny et al., 2018). Building on these results, I used the DGE outputs to execute NMA, constructing treatment networks for individual genes. This process generated a 4x4 fold-change (FC) matrix with associated p-values for each gene (Figure 3.1), enabling systematic pairwise comparisons across different IFN treatments.

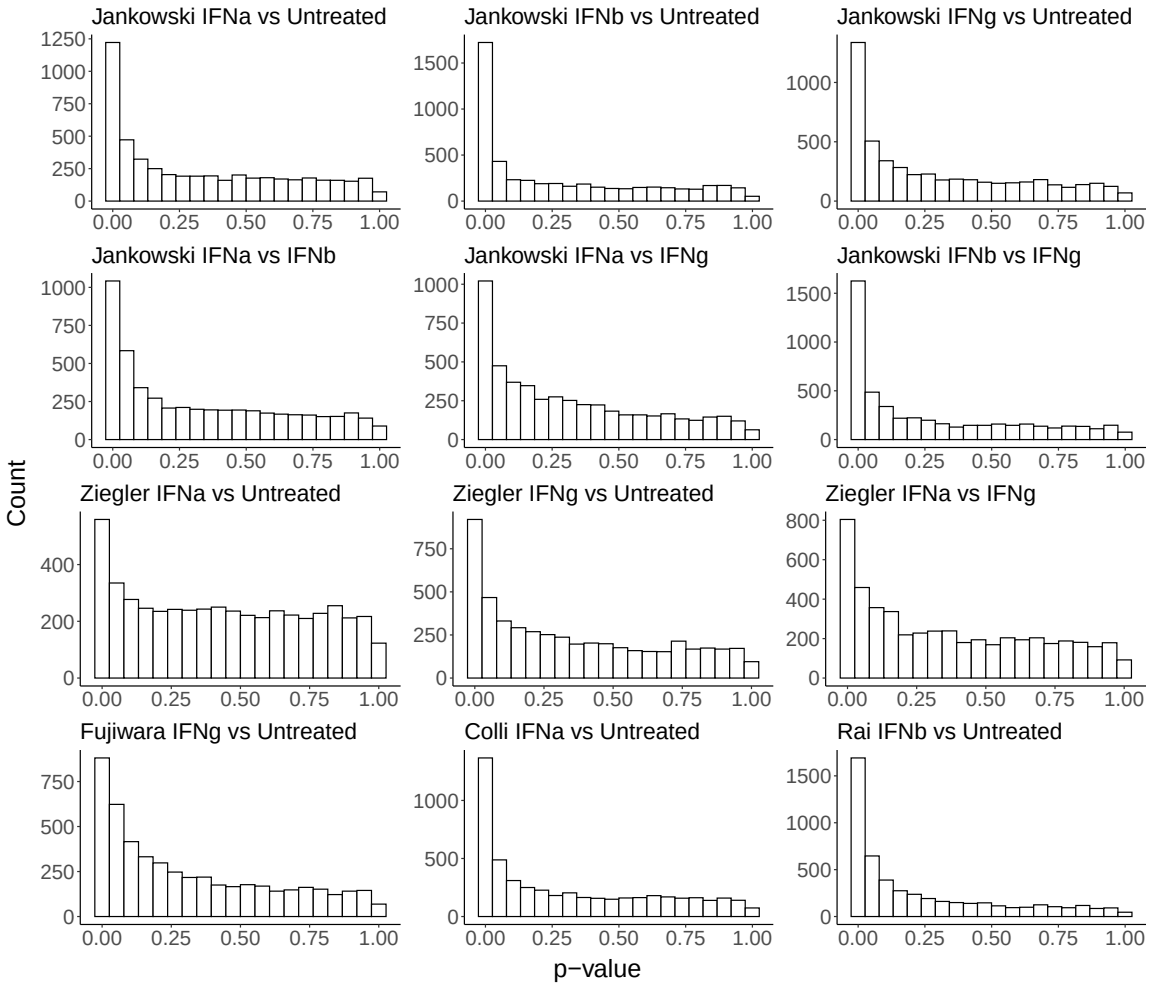

Figure 3.2: P-value distributions of differential gene expression tests for each treatment comparison in discovery datasets.

The p-value distributions coming from DGE analysis of top 5,000 highly variables genes common across datasets are shown. The shape of the distributions with peaks close to zero confirm that there is sufficient signal to identify differentially expressed genes after IFN stimulation in each of the discovery datasets.

To create IFN type-specific GESs, I implemented a two-step filtering process involving treatment-versus-treatment and treatment-versus-control comparisons. For the treatment-versus-treatment analysis, I compared each IFN stimulation against the others, generating three gene lists (Figure 3.1). I excluded genes without significant differences between treatments ($|FC| < 2.5$ and $FDR > 0.05$). This stringent filtering identified 16 DEGs for IFN-a vs. IFN-b, 26 DEGs for IFN-a vs. IFN-g, and 79 DEGs for IFN-b vs. IFN-g. As expected, IFN-a and IFN-b exhibited the fewest distinct DEGs, reflecting their similar transcriptional programs, while IFN-b and IFN-g displayed the most distinct profiles. For the treatment-versus-control analysis, I created three additional gene lists, keeping only genes with significantly higher expression in treatments compared to controls ($FC > 3$, $FDR < 0.05$) (Figure 3.1). IFN-g affected the fewest genes ($n = 38$), while IFN-b influenced the most ($n = 111$), suggesting that IFN-b has a more pronounced impact on downstream gene regulation, whereas IFN-g has a more limited effect.

To finalize my IFN-type specific response GESs, I joined the results from the two-level analyses. For each IFN type, I took the union of upregulated genes from the treatment-versus-treatment comparisons and intersected them with genes identified in the treatment-versus-control analysis (Figure 3.1). As expected, due to the close transcriptional similarity between IFN-a and IFN-b, all IFN-a genes ($n = 20$) were also present in the IFN-b gene set ($n = 60$), demonstrating their shared transcriptional programs (Thomas et al., 2011; de Weerd et al., 2013). To address this overlap, I removed the 20 common genes from the IFN-b signature, leaving 40 unique IFN-b genes to later evaluate whether they could distinguish IFN-a and IFN-b signals. For now, the IFN-a signature can be considered as a general IFN-I or common IFN-a/IFN-b GES. Of note, all IFN-g genes have been independently published as IFN-g ISGs across various cellular contexts and studies in single studies across various contexts, but have never been described in their entirety in single study (Chang et al., 2002; Kim et al., 2018; Liu et al., 2018; Morrow et al., 2011; Pallotta et al., 2022). The final IFN response GESs consisted of 20 genes for IFN-a (general IFN-I), 40 genes for IFN-b, and 6 genes for IFN-g (Table 3.3), referred to as IFNa-Aybey, IFNb-Aybey, and IFNg-Aybey, respectively. I will further evaluate these GESs in the discovery and validation datasets.

Table 3.3: Gene lists for my IFN signatures.

IFNa/IFN-I-Aybey (n=20)	IFNb-Aybey (n=40)	IFNg/IFN-II-Aybey (n=6)
CMPK2	BST2	CD74
DDX58	BTC	CXCL9
GMPR	C3AR1	GBP2
HERC5	CD7	ICAM1
HERC6	CYP2J2	IDO1
HRASLS2	DDX60L	IRF1
HSH2D	DHX58	
IFI27	DLL1	
IFI6	GCH1	
IFIT1	IFI44	
IFIT3	IFI44L	
ISG15	IFIH1	
LAMP3	IFIT1B	
MX1	IL22RA1	
MX2	IL4I1	
OAS1	IRF7	
OAS2	ISG20	
OASL	LGALS9	
RSAD2	LMO2	
USP18	MMP13	
	MYD88	
	NOD2	
	OAS3	
	PDGFRL	
	PLSCR1	
	PNPT1	
	PPM1K	
	RTP4	
	SAMD9	
	SIDT1	
	SLFN12L	
	SSTR2	
	STARD5	
	THEMIS2	
	TLR3	
	TMEM229B	
	TNFSF13B	
	TRANK1	
	TSPAN33	
	ZBP1	

3.3.2 IFN-I and IFN-II response GESs distinguished IFN-I and IFN-II signals in discovery datasets

I first assessed how well IFN GESs could distinguish different IFN signals in the discovery datasets. To do this, I calculated the differences in mean signature scores between each treatment and control (d_{mean}) (Figure 3.3A). As expected, IFN-g samples showed a greater difference in d_{mean} with IFNg-Aybey than with IFNa-Aybey or IFNb-Aybey, while the opposite was true for IFN-a or IFN-b samples. This effect was consistent across various conditions, including time points and concentrations, demonstrating the expected ability of the signatures to distinctly classify IFN-I and IFN-II responses.

Next, I examined the differences between IFN-I GESs, IFNa-Aybey and IFNb-Aybey, in their ability to distinguish between IFN-I and IFN-II signals. The common IFN-I signature (IFNa-Aybey) outperformed IFNb-Aybey, with larger d_{mean} differences between IFNg-Aybey and IFNa-Aybey compared to those between IFNg-Aybey and IFNb-Aybey in nearly all discovery datasets. For example, in multi-IFN perturbation datasets, the differences ranged from 0 to 0.4 in Jankowski dataset (Jankowski et al., 2021) and 0 to 0.75 in Ziegler dataset (Ziegler et al., 2020) on the summed Z score scale. These results confirm that IFNa-Aybey provided the better distinction between IFN-I and IFN-II signals compared to IFNb-Aybey.

I aimed to investigate whether IFN-a and IFN-b could be distinguished from each other. However, the d_{mean} differences between IFNa-Aybey and IFNb-Aybey were close to 0 (two-sided Student's t-test comparing IFNa-Aybey and IFNb-Aybey in each stimulation generally yielded p-values > 0.05). This indicated that their signals were not significantly separable and reaffirmed that distinguishing their signals is challenging, consistent with previous findings from NMA.

Based on these results, I confirmed that IFNg-Aybey and the common IFN-I signature (IFNa-Aybey) effectively separated IFN-I and IFN-II signals. For further validation, I continued with IFNa-Aybey and IFNg-Aybey.

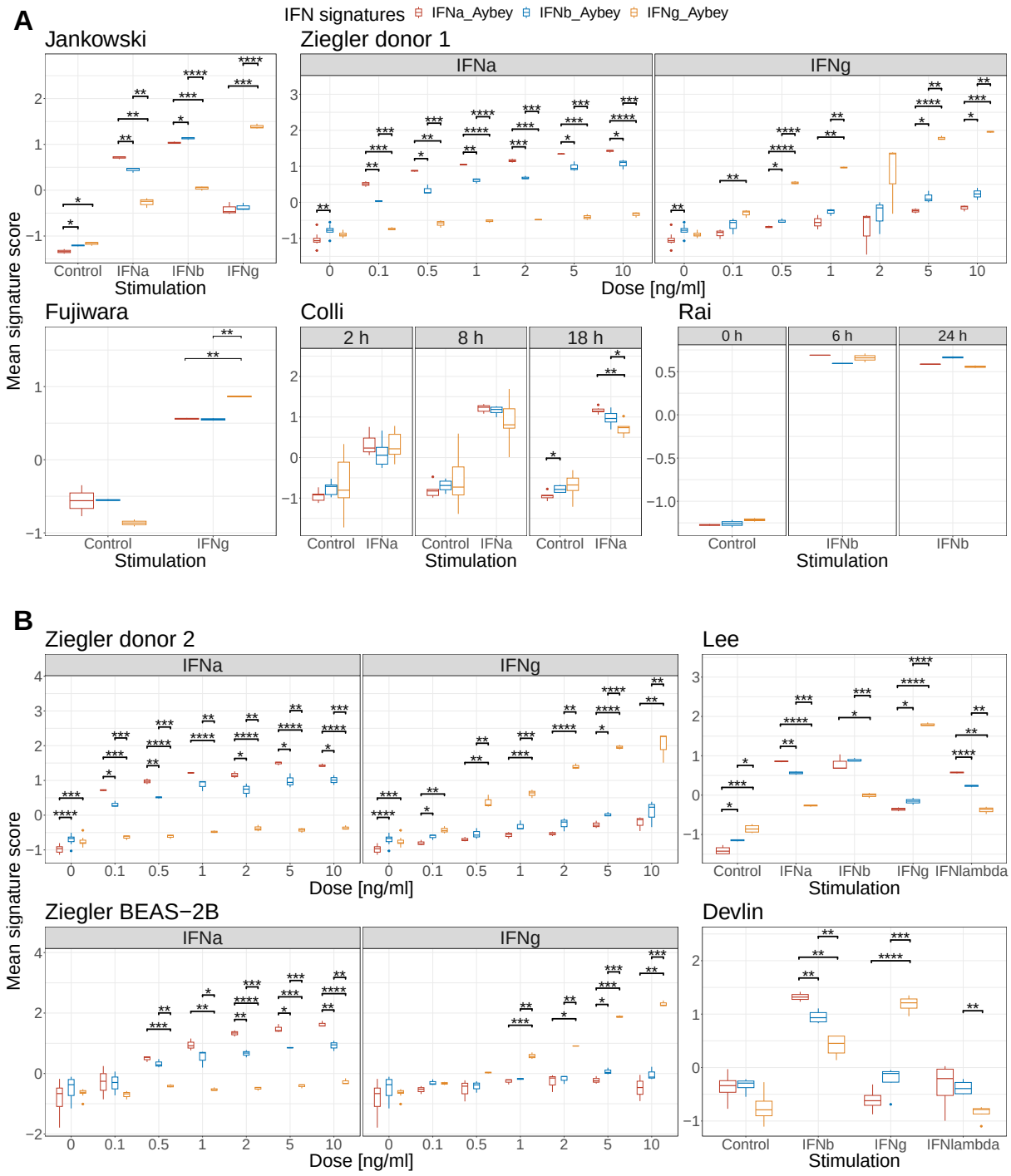

Figure 3.3: Discovery and validation of my IFN signatures.
Mean signature scores for each signature are shown on the y-axis. Data points for IFNa-Aybey, IFNb-Aybey, and IFNg-Aybey are colored differently. **(A)** Discovery datasets. In Ziegler dataset, on the x-axis, IFN concentrations are shown, and each box represents different stimulations while in other datasets different conditions are shown on the x-axis. Different boxes in Colli and Rai datasets represent different time points. **(B)** Validation datasets. In two Ziegler datasets, on the x-axis, different IFN concentrations are shown while in the other two validation datasets, different conditions are shown on the y-axis. p-values comparing different IFN scores are shown. (* = $p < 0.05$, ** = $p < 0.01$, *** = $p < 0.001$, and **** = $p < 0.0001$).

3.3.3 Validation confirmed that IFN-I and IFN-II GESs differentiated IFN signals across independent datasets

I evaluated my IFN GESs in three independent datasets not used in the discovery phase, each serving a different validation purpose (Table 3.2, Figure 3.3B). These validation steps tested the robustness and applicability of my IFN GESs across different cell types, experimental conditions, and multiple IFN stimulations.

I conducted the first validation using the Ziegler dataset (Ziegler et al., 2020), which included IFN-a and IFN-g treated lung basal cell samples from a second donor, not used in the discovery phase, and the BEAS-2B lung cell line. In this dataset, the differences in d_{mean} between IFN-I and IFN-II signals increased with higher doses, ranging from 0.4 to 2 for IFN-a and 0.6 to 2.8 for IFN-g stimulations (two-sided Student's t-tests comparing IFN-I and IFN-II scores at each dose level yielded p-values < 0.05). These validated the utility of my IFN GESs in lung basal cells and epithelial cells across varying doses and experimental conditions.

The second analysis for validation used the Lee dataset (Lee et al., 2020), which encompassed lung small airway epithelial cells exposed to multiple IFN stimulations (IFN-a, IFN-b, IFN-g, or IFN-lambda). The differences in d_{mean} between IFN-I and IFN-II signals were significantly high (2, 1.6, and 1.6 for IFN-a, IFN-b, and IFN-g stimulations, respectively; two-sided Student's t-tests comparing IFN-I and IFN-II scores for each stimulation yielded p-values < 0.05). Furthermore, IFN-a, IFN-b, and IFN-g stimulations exhibited higher d_{mean} for my IFN GESs than IFN-lambda treatments, demonstrating the higher selectivity of my IFN GESs for IFN-I/II compared to IFN-III. This validation demonstrated the robustness of my IFN GESs in datasets with multiple IFN stimulations. It also confirmed their applicability to another cell line similar to the Ziegler dataset, and verified their ability to distinguish IFN-I/II from IFN-III.

The last validation dataset from Devlin et al. (2020) stem from a completely different cellular environment, featuring a more heterogeneous and complex setup with whole blood samples. The dataset included multiple IFN stimulations (IFN-b, IFN-g, or IFN-lambda). In every stimulation, IFN-I and IFN-II signals differed highly and significantly (the differences in d_{mean} 0.6 and 2.3 for IFN-b and IFN-g stimulations, respectively; two-sided Student's t-test comparing IFN-I and IFN-II scores for each stimulation yielded p-values < 0.05). This confirmed that the IFN GESs are effective even in complex, heterogeneous environments.

In conclusion, the common IFN-I (IFNa-Aybey) and IFN-II (IFNg-Aybey) signatures showed the highest separability. These signatures demonstrated their robustness, utility,

and selectivity across various datasets, experimental conditions, biological contexts, and stimulations. Further analyses will focus only on the 20-gene IFN-I signature and the 6-gene IFN-II signature.

3.3.4 IFN GESs were comparable with published IFN GESs and showed similar or better coherence and signal separability

I compared my IFN GESs with ten published IFN-I and seven IFN-II GESs, evaluating their similarity, signal separation, and coherence. I visualized the mean signature scores using clustered heatmaps (Figure 3.4) for both discovery and validation datasets. IFN-I-Aybey clustered with published IFN-I GESs that exhibited greater separation between IFN-I and IFN-II signals. Other signatures, such as IFNa-Hallmark, IFN-Chaussabel-M5-12, and IFN-Chaussabel-M3-4, did not cluster closely with IFN-I-Aybey and failed to distinguish IFN-I and IFN-II signals, particularly in multi-IFN perturbation datasets. Similarly, IFN-II-Aybey clustered with IFN-II GESs, such as IFNg-Ayers, IFNg-Azizi-Platanias, and IFNg-Dummer, that showed better separation between IFN-I and IFN-II signals. The clustering results indicated that my IFN GESs displayed similar activation patterns to published GESs but with stronger selectivity between IFN-I and IFN-II signals.

To quantitatively assess the transferability of these IFN GESs across datasets, I used coherence score (CS) (Rahnenführer et al., 2004; Staub, 2012). CS measures the degree to which gene sets are co-regulated—whether the genes in the set are up- or downregulated coordinately across samples. This approach has been used as a surrogate for pathway relevance or activity. IFN-I-Aybey had one of the highest CSs, particularly in validation datasets (Figure 3.4B). GESs that clustered with IFN-I-Aybey also had high CSs, while interestingly IFNa-Hallmark, a widely used IFN-I GES, had a lower CS. Similarly, IFN-II-Aybey had the highest CSs among IFN-II GESs. In contrast, IFNg-Hallmark, a commonly used IFN-II GES, showed weak CS, as did IFNg-Waddell and IFNg-Sharma, suggesting a poor association with IFN-II responses. In summary, my IFN GESs exhibited similar expression patterns to most published IFN GESs, while showing stronger distinction and higher coherence. These results suggest that my IFN GESs are highly translatable and coherent across datasets, better distinguishing IFN-I and IFN-II biology than most published signatures.

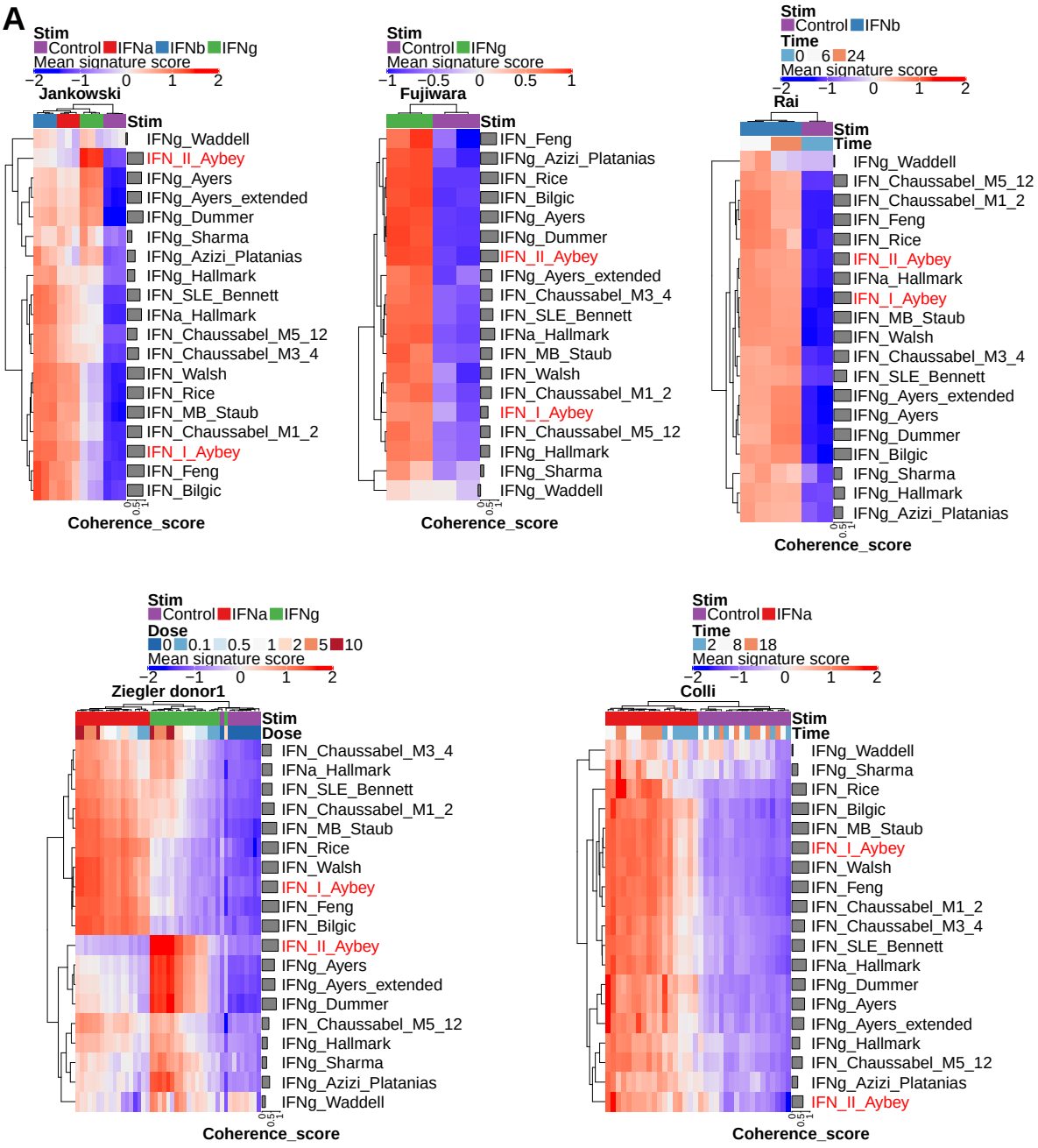
A
Stim
Control IFNa IFNb IFNg
Mean signature score
−2 −1 0 1 2
Jankowski
Stim
IFNg_Waddell
IFN_II_Aybey
IFNg_Ayers
IFNg_Ayers_extended
IFNg_Dummer
IFNg_Sharma
IFNg_Azizi_Platanias
IFNg_Hallmark
IFN_SLE_Bennett
IFNa_Hallmark
IFN_Chaussabel_M5_12
IFN_Chaussabel_M3_4
IFN_Walsh
IFN_Rice
IFN_MB_Staub
IFN_Chaussabel_M1_2
IFN_I_Aybey
IFN_Feng
IFN_Bilgic
Coherence_score
Stim
Control IFNg
Mean signature score
−1 −0.5 0 0.5 1
Fujiwara
Stim
IFN_Feng
IFNg_Azizi_Platanias
IFN_Rice
IFN_Bilgic
IFNg_Ayers
IFNg_Dummer
IFN_II_Aybey
IFNg_Ayers_extended
IFN_Chaussabel_M3_4
IFN_SLE_Bennett
IFNa_Hallmark
IFN_MB_Staub
IFN_Walsh
IFN_Chaussabel_M1_2
IFN_I_Aybey
IFN_Chaussabel_M5_12
IFNg_Hallmark
IFNg_Sharma
IFNg_Waddell
Coherence_score
Stim
Control IFNb
Time
0 6 24
Mean signature score
−2 −1 0 1 2
Rai
Stim
Time
IFNg_Waddell
IFN_Chaussabel_M5_12
IFN_Chaussabel_M1_2
IFN_Feng
IFN_Rice
IFN_II_Aybey
IFNa_Hallmark
IFN_I_Aybey
IFN_MB_Staub
IFN_Walsh
IFN_Chaussabel_M3_4
IFN_SLE_Bennett
IFNg_Ayers_extended
IFNg_Ayers
IFNg_Dummer
IFN_Bilgic
IFNg_Sharma
IFNg_Hallmark
IFNg_Azizi_Platanias
Coherence_score
Stim
Control IFNa IFNg
Dose
0 0.1 0.5 1 2 5 10
Mean signature score
−2 −1 0 1 2
Ziegler donor1
Stim
Dose
IFN_Chaussabel_M3_4
IFNa_Hallmark
IFN_SLE_Bennett
IFN_Chaussabel_M1_2
IFN_MB_Staub
IFN_Rice
IFN_Walsh
IFN_I_Aybey
IFN_Feng
IFN_Bilgic
IFN_II_Aybey
IFNg_Ayers
IFNg_Ayers_extended
IFNg_Dummer
IFN_Chaussabel_M5_12
IFNg_Hallmark
IFNg_Sharma
IFNg_Azizi_Platanias
IFNg_Waddell
Coherence_score
Stim
Control IFNa
Time
2 8 18
Mean signature score
−2 −1 0 1 2
Colli
Stim
Time
IFNg_Waddell
IFNg_Sharma
IFN_Rice
IFN_Bilgic
IFN_MB_Staub
IFN_I_Aybey
IFN_Walsh
IFN_Feng
IFN_Chaussabel_M1_2
IFN_Chaussabel_M3_4
IFN_SLE_Bennett
IFNa_Hallmark
IFNg_Dummer
IFNg_Ayers
IFNg_Ayers_extended
IFNg_Hallmark
IFN_Chaussabel_M5_12
IFNg_Azizi_Platanias
IFN_II_Aybey
Coherence_score

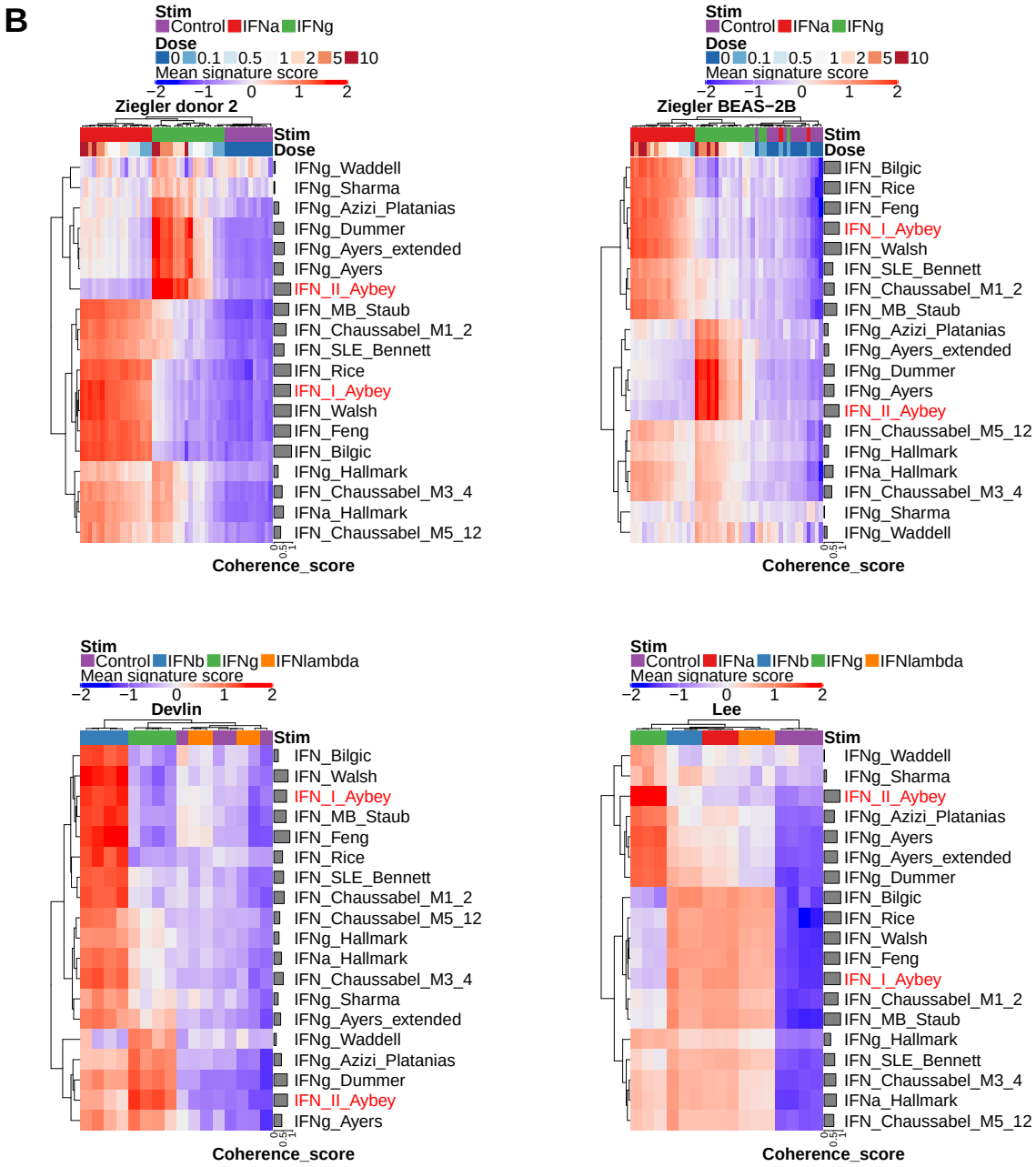

Figure 3.4: Evaluation of my IFN GES and other published GES in (A) discovery and validation (B) datasets.

Mean signature score and coherence scores are shown for each signature separately in the discovery and validation datasets. My IFN signatures are colored in red and others in black. Different experimental conditions such as time and IFN concentrations are shown on the column annotations. Hierarchical clustering is applied column- and row-wise. Mean signature scores are shown from low (blue) to high (red).

3.3.5 IFN GESs were applicable to scRNA-seq data from immune cells, separating IFN-I/II signals

Previously, I demonstrated the applicability of my IFN GESs in bulk tissue RNA-seq datasets. To assess their cell-type-specific utility in scRNA-seq datasets, I analyzed an IFN-stimulation PBMC scRNA-seq dataset (GSE181897) (Hartoularos et al., 2023). PBMCs from 64 healthy donors were stimulated with IFN-b, IFN-g, or left unstimulated, and samples were taken 9 h post-stimulation. As a negative control, I included TNF-a stimulation. This experimental setup allowed me to evaluate the performance of my IFN GESs and other published IFN GESs in a single-cell context.

In the previous chapter, I developed a RF classifier for unbiased immune cell type classification, particularly suited for complex datasets with varying experimental variables, such as the one used here. Using UMAP for dimensionality reduction (Figure 3.5) with my 167 immune cell type genes, cells were separated by cell types rather than treatment groups. This demonstrates that a relatively small number of robust, cell-type-specific genes are sufficient to capture intrinsic cellular composition and define cell types independently of other conditions. These findings further emphasize the robustness and versatility of my immune cell type GESs and suggest that my RF classifier performed well in this different experimental context.

The analysis of IFN GESs in the context of single-cell data showed distinct activation patterns. Visually, the mean signature expression scores for my IFN GESs as overlayed on an UMAP analysis based on my 167 immune cell type genes were elevated in the cells treated with the corresponding IFN type (Figure 3.5). These differences were statistically significant, based on one-sided Student's t-tests (Bonferroni-adjusted p-values < 0.05), comparing mean signature scores across different treatments (Figure 3.6, first row). While IFN-I response was activated in all immune cell-type populations, the IFN-II response was primarily restricted to myeloid cells and other cell types like B cells. These patterns confirm the utility of my IFN GESs in characterizing cell-type-specific IFN responses in scRNA-seq datasets.

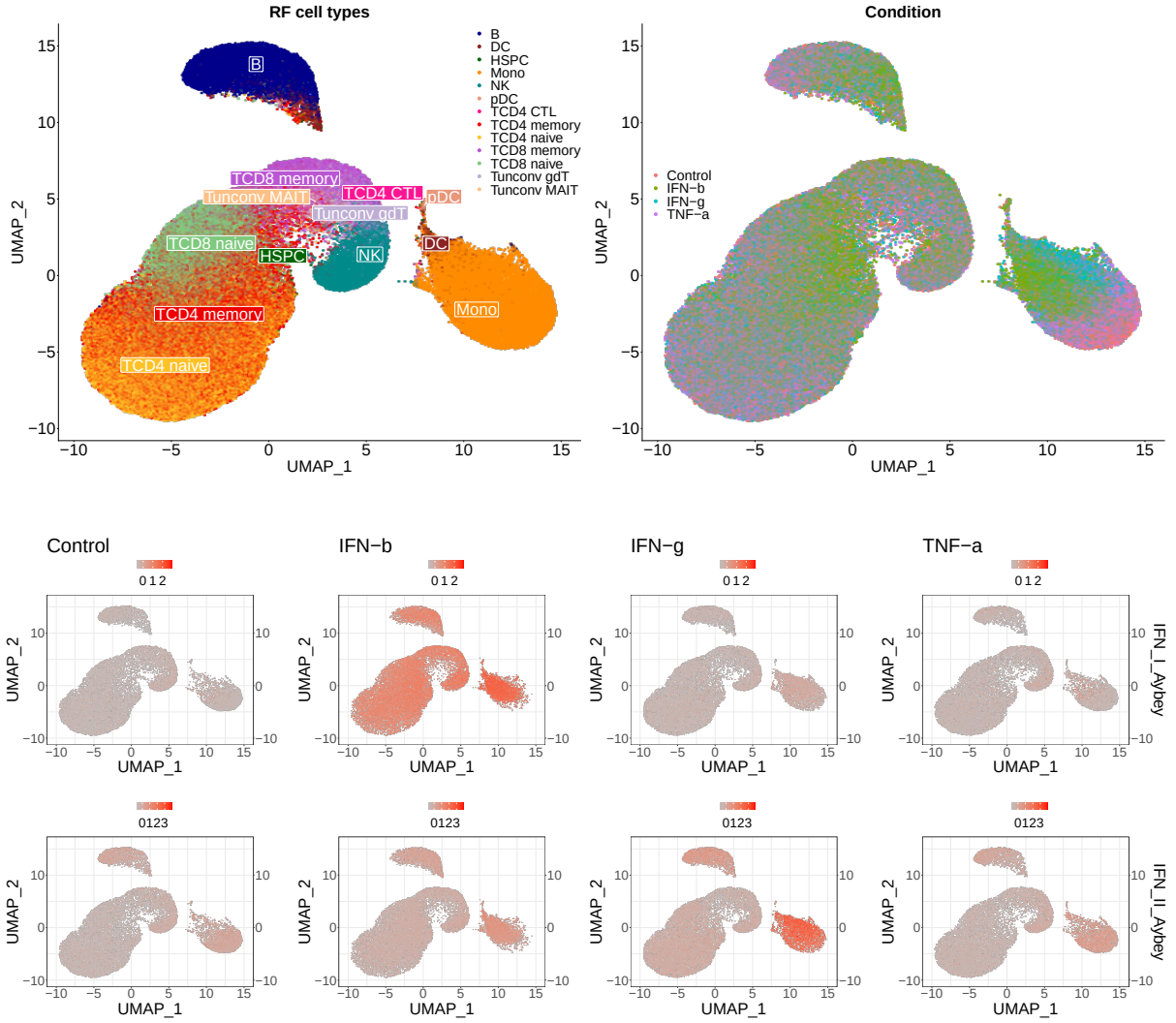

Figure 3.5: FeaturePlots showing mean signature expression scores of IFN Aybey signatures on UMAP plots in IFN-b, IFN-g, and TNF-a stimulation single-cell gene expression dataset. (Upper) UMAP based on my immune cell type specific genes showing different cell types defined by my random forest cell type classification method and different conditions. (Lower) Mean signature score levels are shown for IFN-I- and IFN-II-Aybey signature from low (gray) to high (red) on UMAP from the upper figure. Each condition is shown in a separate FeaturePlot.

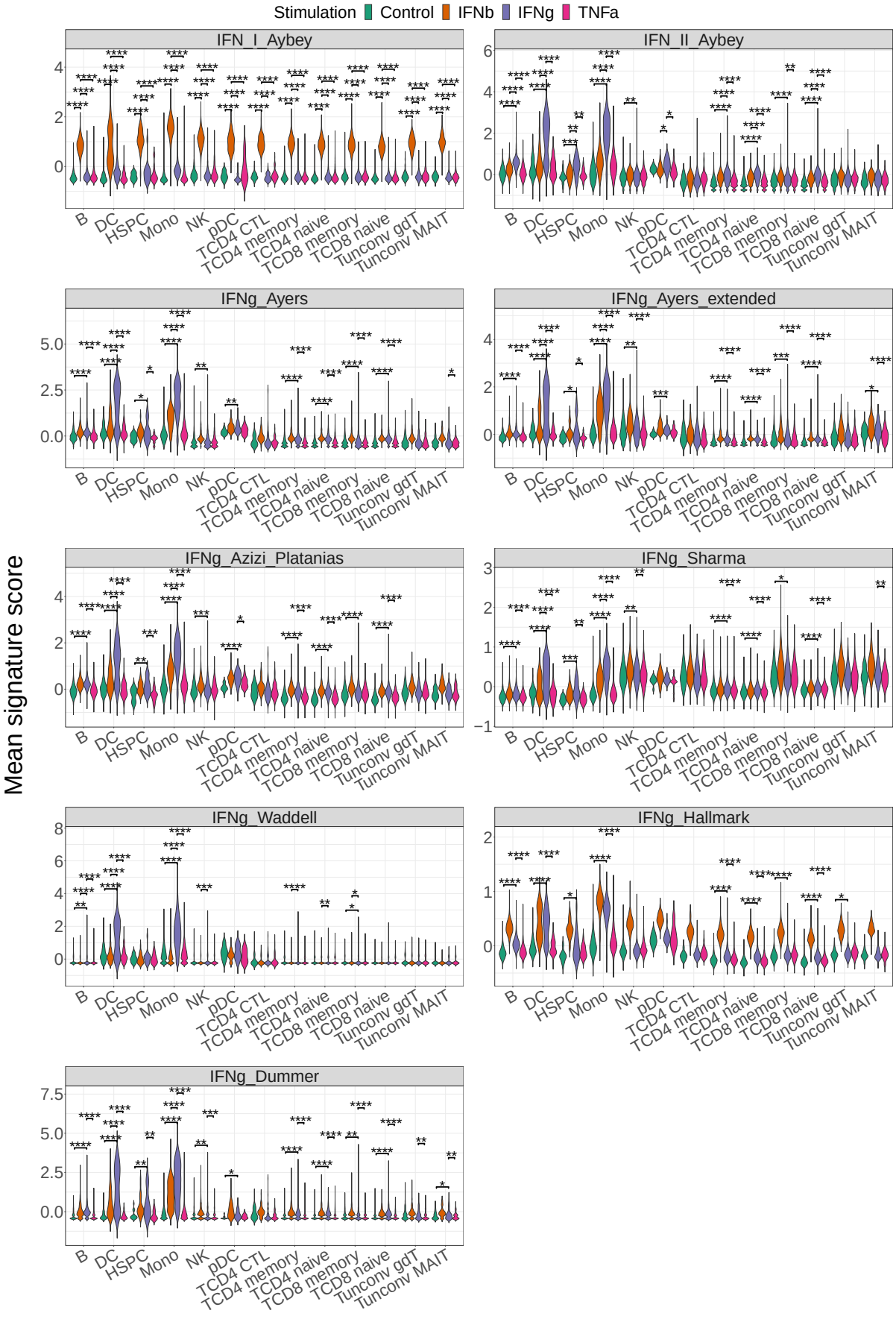
Stimulation Control IFNb IFNg TNFa
IFN_I_Aybey
IFN_II_Aybey
IFNg_Ayers
IFNg_Ayers_extended
IFNg_Azizi_Platanias
IFNg_Sharma
IFNg_Waddell
IFNg_Hallmark
IFNg_Dummer
Mean signature score
B
DC
HSPC
Mono
NK
pDC
TCD4 CTL
TCD4 memory
TCD4 naive
TCD8 memory
TCD8 naive
Tunconv gdT
Tunconv MAIT
Cell types

Figure 3.6: My IFN-I and IFN-II signatures compared with published IFN-II signatures in IFN-b, IFN-g, and TNF-a stimulation single-cell gene expression dataset.
For the evaluation of my IFN signatures and comparing those with published IFN-II signatures, GSE181897 scRNA-seq IFN stimulation dataset is used. Mean signature scores (y-axis) are calculated for each cell and shown for each signature (box) while cell type annotations defined by my random forest cell type classification method are shown on the x-axis. The stimulations (IFN-b, IFN-g, and TNF-a) are shown in different colors. Each IFN score is pairwise compared in its corresponding IFN treatment with other conditions within each cell type using one-sided Student's t-test. Bonferroni-adjusted p-values are displayed. (* = $p < 0.05$, ** = $p < 0.01$, *** = $p < 0.001$, and **** = $p < 0.0001$).

Next, I examined whether IFN-I- and IFN-II genes yield separate expression patterns in the GSE181897 scRNA-seq dataset. To this end, I applied UMAP on two gene expression data matrices: the gene x cell matrix for all genes of my IFN-I/-II GESs, and the analogous data matrix for all genes of public IFN-I/II GESs. I categorized the genes from public signatures into three groups: common genes shared between IFN-I and IFN-II GESs ('common IFN-I/II genes'), IFN-I-specific genes, and IFN-II-specific genes. The first UMAP dimension separated IFN-II-Aybey from IFN-I-Aybey genes (Figure 3.7A), demonstrating that IFN-I and IFN-II genes could be differentiated in a single-cell context. In contrast, the genes from the published signatures formed three types of clusters (Figure 3.7B): mixed clusters containing both IFN-I, IFN-II, and common genes; a cluster of common genes and IFN-I genes; and a cluster containing both IFN-I and IFN-II genes. This pattern suggests significant overlap among the gene sets. Published IFN genes showed a lack of exclusivity, demonstrating that my IFN genes could distinguish IFN type signals in a complex single-cell context, whereas published IFN genes do not differentiate between IFN-I and IFN-II signals.

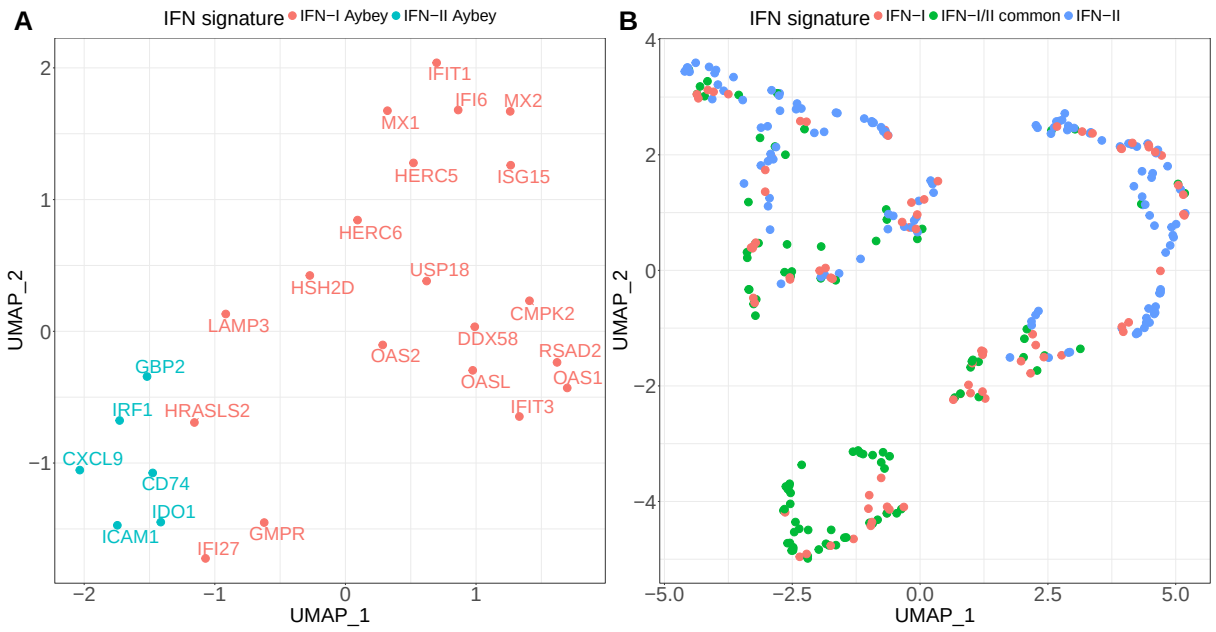

Figure 3.7: UMAPs based on different IFN gene set collections in IFN-b and IFN-g stimulation single-cell gene expression dataset: (A) IFN-I-Aybey and IFN-II-Aybey genes or (B) published IFN-I and IFN-II genes.

Expression data of samples from different conditions (control, IFN-b stimulation, and IFN-g stimulation) are used to derive a UMAP based on different IFN gene sets. Each gene set is colored differently, and gene names are shown for my IFN signatures. For published gene sets unique IFN-I or IFN-II genes as well as common genes between those two subtypes are colored. Note that in (A) my IFN-I and IFN-II signature genes are perfectly separated while in (B) for IFN-I/II genes from other published signatures genes do not cluster by annotated IFN type.

3.3.6 IFN-II-Aybey detected IFN-II response more effectively than previously published GESs and in more cell types

I evaluated the ability of IFN-II-Aybey to detect cell type-specific IFN-II responses compared to other published IFN GESs in the GSE181897 dataset (Figure 3.6). Expectedly, myeloid cells were activated more strongly upon IFN-g stimulation (Waddell et al., 2010). All IFN-II GESs except IFNg-Hallmark could detect myeloid cell specific IFN-II response by having significantly higher scores (one-sided Student's t-test, Bonferroni-adjusted p-values < 0.05) upon IFN-g stimulation compared to other stimulations. Notably, IFN-II-Aybey was the only GES which showed significantly higher scores at other IFN-g treated cell type populations such as hematopoietic stem cells (HSC), B cell, naïve $CD8^+$ T cell, naïve $CD4^+$ T cell, and memory $CD4^+$ T cell populations (one-sided Student's t-test, Bonferroni-adjusted p-values < 0.05). IFNg-Hallmark again showed a weak association with IFN-II specific response, which I have already demonstrated in my previous analysis

(Figure 3.4). Similarly, other signatures such as IFNg-Ayers and IFNg-Azizi-Platanias exhibited higher scores at IFN-b treatment compared to IFN-g treatment, indicating lack of IFN-II specificity. Additionally, some signatures such as IFNg-Sharma showed cell type specificity by having higher scores in T and NK cell populations across all conditions. In summary, my IFN-II GES detected IFN-II specific response with higher selectivity and in more immune cell type populations than any published IFN-II GES.

3.3.7 IFN-I-Aybey showed high coherence and was highly correlated with disease severity in SLE

To investigate the relevance of my IFN GESs in the diseased context, I focused on SLE, an autoimmune disease where many studies have linked IFN-I signaling with disease severity, particularly the SLEDAI score (Bengtsson et al., 2000; Chasset et al., 2022; Chaussabel et al., 2008; Gómez-Bañuelos et al., 2024). I used three independent SLE microarray datasets to calculate Spearman correlation (SC) between the SLEDAI score and the IFN signature score, as well as the CS for each individual IFN GES (Table 3.4). In general, both SC and CS of IFN-I GESs were higher than those of IFN-II GESs, emphasizing the predominant role of IFN-I over IFN-II in driving SLE progression. IFN-I-Aybey ranked among the GESs with the highest SC, just after SLE-driven IFN GESs like IFN-SLE-Bennett and IFN-Chaussabel (M3/4 and M5/12, except M1/2). It also demonstrated a high CS ($0.55 - 0.71$). In contrast, most IFN-II GESs, except for IFNg-Hallmark, showed low SC (< 0.2), indicating low or no association with SLE disease activity. However, IFNg-Hallmark exhibited a mixture of both IFN-I and IFN-II signaling, as shown previously, which was indicated here by its higher SC value. Overall, IFN-I-Aybey demonstrated strong coherence across clinical SLE samples and was associated with disease severity in SLE, while IFN-II did not show the same relevance, affirming the distinct roles for IFN-I and IFN-II in SLE disease progression.

Table 3.4: Relevance of IFN signatures in three SLE datasets.

Spearman correlation between mean signature scores and SLEDAI along coherence scores for each IFN signature are shown. The number of genes for each IFN signature is shown in brackets. IFN signatures are ordered by the ranking based on correlation coefficients in three SLE datasets.

IFN signature	Spearman correlation			Coherence score		
	GSE121239	GSE49454	GSE65391	GSE121239	GSE49454	GSE65391
IFN_SLE_Bennett (26)	0.34	0.20	0.48	0.51	0.44	0.45
IFN_Chaussabel_M3_4 (59)	0.34	0.14	0.50	0.52	0.50	0.54
IFN_Chaussabel_M5_12 (58)	0.32	0.21	0.47	0.35	0.36	0.36
IFN_I_Aybey (20)	0.32	0.19	0.46	0.71	0.58	0.55
IFN_Walsh (6)	0.32	0.16	0.45	0.93	0.94	0.91
IFN_Chaussabel_M1_2 (32)	0.32	0.11	0.45	0.79	0.62	0.64
IFNa_Hallmark (97)	0.31	0.11	0.46	0.35	0.31	0.31
IFN_Rice (4)	0.30	0.17	0.43	0.92	0.80	0.62
IFN_Bilgic (3)	0.31	0.16	0.42	0.76	0.39	0.13
IFN_Feng (5)	0.30	0.11	0.44	0.92	0.78	0.72
IFN_MB_Staub (10)	0.31	0.08	0.42	0.78	0.64	0.63
IFNg_Hallmark (200)	0.25	0.05	0.43	0.13	0.14	0.15
IFNg_Dummer (5)	0.09	-0.12	0.21	0.29	0.06	0.11
IFNg_Waddell (10)	-0.02	0.11	0.12	0.12	0.07	0.09
IFNg_Azizi_Platanias (11)	-0.01	-0.14	0.15	0.07	0.04	0.07
IFN_II_Aybey (6)	-0.12	-0.09	0.15	0.16	0.13	0.14
IFNg_Ayers (6)	0.06	-0.19	0.09	0.22	0.17	0.15
IFNg_Ayers_extended (10)	0.01	-0.21	0.06	0.25	0.13	0.12
IFNg_Sharma (25)	-0.11	-0.27	0.03	0.17	0.18	0.18

3.3.8 IFN-I and IFN-II signals were separable in bulk tissue cancer datasets using my IFN GESs

To assess the separation of IFN-I and IFN-II signals in the cancer context, I examined TCGA cohorts from 32 different cancer indications. I calculated the Pearson correlation between sample mean signature scores of IFN-I-Aybey or IFN-II-Aybey and published IFN-I or IFN-II GESs in each cancer indication. I then transformed the correlation coefficients using Fischer's z-transform to represent the correlation distributions as normal distributions for further statistical analysis (Figure 3.8).

First, I compared the similarity between my IFN GESs and published IFN GESs (Figure 3.8A). The comparison between published IFN-I GESs and IFN-I-Aybey showed a significantly higher mean correlation Z score compared to the pairwise comparisons among published IFN-I GESs (difference between the means d_{mean}= 0.19, two-sided Student's t-test, $p < 0.001$). Similarly, IFN-II-Aybey showed a significantly higher mean correlation Z score compared to pairwise comparisons among published IFN-II GESs (d_{mean}= 0.07, two-sided Student's t-test, $p < 0.01$). These results suggest that my IFN GESs are strongly correlated with published GESs.

Next, I evaluated how well IFN-II-Aybey could be separated from published IFN-II GESs, and vice versa for IFN-I-Aybey (Figure 3.8A). I first compared the correlation between published IFN-I GESs and IFN-II-Aybey. The mean correlation Z score for

published IFN-I GESs and IFN-II-Aybey was significantly lower than the pairwise correlations from published IFN-I GESs (d_{mean}= 0.59, two-sided Student's t-test, p < 0.001). This shows that IFN-II-Aybey does not strongly correlate with IFN-I signatures. I then compared the published IFN-II GESs with IFN-I-Aybey. Similarly, the correlation was significantly lower than the pairwise correlations among the published IFN-II GESs (d_{mean}= 0.52, two-sided Student's t-test, p < 0.001). This further supports the idea that IFN-I-Aybey is distinct from published IFN-II GESs. These results show that my IFN GESs exhibit minimal overlap or cross-correlation with the opposing IFN type. Across various cancer samples and indications, my IFN GESs successfully identified distinct signals of IFN-I and IFN-II.

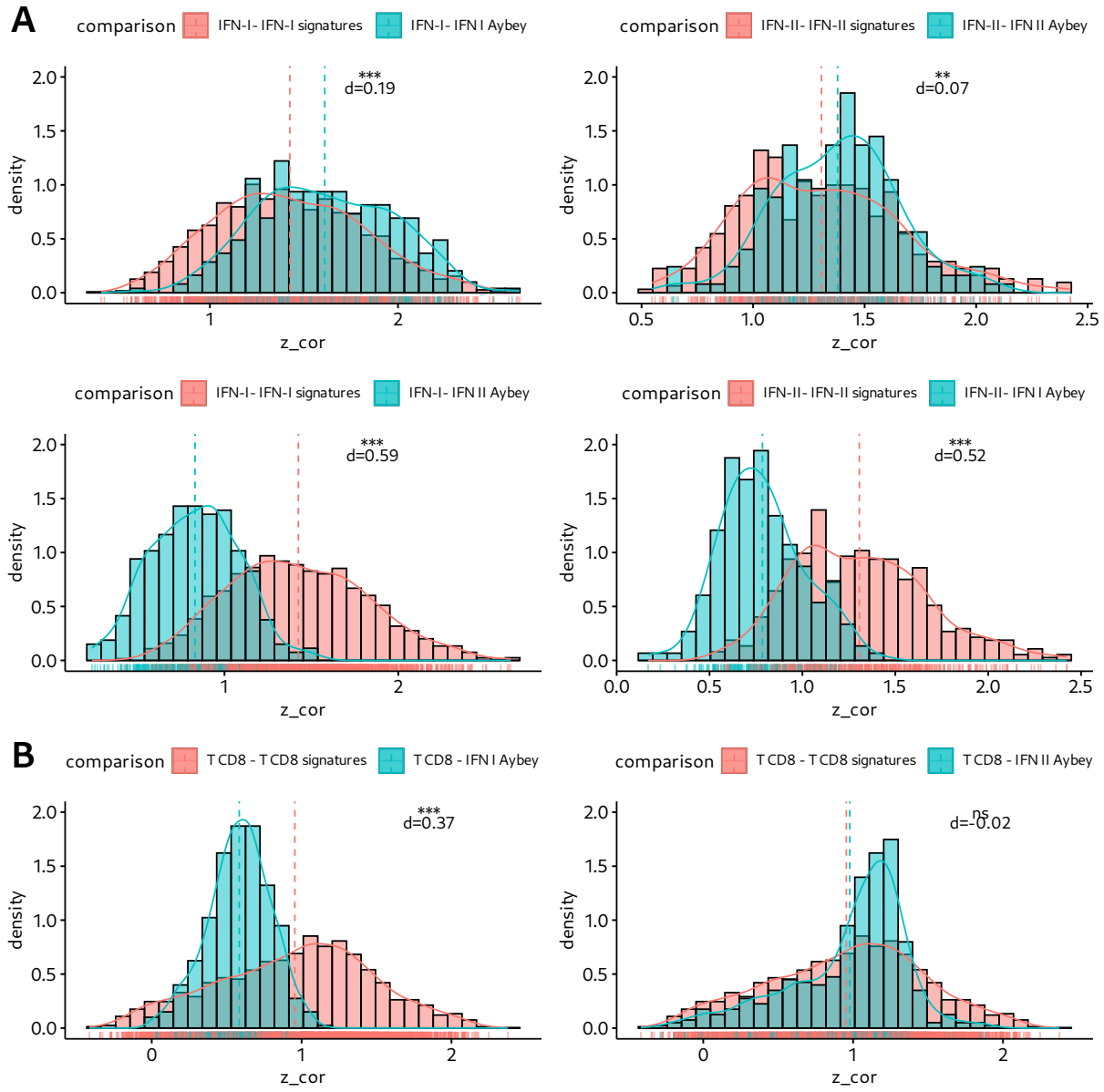

Figure 3.8: Correlation histograms between IFN-I- or IFN-II-Aybey signatures and published IFN signatures (A) or CD8$^+$ T cells (B) in all TCGA cohorts (n = 32).

Mean signature scores for each signature are calculated in each TCGA cohort separately. Within each cohort, Pearson correlation coefficients are calculated between my IFN signatures and all other published signatures for IFN-I, IFN-II, or CD8$^+$ T cells. Correlation values are z-transformed (Fisher transformation) and shown on x-axis while y-axis represents the density of the distributions. Each color shows different comparisons e.g., IFN-I against IFN-I or IFN-I against IFN-I-Aybey. Two-sided Student's t-test is used to compare the similarity between the distribution of the histograms, i.e., the means of the distributions. (ns = non-significant ($p > 0.05$); ** = $p < 0.01$ and *** = $p < 0.001$). The differences between the means of the histograms are denoted as d.

3.3.9 IFN-II-Aybey was correlated with CD8$^+$ T cell infiltration in TCGA cancer samples

CD8$^+$ T cells are the main producers of IFN-g, and their infiltration has been linked to high IFN-II signaling (Burke and Young, 2019; Kambayashi et al., 2003; Yan et al., 2021). Since I cannot directly measure IFN-g levels using my IFN-II GES, I tested the association by evaluating the downstream effects of IFN-g signaling in the TME across 32 TCGA cohorts. I compared the mean Z score Pearson correlation between published CD8$^+$ T cell GESs and my IFN GESs, similar to the previous analysis (Figure 3.8B). The correlation between published CD8$^+$ T cell GESs and IFN-I-Aybey was lower than that of pairwise correlations among CD8$^+$ T cell GESs (d_{mean}= 0.37, two-sided Student's t-test, $p < 0.001$). In contrast, the correlation between published CD8$^+$ T cell GESs and IFN-II-Aybey showed no significant difference (d_{mean}= 0.02, two-sided Student's t-test, $p > 0.05$). These findings confirmed the strong correlation between IFN-II response and CD8$^+$ T cell infiltration, but a weaker association with IFN-I response.

To better understand the relationship between IFN-II response and CD8$^+$ T cell infiltration, I expanded my analysis to include a wider range of GESs related to immune and cellular functions. Specifically, I aimed to assess how the activity of CD8$^+$ T cell GESs aligned with my IFN GESs, compared to other immuno-oncology signatures. I used a methodology similar to that of Kreis et al. (2021), which analyzed the coherence and associations of multiple GESs in a cancer-specific context, particularly in the TCGA-BRCA cohort. To achieve this, I calculated the covariance between published GESs and IFN-I-Aybey or IFN-II-Aybey, ranking the signals based on covariance. I displayed the results in two separate heatmaps, with the top 20 signatures shown in Figure 3.9 (all signatures are shown in Appendix Figure A.2). This approach provides a comprehensive view of how different immune and cellular processes interact in a given dataset.

Most IFN-I GESs showed the highest covariance with IFN-I-Aybey, with the top three being IFN-Walsh, IFN-Staub, and IFN-Rice (covariance ranging from 0.6 to 0.7) (Figure 3.9). This indicates that my IFN-I GESs are highly consistent with existing published IFN-I GESs. Interestingly, some IFN-II GESs, including IFN-g-Dummer, IFN-g-Ayers, and IFNg-Azizi-Platanias, showed high similarity to IFN-I-Aybey (covariance > 0.3). In contrast, IFN-II-Aybey had the lowest covariance to IFN-I-Aybey among all IFN-II GESs (Appendix Figure A.2), reaffirming its ability to differentiate IFN signals more effectively than most published IFN-II GESs.

When I compared IFN-II-Aybey with other signatures, the GESs with the highest covariances were published IFN-II GESs and CD8$^+$ T cell GESs (Figure 3.9). Notably, none of the IFN-I GESs appeared among the top-ranked signatures, showing the high specificity

of IFN-II-Aybey. Interestingly, IFNg-Hallmark showed the least covariance with IFN-II-Aybey compared to other IFN-II GESs, suggesting its dissimilarity to IFN-II-Aybey and other IFN-II GESs (Appendix Figure A.2). These results further asserted the strong association between IFN-II-Aybey and $CD8^+$ T cell GESs and highlighted the superior capability to distinguish IFN-I and IFN-II gene expression responses, demonstrating even greater separation than other published IFN GESs in the TCGA BRCA cohort.

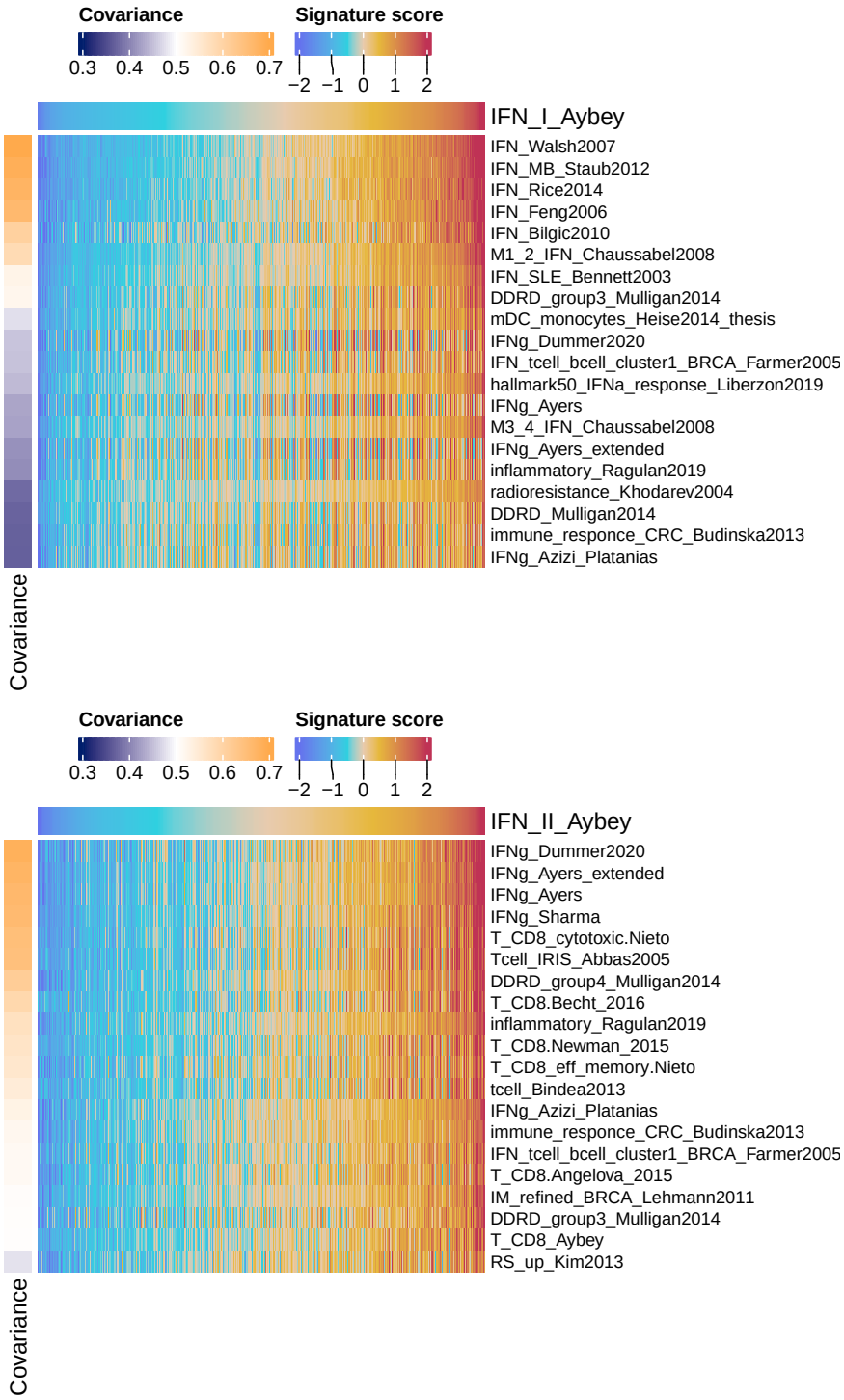

Figure 3.9: RosettaSX analysis: top 20 related signatures to my IFN signatures in TCGA BRCA cohort.

The signatures are compiled from Kreis et al. (2021) and additional published $CD8^+$ T cell and IFN-II GESs. Mean signature scores are calculated only for coherent signatures (coherence score > 0.2). Covariance between each of my IFN signatures and coherent signatures are calculated. Only top 20 signatures with the highest covariances to IFN-I-Aybey or IFN-II-Aybey are depicted. Mean signature scores are shown from low (blue) to high (red). Covariance values are shown from low (dark blue) to high (orange).

3.3.10 IFN-II-Aybey was associated with response to ICI therapy

Finally, I applied my IFN GESs to better understand the effect of cancer immunotherapy, specifically ICI therapy. I aimed to validate the positive association between IFN-II signaling and ICI response, as reported in several studies based on baseline samples (Ayers et al., 2017; Grasso et al., 2020; Karachaliou et al., 2018; Mo et al., 2018). To this end, I calculated mean signature scores for my IFN GESs across three ICI treatment bulk tissue RNA-seq datasets from three different cancer types: bladder cancer (Mariathasan et al., 2018), melanoma (Van Allen et al., 2015), and gastric cancer (Kim et al., 2018) (Figure 3.10). In all datasets, IFN-II-Aybey scores were significantly higher in responders (two-sided Student's t-test, $p < 0.01$), while IFN-I-Aybey scores showed no significant difference (two-sided Student's t-test, $p > 0.05$). These results suggest that IFN-II, rather than IFN-I, is a predictive biomarker for ICI response.

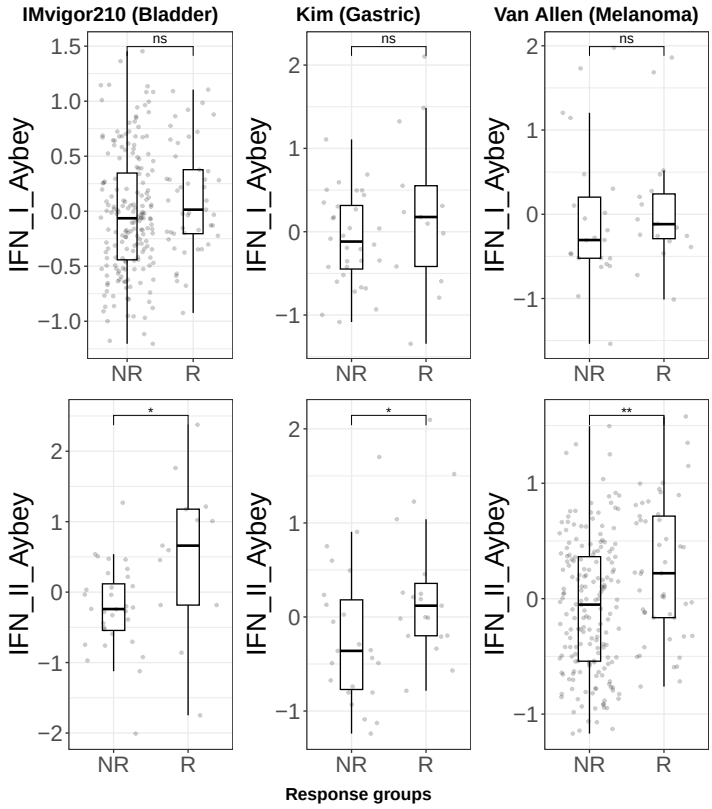

Figure 3.10: Boxplots showing mean signature scores of IFN-I- and IFN-II-Aybey signatures between responders and non-responders of ICB therapy in three different cancer cohorts. Three bulk tissue RNA-seq datasets of three different cancer types are used: gastric cancer (Kim et al., 2018), melanoma (Van Allen et al., 2015) and bladder cancer- IMvgor210 (Mariathasan et al., 2018). Mean signature scores for each signature (y-axis) are calculated in each cohort separately. Responders (R) and non-responders (NR) are shown on the x-axis. Two-sided Student's t-test is used to compare differences in the mean signature scores between R and NR. (ns = non-significant ($p > 0.05$); * = $p < 0.05$ and ** = $p < 0.01$).

3.4 Discussion

To disentangle the transcriptional effects of responses to different IFN types, IFN-I and IFN-II, I developed IFN type-specific response GESs. Until now, no GES repertoire has been published that clearly separates IFN-I and IFN-II responses, derived and validated from multiple expression datasets. For instance, as shown in my analyses, a prominent IFN-II GES, IFNg-Hallmark, has mixed characteristics, representing both IFN-I and IFN-II signaling (Figure 3.4, Figure 3.6, Appendix Figure A.2, and Table 3.4). Further, no study has comprehensively compared different published IFN GESs across multiple datasets from varying experimental conditions, which is essential to assess their translatability and relevance. To address these gaps, I utilized a meta-analysis-based workflow, leveraging five diverse healthy bulk tissue RNA-seq datasets and applied an extensive discovery, validation, and application process involving multiple datasets from different sequencing platforms, cellular environments, experimental conditions, and healthy-disease datasets. These steps ensured broad application, versatility, validation, and statistical power of my IFN GESs.

A network meta-analysis approach was particularly useful for discovery, given the variability in IFN stimulations, cellular contexts, experimental setups, and normalization methods across datasets. This approach has been successfully applied in GES discovery and candidate gene detection, yielding highly comparable results to analyses of merged independent gene expression data (Winter et al., 2019). This method allowed pairwise comparisons between treatments, by utilizing the information from all datasets available. The power of NMA lies in its ability to synthesize indirect evidence, providing a comprehensive view that might otherwise be ignored in studies with limited direct comparisons. Using the available datasets, I successfully obtained IFN-I and IFN-II GESs; however, disentangling IFN-a and IFN-b signals was not always possible, as it largely depended on the cellular context. This finding also reaffirmed the proximity of IFN-a and IFN-b signals (Chow and Gale, 2015; Thomas et al., 2011; de Weerd et al., 2013).

Throughout all steps of my study, my IFN GESs demonstrated strong coherence and high separation of IFN-I/II signals across various conditions, including healthy, SLE, and cancer, as well as in heterogeneous cell populations and at the single-cell level. Notably, IFN-II-Aybey exhibited the highest coherence score among other IFN-II GESs and separated itself from IFN-I GESs, including IFN-I-Aybey. This differentiation was crucial, as it helped to identify distinct patterns of immune response associated with IFN-II signaling, which were not confounded by IFN-I signals. These results provided strong evidence that my IFN GESs were capturing biologically meaningful and context-specific information.

My analysis further reaffirmed the distinct roles of IFN-I and IFN-II in SLE and can-

cer. Specifically, IFN-II-Aybey was strongly associated with $CD8^+$ T cell infiltration and response to ICI therapy, aligning with findings from previous studies (Ayers et al., 2017). In contrast, IFN-I-Aybey, but not IFN-II-Aybey, was linked to disease severity in SLE, as reported earlier (Bengtsson et al., 2000; Chasset et al., 2022; Gómez-Bañuelos et al., 2024). Notably, the roles of IFN-I signaling in ICI response and IFN-II signaling in SLE disease severity have not been explicitly compared in previous studies. These translational findings suggest the unique and context-dependent roles of IFN-I and IFN-II signaling, emphasizing the utility of my IFN GESs and evaluation framework in better understanding separate impacts of IFNs on immune responses and disease progression.

The evaluation of IFN GESs in terms of cell-type-specific IFN responses based on single-cell data has not been extensively explored. My analysis using a published scRNA-seq PBMC dataset from a large group of healthy donors (Hartoularos et al., 2023) showed that IFN-II-Aybey captured the IFN-II-specific response in a broader range of cell types, including HSC, B cells, and naïve T cells, in addition to myeloid cells (Figure 3.6). This was in contrast to most other IFN-II GESs, which were predominantly restricted to myeloid cells. Furthermore, some IFN-II GESs, such as IFNg Sharma, exhibited specificity for particular cell types, while others, like IFNg-Ayers, IFNg-Azizi-Platanias, and IFNg-Hallmark, were also upregulated upon other treatments, showing treatment-unspecific 'mixed signals'. The low signal-to-noise ratio, particularly in IFNg-Hallmark, was a striking result, given its widespread use in the literature. This shows the importance of cellular resolution and performing external validation for any GES, especially IFN GESs, to ensure their validity and translatability for specific use cases.

In summary, I derived robust, broadly applicable, and disease-relevant IFN-I and IFN-II response-specific GESs, addressing the limitations of existing signatures. My signatures enhance the understanding of IFN responses across diverse experimental settings, cell types, and disease contexts. My IFN GESs were particularly useful for dissecting cell type-specific responses in single-cell studies and comparing the differential effects of IFN-I and IFN-II signaling in disease progression and therapy in SLE and cancer. This study provides new tools to investigate the downstream effects of IFN-I and IFN-II signaling, even in complex tisssues, in the form of IFN-I and IFN-II GESs.

4 Chapter 3: Resolving temporal interferon signaling across immune cells

"We are all time travelers journeying together into the future."
Stephen Hawkings, "Brief Answers to the Big Questions"

In the final chapter, I describe my investigation of temporal IFN type-specific responses in diverse immune cell populations using the tools which I described in previous chapters. For this, I analyze a novel dataset generated for this study: temporal CITE-seq dataset of PBMCs stimulated with IFN-a or IFN-g. I examine the strength and dynamics of responses in various immune cell types to IFN-I and IFN-II. Finally, I identify genes specifically activated by distinct IFN types in individual cell types, particularly in monocytes, which display unique temporal activation patterns.

(I adapted this chapter based on my unpublished manuscript (Aybey et al., 2025b), in which I was the lead author and for which I have conducted all analyses. I will submit the manuscript to a peer-reviewed journal as soon as I submit my thesis for assessment.)

4.1 Introduction

4.1.1 Limitations of previous studies characterizing immune cell type-specific IFN response dynamics

Understanding immune cell type-specific IFN response dynamics is critical for characterizing the complexities of immunological processes. Existing datasets often lack resolution at the cellular, temporal, or cross-IFN type comparison levels. Many previous studies, that investigate the gene expression response to IFNs, rely on bulk tissue populations or purified immune cells (Devlin et al., 2020; Reyes et al., 2019; Waddell et al., 2010). These fail to capture the heterogeneity within immune populations. For instance, Waddell et al. (2010) identified temporal expression profiles for cell type-specific and general IFN-I and IFN-II response genes in a temporal microarray study on purified immune cells. They also emphasized the importance of intercellular interactions in interpreting and better characterizing cell type-specific IFN signaling. However, no comparable temporal bulk tissue RNA-seq or microarray dataset has since been generated.

Previously published scRNA-seq datasets of PBMCs stimulated with IFNs also have limitations. Some focus on the response to a single IFN type across multiple time points (de Cevins et al., 2023; Kartha et al., 2022), but lack cross-comparisons between IFN

types. Others examine only a single time point upon stimulation with a single IFN type (Karagiannis et al., 2020), ignoring both temporal dynamics and cross-treatment comparisons. Multi-IFN perturbation datasets (Hartoularos et al., 2023; Goel et al., 2021) capture cross-treatment responses but fail to explore temporal changes. Until now, no dataset has sufficiently addressed these three resolution levels, that are essential for enabling comprehensive understanding of the dynamic cell- and IFN-type specific responses.

To address these gaps, I designed and analyzed a new CITE-seq dataset using PBMCs stimulated with IFN-a or IFN-g, with samples taken after four time points. This approach would also allow me to explore the relationships between different immunological pathways and IFN signaling, dissecting cell- and IFN-type specific temporal expression patterns.

4.2 Methods

4.2.1 Experimental design and data generation for IFN-stimulated PBMC samples

I designed the experimental setup to investigate immune cell-type-specific temporal responses to IFN stimulation. PBMCs were isolated from three healthy female donors and stimulated with IFN-a and IFN-g, or left untreated. Samples were collected at four time points: 0 hours, 1 hour, 3 hours, and 9 hours post-stimulation. Single Cell Discoveries (Utrecht, Netherlands) generated and sequenced the data. The sample for IFN-a (9 h) from donor 10881 could not be sequenced due to sample being shipped without dimethyl sulfoxide.

The sequencing workflow followed standard 10x Genomics and BioLegend protocols, using the TotalSeq-B TBNK panel to profile nine immune cell surface markers: CD19, CD4, CD14, CD8, CD56, CD16, CD11c, CD45, and CD3. The resulting CITE-seq data was processed into raw count matrices and provided for preprocessing and downstream analysis.

4.2.2 Single-cell data analysis

To preprocess the data, I filtered out genes detected in fewer than three cells and removed cells with fewer than 200 detected genes. Additionally, I excluded cells with more than 5,000 unique gene counts or a mitochondrial gene fraction exceeding 15%. For gene expression normalization, I used LogNormalize method from Seurat (v.4.3.0) (Stuart et al., 2019). For surface protein expression, I used centered log-ratio (CLR) normalization in

Seurat. This method transforms raw protein counts by calculating the geometric mean across all proteins for each cell and then taking the log-ratio of each protein's count relative to this geometric mean. After preprocessing, I obtained two data matrices: (1) a gene expression matrix with genes (n = 28,865) as rows and cells (n = 212,761) as columns, containing log-normalized transcript counts, and (2) a protein expression matrix with surface protein markers (n = 9) as rows and cells (n = 212,761) as columns, containing CLR-normalized protein expression values.

For the classification of immune cell types, I utilized my random forest classification approach as described in Chapter 1. I used medium-grained cell type annotations from the PBMC reference dataset, specifically the Hao dataset (Hao et al., 2021). For further downstream analysis, I excluded immune cell type genes (n = 167) and was left with 28,698 genes.

4.2.3 Gene expression change score

To quantify absolute gene expression changes in response to different IFN stimulations across immune cell types, I adapted the "change score" method from Bouman et al. (2024). This score measures how gene expression fluctuates over time within a specific cell type and stimulation condition, such as monocytes stimulated with IFN-g (monocytes-IFNg). For each gene, I calculated the absolutes sum of the derivative of the average expression at each time point. This captures the magnitude of expression change between consecutive time points:

$$\text{Absolute sum of derivaties}_t = |\text{Z}_t - \text{Z}_{t-1}| \tag{7}$$

Where Z_t is the Z-scaled average gene expression value at time point t and Z_{t-1} is the Z-scaled average gene expression value at the previous time point $(t-1)$.

Next, I computed the overall change score for each gene by summing the absolute derivatives across time intervals for a given stimulation and cell type:

$$\text{Change score}_{\text{gene}} = \sum_{t=2}^{n} |\text{Z}_t - \text{Z}_{t-1}| \tag{8}$$

Where t represents the time point index (from 2 to n), and n is the total number of time points.

4.3 Results

4.3.1 Novel temporal IFN stimulated PBMC CITE-seq dataset

To characterize immune cell- and IFN-type specific expression profiles, a CITE-seq dataset was generated from PBMCs isolated from three different healthy female donors with similar demographics (Table 4.1). Cells were stimulated with IFN-a or IFN-g, or left untreated, with samples collected at four time points (0 h, 1 h, 3 h, and 9 h) to capture temporal changes in transcriptional programs. Untreated control samples were included in each time point to account for baseline effects. This experimental design ensures a robust, temporal comparison of the response to IFN-a and IFN-g across immune cell populations.

Table 4.1: Donor demographics.

Donor	Age at collection	Gender	Race	Ethnicity	Tobacco history	Alcohol history	Body mass index (calculated)
M-10881	29	Female	White	Non-Hispanic	Previous Use	Current Use	25.4
M-10882	30	Female	White	Non-Hispanic	Never Used	Current Use	27.3
M-10883	30	Female	White	Non-Hispanic	Never Used	Current Use - Infrequent	24.4

To prepare the data for further analysis, I assessed various quality control metrics related to sample differences, as well as mRNA-protein translatability (Figure 4.1). Cells were evenly distributed across samples, with a median of 7,161 cells per sample, totaling 212,761 cells. Interestingly, unstimulated control samples contained higher numbers of cells, suggesting a possible impact of IFN stimulation on cell viability (Figure 4.1A). There were no significant differences (two-sided Student's t-test, $p > 0.05$) in cell surface protein expression between samples, indicating that the cell surface protein markers were consistently expressed across the experimental conditions (Figure 4.1B). Further, almost all cell surface markers showed strong correlation (Pearson correlation PC $>$ 0.3) to mRNA expression, indicating overall agreement between mRNA and protein expression (Figure 4.1C). These initial assessments demonstrated the overall homogeneity of cell distribution and consistent protein expression across samples, as well as a

strong mRNA-protein translatability, confirming the data's suitability for further analysis.

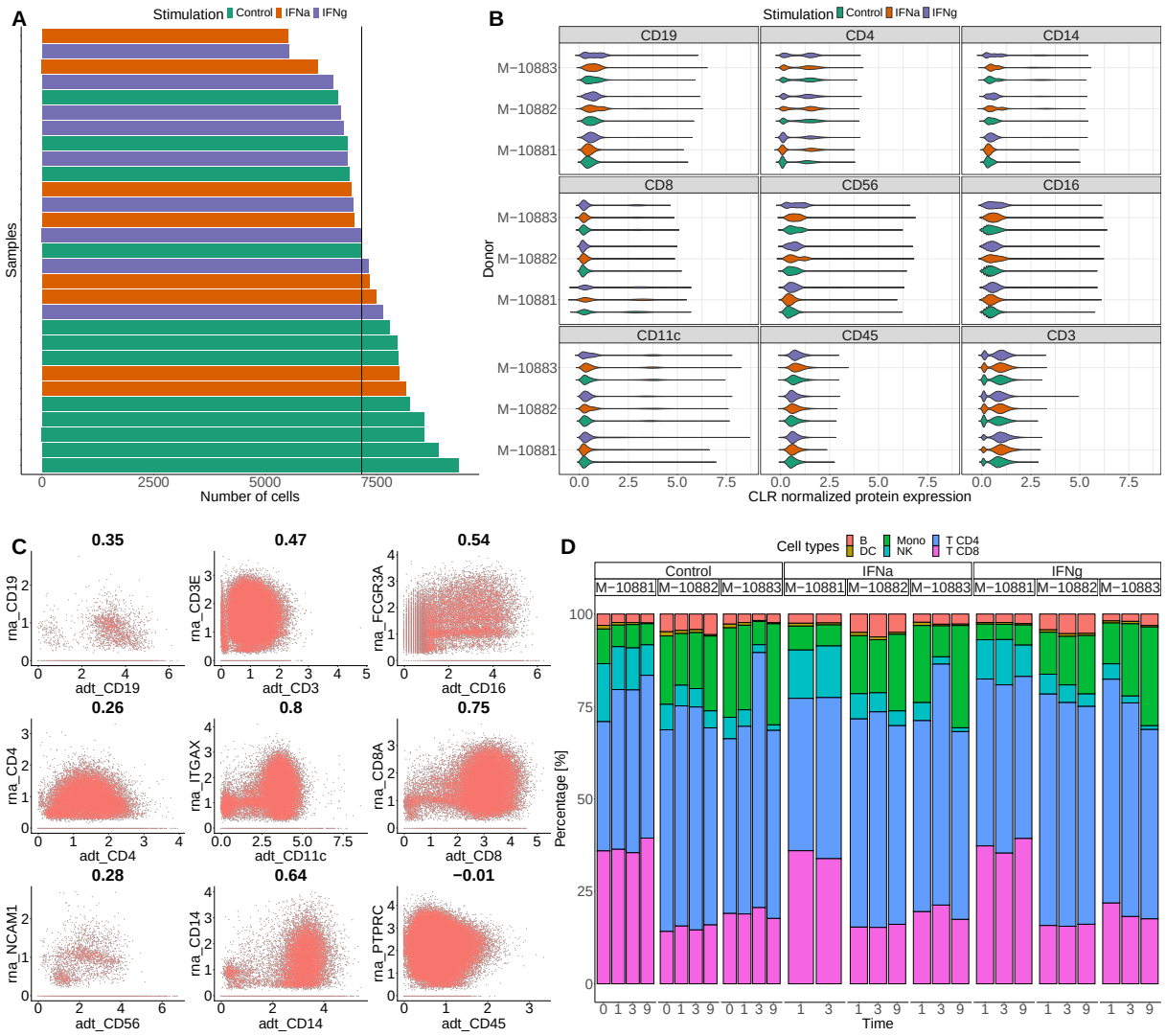

Figure 4.1: Quality control of novel IFN CITE-seq dataset.

(A) Distribution of number of cells per sample. The bar plot shows the number of cells for each sample, with different colors indicating the type of stimulation (IFN-a, IFN-g, or untreated) and time point (0 h, 1 h, 3 h, 9 h) after stimulation. The y-axis represents the number of cells, and the median of the distribution is 7,161 cells, marked by a line. The cells are evenly distributed across samples. **(B)** Distribution of protein expression between donors under different conditions. Centered log ratio (CLR) normalized protein expression values are plotted for each donor under different conditions as violin plots. Note the homogeneous distribution of protein expression across samples. **(C)** Correlation of gene and protein expression of cell surface markers. Normalized expression values of protein and mRNA expression are used for the x and y axes, respectively. Pearson correlation coefficients for each gene and protein expression comparison are reported for all samples. Most protein markers are strongly correlated. **(D)** Distribution of cell types in each sample. Cell type percentages are shown for each sample. Different cell types are depicted in different colors and each condition is shown separately. Overall, there are similar distributions among the different samples.

4.3.2 Random forest classifier effectively assigned immune cell types

In the first chapter, I described the development of a RF cell type classifier specifically designed for unbiased downstream analyses for such complex single-cell datasets. Here, I applied this classifier to assign immune cell type labels (see Methods). To assess whether my selected immune cell type genes could separate cells by cell type, I performed UMAP analysis based on my immune cell type genes (n = 167). The UMAP plots showed that cells clustered primarily by cell type rather than by experimental variables such as time points, stimulations, or donors (Figure 4.2A). This confirmed that my small set of immune cell type genes used for classification effectively captured cell type-specific patterns and was sufficient to distinguish cell types.

To further validate the cell type assignments from the RF classifier, I compared the clustering results with immune cell surface marker protein expression. The cell type clusters in the UMAP plot (Figure 4.2A) aligned visually with their expected surface marker expression patterns, which I confirmed by boxplots displaying protein expression levels across different immune cell type populations (Figure 4.2B). Moreover, the overall immune cell type composition remained consistent across samples (Figure 4.1D), indicating the consistency of the classifier across different experimental conditions. These findings validated the cell type assignments from the RF and demonstrated the robustness of my classifier in accurately identifying immune cell types, even in the presence of biological and experimental variability.

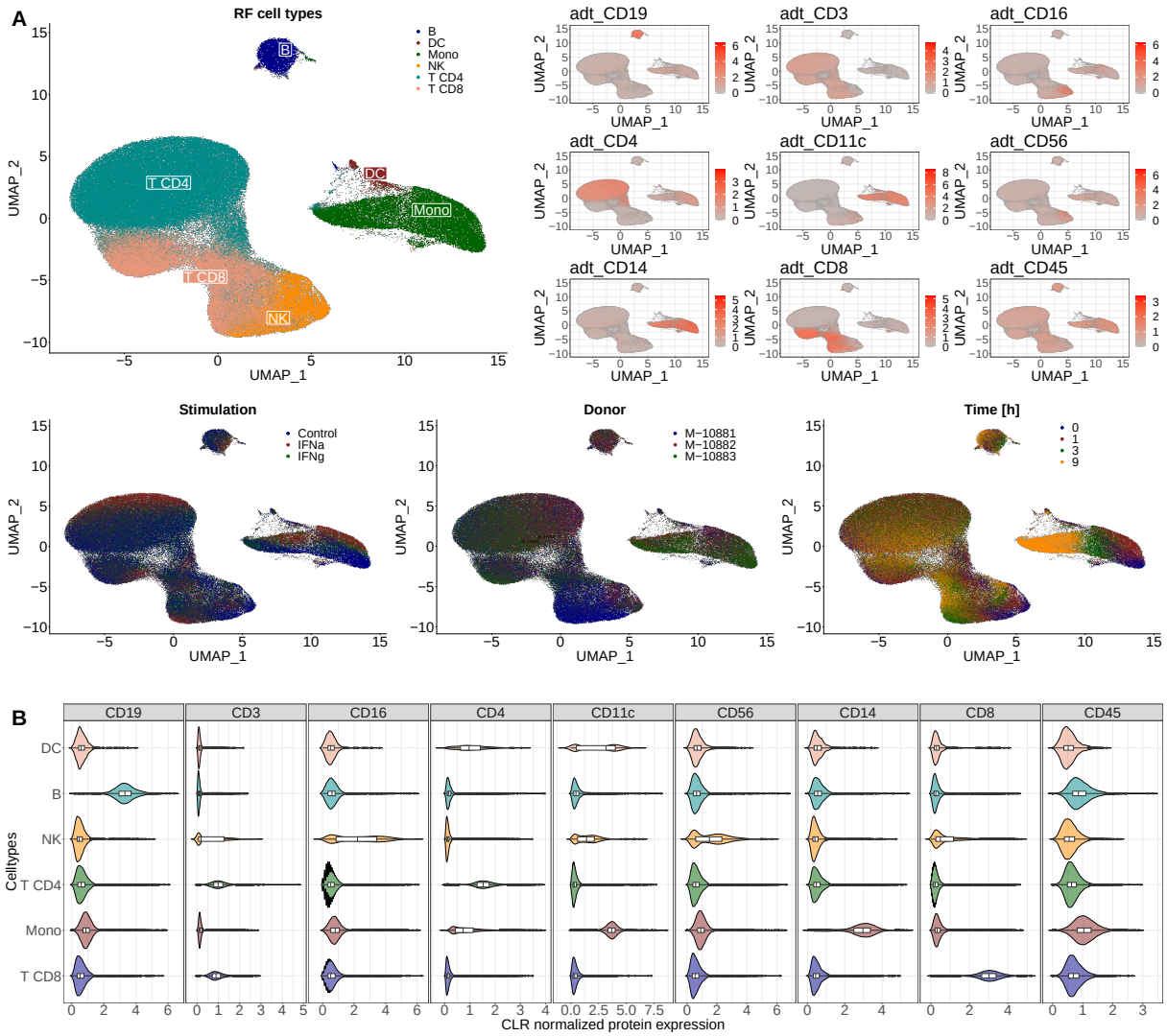

Figure 4.2: Cell type classification using random forest classifier based on robust immune cell type genes and its alignment with surface marker expression.

(A) UMAP plots based on my immune cell type genes showing different experimental variables along cell surface marker protein expression. Each point represents a single cell, and each cell is colored either by my cell type annotation or other experimental variables such as stimulation, donor, and time point. Centered log ratio (CLR) normalized protein expression values (right) are shown from gray to red indicating low to high expression. Regions with high expression match with my cell type classification results. **(B)** Alignment of cell surface markers with cell type annotations. CLR normalized protein expression values are plotted for each cell type. Boxplots and violin plots depict the consistent correlation between cell surface marker protein expression levels and their respective cell type annotations.

4.3.3 IFN-I response was activated transiently across all immune cell types, with strongest activation in myeloid cells

I assessed the strength of the IFN-I response across immune cell types using the mean signature scores of IFN-I GESs. The scores were significantly higher at all time points and across all cell types for nearly all IFN-I GESs (two-sided Student's t-test, Bonferroni-adjusted p-values < 0.05) (Figure 4.3). Monocytes, followed by DCs and B cells, exhibited the highest overall IFN-I signature scores. These results demonstrated differences in IFN-I response strength among immune cells, with myeloid cells showing the strongest responses.

Among the GESs, IFN-I-Aybey showed one of the highest differences in signature scores between IFN-I and other treatments. This indicated its strong specificity for IFN-I over IFN-II signal. In contrast, some GESs such as IFN-SLE-Bennet, IFNa-Hallmark, and IFN-Chaussabel showed relatively smaller differences between IFN-I and other treatments compared to other GESs particularly at 9 h. These suggested that the ability of each IFN-I GESs to distinguish IFN-I from IFN-II varied.

The IFN-I response displayed transient activation, as captured by most IFN-I GESs, particularly IFN-I-Aybey. The response increased at 1 h, plateaued at 3 h, and returned to levels similar to those at 1 h by 9 h (Figure 4.3). This pattern was consistent across all immune cell type populations. However, some GESs such as IFN-Bilgic and IFN-Rice did not show this temporal effect, showing variability in how different signatures capture IFN-I dynamics. These demonstrated the transient nature of the IFN-I response across all immune cell types.

I further supported these results by DGE analysis. I compared the number of significant DEGs (FC > 1.5, Wilcoxon rank sum test Bonferroni-adjusted p-values < 0.05) after IFN-I stimulation compared to controls (Figure 4.4). The highest number of significant DEGs occurred at 3 h, while the number of significant DEGs at 1 h and 9 h was similar or lower across all cell types. Monocytes, followed by DCs and B cells, showed the strongest IFN-I response as measured by the number of DEGs. The results from DEG analysis were congruent with the IFN-I-Aybey signature analysis in both the current and previous chapters.

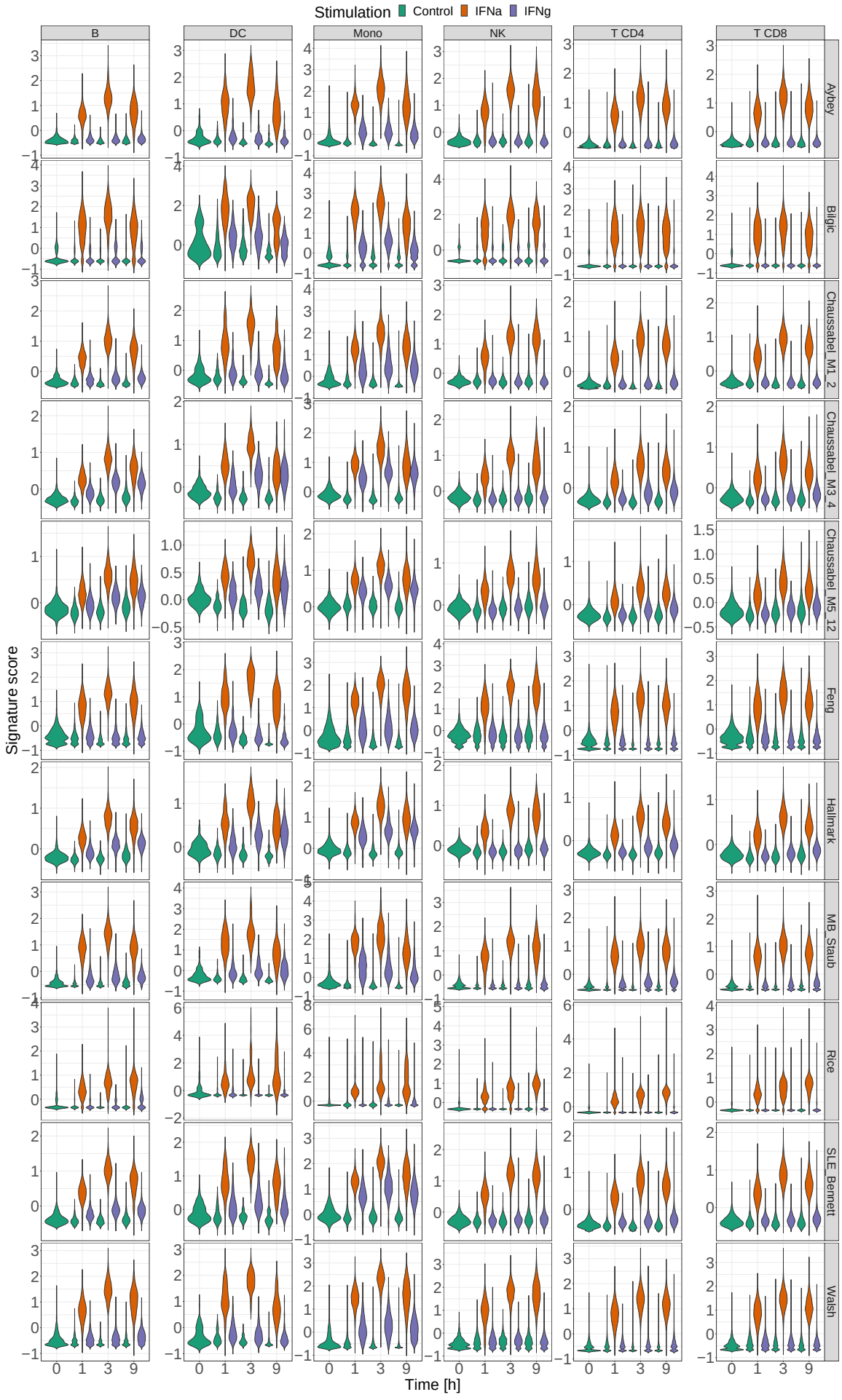
Stimulation Control IFNa IFNg
B
DC
Mono
NK
T CD4
T CD8
Aybey
Blgic
Chaussabel_M1_2
Chaussabel_M3_4
Chaussabel_M5_12
Feng
Hallmark
MB_Staub
Rice
SLE_Bennett
Walsh
Signature score
Time [h]
0 1 3 9

Figure 4.3: Analysis of temporal IFN-I response across immune cells.

The mean signature scores for published IFN-I signatures along with my IFN-I signature, depicted on the y-axis, are computed for individual cells, and illustrated using violin plots. The stimulations are distinguished by different colors, and the x-axis displays different time points. Each row corresponds to a single IFN-I signature. All immune cells respond transiently to IFN-I. Myeloid cells show the strongest response.

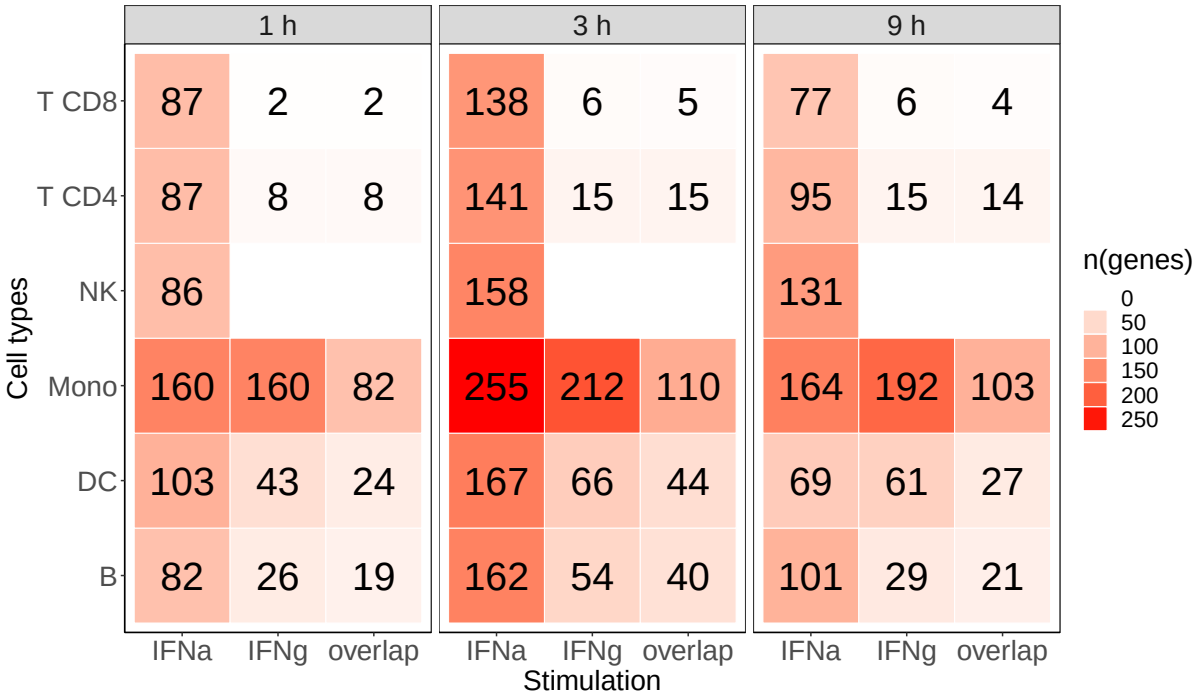

Figure 4.4: Cell type specific IFN responses.

Differential gene expression analysis based on Wilcoxon rank sum test is applied between treatment and control samples for each stimulation, cell type and time point separately. Number of significantly upregulated genes (fold-change FC > 1.5, Wilcoxon rank sum test Bonferroni-adjusted p-values < 0.05) for different conditions are shown for each stimulation along with the overlap between stimulations. The scale color ranges from low (white) to high (red) number of genes. Monocytes, DCs, and B cells respond the highest to the IFN-g stimulation while all cell types respond to IFN-a stimulation.

4.3.4 IFN-II-Aybey provided better representation of cell-type specific IFN-II responses, highlighting distinct myeloid and B cells dynamics

In Chapter 2, I showed that IFN-II-Aybey was the only IFN-II GES capable of detecting IFN-II responses across diverse immune cell types, including B cells, whereas other IFN-II GESs detected responses only in myeloid cells (Figure 3.6). Here, I investigated cell type-specific IFN-II response dynamics and confirmed these findings using a similar approach to the IFN-I GES analysis in the previous section.

In this dataset, IFN-II-Aybey showed significant and high score changes in IFN-g treated myeloid and B cells at all time points compared to other treatments (two-sided Student's t-test, Bonferroni-adjusted p-values < 0.05)(Figure 4.5). Some other IFN-II GESs, including IFNg-Ayers and IFNg-Waddell, showed elevated scores only in IFN-g stimulated myeloid cells. In contrast, other GESs, such as IFNg-Hallmark, IFNg-Azizi-Platanias, and IFNg-Sharma, displayed higher IFN-II scores in other conditions. These results showed superior representation of IFN-II responses and higher specificity of my IFN-II GES compared to other IFN-II GESs.

Using IFN-II-Aybey, I identified distinct temporal response patterns for B cells and myeloid cells. Monocytes and DCs responded to IFN-II stimulation with a gradually increasing GES signal, while B cells showed a transient activation. The strongest response was observed in myeloid cells, followed by B cells. I further confirmed this trend by DGE analysis (Figure 4.4). The number of significant DEGs (FC > 1.5, Wilcoxon rank sum test Bonferroni-adjusted p-values < 0.05) was the highest in monocytes, DCs, and B cells, while NK cells and T cells exhibited a small number of genes affected by IFNs (around 2-15 DEGs) (Figure 4.4). This means that the primary IFN-II responsive populations were myeloid cells and B cells, while gene expression in NK and T cells were minimally affected by IFN-II.

Overall, IFN-II-Aybey provided better representation of the IFN-II responses across a broader range of immune cell types and offered higher discrimination between IFN-I and IFN-II signals compared to other IFN-II GESs. Further, it enabled the identification of distinct temporal IFN-II response patterns for B and myeloid cells, which was not possible using published IFN-II GESs.

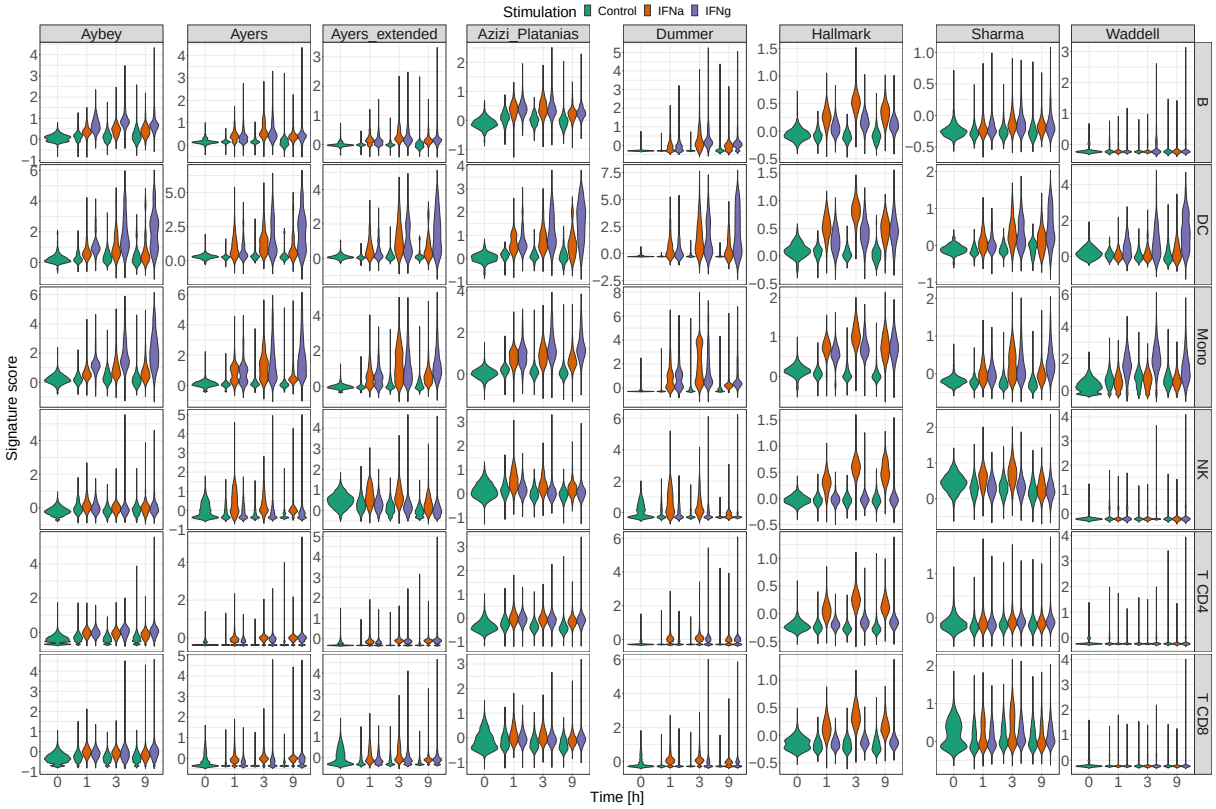

Figure 4.5: Analysis of IFN-II response.

Mean signature scores (y-axis) for published IFN-II signatures along with IFN-II-Aybey are calculated for each cell and represented as violin plots. Different stimulations are colored separately, and different time points are shown on the x-axis. Each cell type is demonstrated in each row separately. Each signature is represented in a single row. IFN-II-Aybey better represents cell type-specific IFN-II responses. It captures signals from both myeloid and B cell populations, which show distinct temporal response profiles.

4.3.5 Multi-faceted IFN response dynamics in monocytes: distinct IFN-I and IFN-II temporal gene modules

Cell-type-specific response kinetics to different IFNs are crucial for understanding the dynamics of immune activation and modulation. However, previous datasets have lacked the resolution necessary to explore for each gene its cell-specific, IFN-specific and temporal expression dynamics. To address this, I used this newly generated data to identify gene modules that represent cell-type-specific IFN responses and examined their temporal profiles, particularly in monocytes.

Initially, I started with genes that were significantly upregulated upon IFN-a or IFN-g stimulation compared to control samples (FC > 1.5, Wilcoxon rank sum test Bonferroni-adjusted p-values < 0.05). I performed the analysis separately for each time point and cell type, resulting in 581 genes (as shown in Figure 4.4). To ensure that the genes selected

were specifically responsive to stimulation and not merely defining basal differences between cell types, I applied a secondary filter. I excluded genes that showed upregulation (FC $>$ 1.25) in only one cell type compared to others under unstimulated conditions. This filtering reduced the feature space to 210 genes for further analysis and ensured to eliminate basal cell-type genes, leaving only those that were specifically responsive to IFN stimulation.

To identify genes exclusively activated by distinct IFN types in a specific immune cell type, I categorized genes based on the highest absolute change in their expression levels over time. To quantify these changes, I used a scoring metric called the 'change score,' as suggested by Bouman et al. (2024), but adapted it for multiple stimulations in my study (see Methods). This score reflects gene expression fluctuations within each cell type and stimulation category (e.g., monocytes-IFNg). I assigned each gene to the category with the highest change score, reflecting the stimulation and cell type that most strongly activated its expression. Specifically, I only kept genes for which the difference between the highest and second-highest change scores exceeded twice the average change score across all categories. This filtering resulted in 54 final genes (Table 4.2). Notably, I identified genes only for B cells, DCs, and monocytes. B-IFNa, B-IFNg, and DC-IFNa each had two genes, while DC-IFNg had three genes. Monocytes were the most exclusively responsive cell type population, with 12 genes for IFN-a and 33 for IFN-g stimulation. These suggest that monocytes exhibit the most unique and dynamic gene activation profile in response to IFN stimulations and highlight their distinct role in immune activation.

Finally, I examined those 45 monocyte genes to further investigate potential temporal patterns. I applied hierarchical clustering on the Euclidean distance matrix calculated using Z-scaled expression values across all monocyte populations. This resulted in five distinct clusters (Figure 4.6A). To assess whether these clusters reflected different temporal characteristics, I displayed the average Z-scaled expression values of each gene as spaghetti plots across time points and treatments within monocyte samples (Figure 4.6B). The clusters revealed distinct temporal patterns, which I annotated and summarized in Table 4.2. Group 1 (Mono-IFNa-transient) was characterized by genes, including CXCL11 and APOBEC3B, that exhibited transient activation in response to IFN-a. These genes play key roles in the immune cell recruitment and activation. Group 2 (Mono-IFNg-transient) was transiently activated upon IFN-g and contained genes like FCGR1A and FCGR1B, Fc receptor genes involved in immune cell activation, phagocytosis, and pathogen defense. Interestingly, group 3 (Mono-IFNg-initial) included genes such as IFNAR1, the IFN-I receptor gene, and TLR genes like TLR1 and TLR8, which displayed an initial increase in expression followed by a decrease in response to IFN-g. These genes are crucial for early immune responses, driving cytokine signaling, pathogen recognition, and IFN production. Group 4 (Mono-IFNg-gradual increase) featured the

immune checkpoint gene CD274, which showed a gradual increase in expression after IFN-g stimulation. Lastly, Group 5 (Mono-IFNg-late increase) exhibited genes with a gradual-late increase in expression. Further, I verified whether the genes from Table 4.2 were specifically activated only in their respective cell type and treatment group, by comparing their expression levels across all cell types using spaghetti plots (Figure 4.7). In summary, these temporal patterns in monocytes activated by IFN-a or IFN-g represent key components of distinct immune responses and IFN signaling pathways, providing valuable insights into their mechanistic roles in immune modulation.

Table 4.2: Cell- and IFN-type specific gene lists.

B IFN-a	B IFN-g	DC IFN-a	DC IFN-g	Group 1 Mono IFNa-transient	Group 2 Mono IFNg-transient	Group 3 Mono IFNg-initial	Group 4 Mono IFNg-gradual increase	Group 5 Mono IFNg-gradual late increase
CACNA1A	GBP7	HESX1	CXCL9	NEXN	MIR3945HG	CISH	SERPING1	F3
SECISBP2L	SLAMF1	CHROMR	UBD	AC124319.1	FCGR1B	SEPHS2	CD274	HMGB3
			CCL19	DEFB1	FCGR1A	LIMK2	ANKRD22	TGM2
				MSR1	PGS1	SNX20	APOL4	CDCP1
				CXCL11	NDST2	ERLIN1	SLAMF8	CD209
				DNAAF1	ACOD1	AC112496.1	SUCNR1	
				SAMD4A	HK1	TLR8		
				JUP	KLHL6	IFNAR1		
				APOBEC3B	RSPO3	STEAP4		
				KIAA1109	KRT17	TLR1		
				SDS		PELI1		
				SIGLEC1		TICAM2		

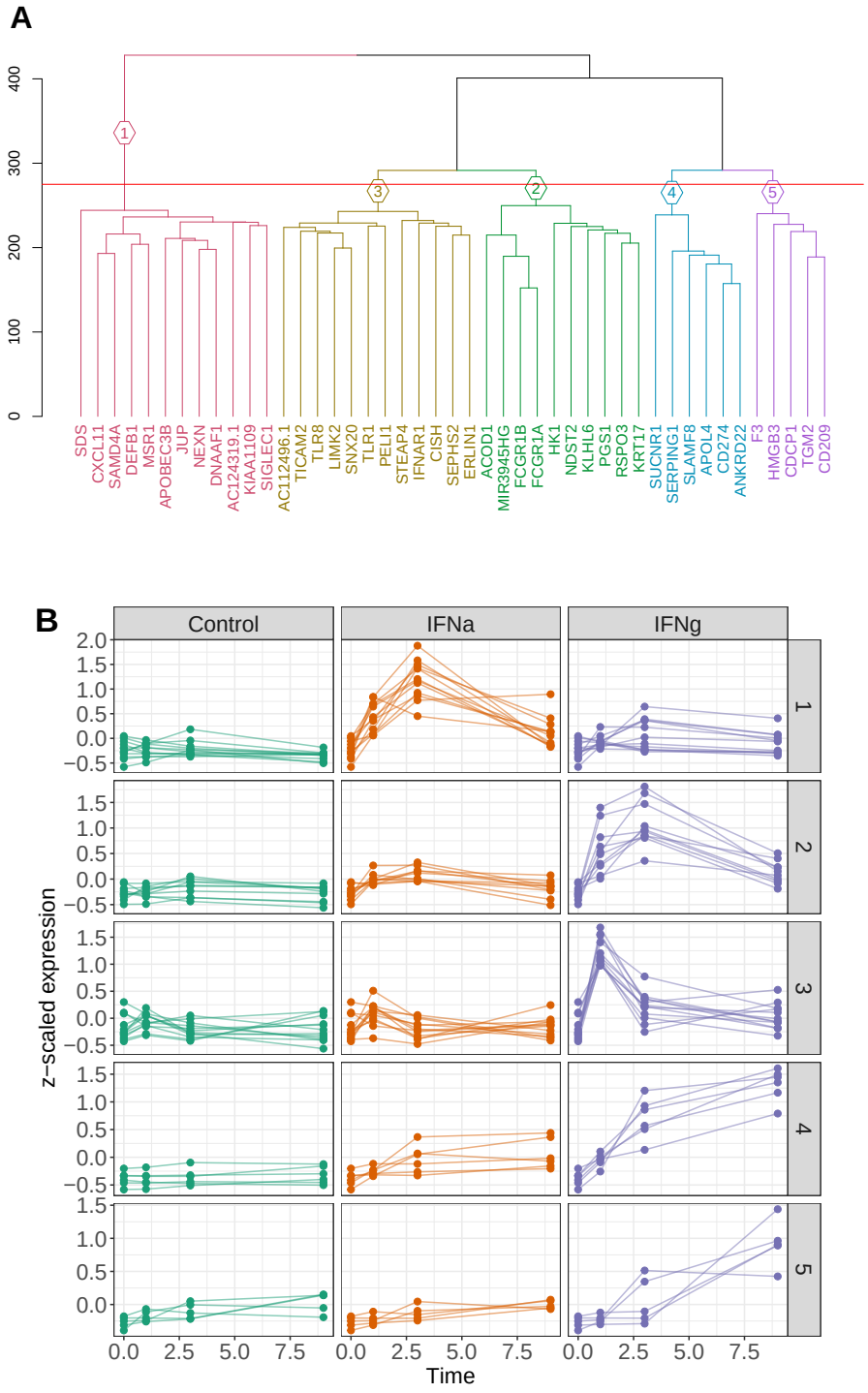

Figure 4.6: Discovery of cell- and IFN-type specific genes.

(A) Clustering dendrogram obtained for 45 monocyte- and IFN-specific genes. Using Z-scaled expression values extracted for monocytes in all conditions, I performed hierarchical clustering. The data form five major clusters, each showing a specific temporal expression pattern. The red line shows the cut point of the dendrogram. **(B)** Average Z-scaled expression of each gene from my five monocyte IFN-specific gene groups are shown on the y-axis along temporal scale on the x-axis. The plot shows only the expression patterns in monocyte populations. Each row represents a single gene cluster, and each column depicts different stimulation conditions.

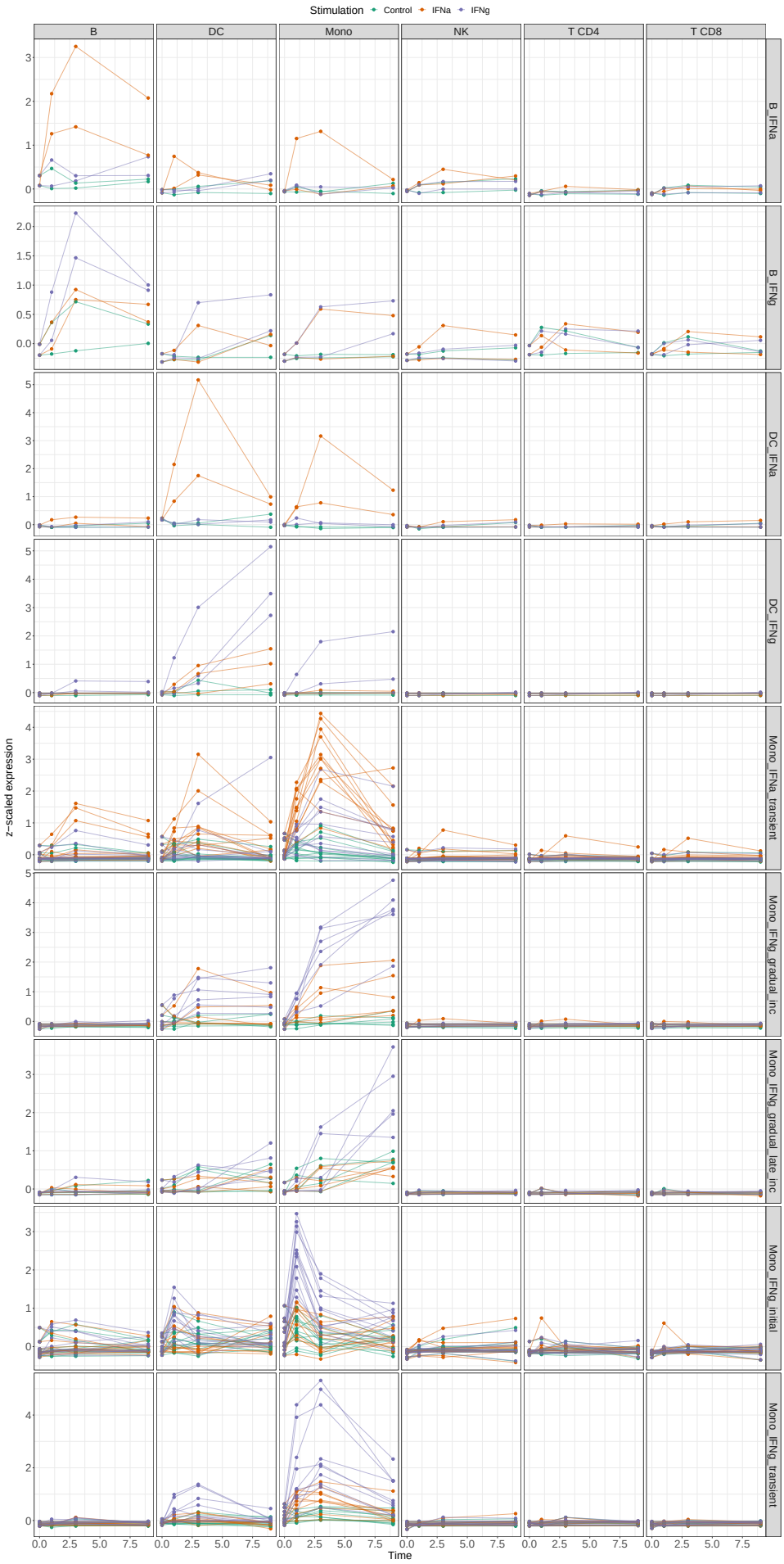
Stimulation
Control
IFNa
IFNg
B
DC
Mono
NK
T CD4
T CD8
B_IFNa
B_IFNg
DC_IFNa
DC_IFNg
Mono_IFNa_transient
Mono_IFNg_gradual_inc
Mono_IFNg_gradual_late_inc
Mono_IFNg_initial
Mono_IFNg_transient
z−scaled expression
Time

Figure 4.7: Examination of my cell- and IFN-type specific genes.

Z-scaled gene expression values of each gene from gene lists from my analysis are averaged for each condition in spaghetti plots in my data (y-axis). Each row represents a gene list, and each column depicts a cell type. Different conditions are colored separately.

4.4 Discussion

The last chapter of my thesis establishes a comprehensive resource for analyzing temporal, cell- and IFN-type-specific gene expression changes, thereby addressing key gaps in earlier studies. Prior studies examined only a single IFN type and ignored the differences between IFN-I and IFN-II responses. They also lacked single-cell resolution or failed to capture dynamic changes by restricting analyses to a single time point. This new dataset addresses these limitations while enabling the application and validation of my RF classifier and IFN signatures, confirming their robustness in a high-resolution, temporal context. It also facilitates the discovery of distinct IFN-driven gene expression dynamics exclusive for monocytes.

Robust immune cell type GESs and unbiased cell type classification are crucial for analyzing complex single-cell datasets, like the one I analyzed in this chapter. In Chapter 1, I demonstrated how the RF classifier eliminated bias in the downstream analysis and misclassification, particularly between DCs and monocyte populations, in an IFN-g stimulation data. This unbiased analysis was particularly critical for myeloid cells, which were key to identifying distinct temporal patterns in this data. In this chapter, cell surface marker expression was consistent with the output of my RF cell type classifier (Figure 4.2). Therefore, the cell type annotation of this IFN stimulation dataset can be regarded as accurate. This independent validation reinforced the reliability of the RF classifier as a versatile tool for robust and unbiased cell type identification in diverse experimental contexts.

Building on my IFN-I and IFN-II response GESs, I demonstrated for the first time immune cell type-specific IFN response dynamics at single-cell and temporal resolution. The broad effect of IFN-I across immune cells has been well established (McNab et al., 2015), and its rapid, transient activation has been reported in multiple studies (Schneider et al., 2014; De Giovanni et al., 2020; Pertsovskaya et al., 2013). However, no single study has mapped the temporal activation patterns across multiple cell types. In my study, upon IFN-a stimulation, all immune cell types were transiently activated (Figure 4.3), showing the universal but short-lived activation of immune responses induced by IFN-a. In contrast, the IFN-II response exhibited greater cell-type specificity: B cells showed a transient

activation upon IFN-g stimulation, similar to the response observed with IFN-a, while myeloid cells displayed a more gradual and sustained increase in activation (Figure 4.5). Several studies (Sindhava et al., 2017; Rubtsova et al., 2017; Peng et al., 2002; Knox et al., 2019) have shown IFN-g-induced gene expression in B cells, but none have examined its temporal dynamics. Notably, only my IFN-II GES accurately captured the IFN-II effect on B cells, whereas most published IFN-II GESs either exhibited mixed IFN-I/II signals in myeloid cells or failed to detect temporal effects. Consistent trends observed in DGE analysis further validated these findings, independently confirming the robustness of the IFN GES analysis and supporting conclusions drawn in Chapter 2 as well.

In this study, I identified gene modules with distinct temporal patterns, particularly in monocyte populations (Table 4.2). The IFN gene expression responses in monocytes followed distinct activation patterns, illustrating the transition between innate and adaptive immune responses. The transient activation of antiviral and immune cell recruitment genes upon IFN-a stimulation aligns with its role in innate immunity and antiviral responses (Schneider et al., 2014). In contrast, between 0 h and 1 h, IFN-g triggered an early activation of genes involved in pathogen recognition and IFN production, suggesting a feedback loop between IFN signaling and immune response initiation. Earlier reviews (Ivashkiv, 2018; Platanias, 2005) have discussed the crosstalk between type I and type II IFN pathways but this coupling of IFN-II signaling and IFN-I translation has not been widely examined. Between 0 h and 3 h, IFN-g further activated genes related to antigen presentation, such as Fc receptors, suggesting a shift towards adaptive immunity. The role of IFN-g in upregulating antigen presentation machinery is well known (Schroder et al., 2003), but my temporal analysis refines this understanding by showing a clear transition from an initial innate response to a later, adaptive-oriented gene expression profile. Between 0 h and 9 h, a group of genes, including CD274, a well known target for for immune checkpoint blockade in cancer therapy, showed gradual expression changes upon IFN-g stimulation. This is in agreement with studies suggesting CD274 as IFN-g induced gene (Galbraith et al., 2020). Similarly, genes from groups 4 and 5, including HMGB3 (Luo et al., 2024), TGM2 (Chang et al., 2024), CD209 (Duval et al., 2024), APOL4 (Zhu et al., 2022), SLAMF8 (Zou et al., 2019), and ANKRD22 (Chen et al., 2023), have been reported as immunosuppressive and linked to therapy resistance in cancer. Likewise, my IFN-II GES, which also served as a predictive ICI response marker (Figure 3.10), detected such late-phase activation of monocytes upon IFN-g stimulation. Groups 4 and 5 might suggest new potential immunotherapy targets. These findings provide valuable novel insights into the dynamic roles of IFN signaling in monocytes, with possible implications for myeloid biology and immune therapy.

In summary, this study provides a high-resolution, temporal map of IFN-driven gene expression dynamics. It addresses key gaps in previous research and offers a level of

granularity unavailable in existing studies. The dataset reveals distinct activation patterns in monocytes, reinforcing the role of IFN signaling in shaping innate and adaptive immune responses. By capturing monocyte-specific IFN responses over time, this study serves as a valuable resource for studying myeloid and IFN biology.

5 Conclusion and outlook

In this thesis, I utilized integrative approaches, combining multiple datasets and technologies, to investigate cell-type-specific IFN biology in both healthy and disease contexts. I established a novel GES discovery workflow for robust immune cell type GESs, immune cell type classifier for unbiased comparative analyses between cell types, and GESs specific to IFN-I and IFN-II response. I applied this set of tools in a temporal single-cell gene expression study of PBMCs that are stimulated by different types of IFNs. This is the most comprehensive study about gene expression response to date: it stands out with regard to its time resolution and coverage of different IFNs. The cell type-specific analysis of this data generated novel insights into several aspects of cell-type- and IFN-specific responses of various gene groups. This comprehensive analysis deepened the understanding of distinct cell-type-specific immune responses, particularly in myeloid cells, to IFNs.

To establish a framework for an unbiased immune cell type classification, I identified robust GESs for ten distinct immune cell types using a novel discovery workflow by leveraging multiple TME scRNA-seq datasets. I applied the genes in these GESs as features in a RF immune cell type classification approach. The classifier outperformed other published methods when using a small set of genes for cell typing. My immune cell type GESs were superior inputs to the classifier compared to previously published gene sets. For the first time, using IFN biology as an example, I demonstrated how commonly used cell type classification methods introduce statistical bias in downstream analyses and how this bias can perturb the biological interpretation of myeloid biology. In contrast, the RF classifier provided an unbiased, clustering-free, and accurate cell type annotation approach for complex single-cell data.

I have developed the GES discovery workflow for TME data and RF classifier using those GESs derived from TME data trained on PBMC. But these frameworks can be extended to other environments, provided sufficient high-quality datasets are available. For future applications and benchmarking, it is essential to include additional cellular environments, particularly TME, to evaluate the classifier's generalizability, robustness, and ability to enable automatic cell type annotation across diverse tissue types. Additionally, further biological systems and perturbation data should be used to assess the misclassification of immune cells and the bias in downstream analyses. These steps will broaden the applicability of my tools and findings.

To thoroughly characterize distinct IFN-I and IFN-II responses, I generated specific GESs that offer finer discrimination than previous GESs. My IFN GESs were clinically relevant. My IFN-I GES is a biomarker for SLE disease severity. My IFN-II GES correlates with $CD8^+$ T cell infiltration, and is a predictive biomarker for ICI therapy response. This

study is the first to comprehensively assess multiple IFN GESs across various experimental setups, cell types, disease contexts, and sequencing platforms. For future signature analyses, it shows the importance of GES evaluation before use. Further research should expand these analyses to longitudinal data to understand the dynamics of IFN responses, especially in ICI therapy. Ultimately, these efforts will refine IFN type-specific response profiling and broaden its clinical application.

After establishing the necessary tools to analyze a single-cell gene expression study focusing on differentiated IFN responses, I designed a PBMC CITE-seq experiment with IFN-I and IFN-II stimulations across four time points. This dataset enables direct comparisons between IFN-I and IFN-II responses at both temporal and cellular resolution, addressing gaps in previous studies. My analysis shows distinct stages of IFN-g responses in monocytes, showing their transition from early innate immune activation to a later adaptive-like profile. The dataset also identifies a previously uncharacterized feedback loop between IFN-II signaling and IFN-I production. Furthermore, it refines the understanding of IFN-g-induced gene regulation in B cells, particularly in a temporal context. Additionally, my study identifies late-phase IFN-g-induced gene modules, including possible immunosuppressive and therapy resistance-associated genes. This research provides valuable insights into immune response dynamics, especially in monocytes, and highlights the significance of temporal and multi-perturbation data in studying IFN-induced immune activation.

Future research could expand on the findings of this single-cell study by exploring the roles of individual genes identified in different monocyte IFN groups, particularly those involved in the late-stage response. These genes, associated with immunosuppression and therapy resistance, could be investigated in diseases like cancer, autoimmune disorders, and chronic inflammation. Studying their regulation of immune responses in monocytes may provide translational insights into myeloid cell differentiation, especially the transition from inflammatory to tolerogenic phenotypes. This could help develop therapeutic strategies for diseases such as cancer, where myeloid-derived suppressor cells contribute to immune evasion.

6 References

Abbas, A. R., Baldwin, D., Ma, Y., Ouyang, W., Gurney, A., Martin, F., Fong, S., van Lookeren Campagne, M., Godowski, P., Williams, P. M., Chan, A. C. and Clark, H. F. (2005). Immune response in silico (IRIS): immune-specific genes identified from a compendium of microarray expression data. Genes Immun *6*, 319–31.

Amezquita, R., Lun, A., Hicks, S. and Gottardo, R. (2021). Basics of Single-Cell Analysis with Bioconductor. Accessed: 2025-01-21. Bioconductor, CC BY 4.0.

Amezquita, R. A., Lun, A. T. L., Becht, E., Carey, V. J., Carpp, L. N., Geistlinger, L., Marini, F., Rue-Albrecht, K., Risso, D., Soneson, C., Waldron, L., Pagès, H., Smith, M. L., Huber, W., Morgan, M., Gottardo, R. and Hicks, S. C. (2020). Orchestrating single-cell analysis with Bioconductor. Nat Methods *17*, 137–145.

Angelova, M., Charoentong, P., Hackl, H., Fischer, M. L., Snajder, R., Krogsdam, A. M., Waldner, M. J., Bindea, G., Mlecnik, B., Galon, J. and Trajanoski, Z. (2015). Characterization of the immunophenotypes and antigenomes of colorectal cancers reveals distinct tumor escape mechanisms and novel targets for immunotherapy. Genome Biol *16*, 64.

Aran, D., Looney, A. P., Liu, L., Wu, E., Fong, V., Hsu, A., Chak, S., Naikawadi, R. P., Wolters, P. J., Abate, A. R., Butte, A. J. and Bhattacharya, M. (2019). Reference-based analysis of lung single-cell sequencing reveals a transitional profibrotic macrophage. Nat Immunol *20*, 163–172.

Ardoin, S. P. and Pisetsky, D. S. (2008). Developments in the scientific understanding of lupus. Arthritis Res Ther *10*, 218.

Aricò, E., Castiello, L., Capone, I., Gabriele, L. and Belardelli, F. (2019). Type I interferons and cancer: An evolving story demanding novel clinical applications. Cancers (Basel) *11*.

Aybey, B. (2020). Exploratory meta-analysis of single cell RNAseq cancer expression datasets: Characterizing cancer immune response and evasion. Master thesis University of Heidelberg.

Aybey, B., Brors, B. and Staub, E. (2025a). Expression signatures with specificity for type I and II IFN response and relevance for autoimmune diseases and cancer. Manuscript in preparation.

Aybey, B., Brors, B. and Staub, E. (2025b). Single cell analysis revealed immune cell type specific temporal IFN activation patterns of blood monocytes. Manuscript in preparation.

Aybey, B., Zhao, S., Brors, B. and Staub, E. (2023). Immune cell type signature discovery and random forest classification for analysis of single cell gene expression datasets. Front Immunol *14*, 1194745.

Ayers, M., Lunceford, J., Nebozhyn, M., Murphy, E., Loboda, A., Kaufman, D. R.,

Albright, A., Cheng, J. D., Kang, S. P., Shankaran, V., Piha-Paul, S. A., Yearley, J., Seiwert, T. Y., Ribas, A. and McClanahan, T. K. (2017). IFN-gamma-related mRNA profile predicts clinical response to PD-1 blockade. J Clin Invest *127*, 2930–2940.

Azizi, E., Carr, A. J., Plitas, G., Cornish, A. E., Konopacki, C., Prabhakaran, S., Nainys, J., Wu, K., Kiseliovas, V., Setty, M., Choi, K., Fromme, R. M., Dao, P., McKenney, P. T., Wasti, R. C., Kadaveru, K., Mazutis, L., Rudensky, A. Y. and Pe'er, D. (2018). Single-cell map of diverse immune phenotypes in the breast tumor microenvironment. Cell *174*, 1293–1308 e36.

Bai, R., Lv, Z., Xu, D. and Cui, J. (2020). Predictive biomarkers for cancer immunotherapy with immune checkpoint inhibitors. Biomark Res *8*, 34.

Balduzzi, S., Rücker, G., Nikolakopoulou, A., Papakonstantinou, T., Salanti, G., Efthimiou, O. and Schwarzer, G. (2023). netmeta: An R package for network meta-analysis using frequentist methods. Journal of Statistical Software *106*, 1 – 40.

Banchereau, R., Hong, S., Cantarel, B., Baldwin, N., Baisch, J., Edens, M., Cepika, A.-M., Acs, P., Turner, J., Anguiano, E., Vinod, P., Khan, S., Obermoser, G., Blankenship, D., Wakeland, E., Nassi, L., Gotte, A., Punaro, M., Liu, Y.-J., Banchereau, J., Rossello-Urgell, J., Wright, T. and Pascual, V. (2016). Personalized Immunomonitoring Uncovers Molecular Networks that Stratify Lupus Patients. Cell *165*, 551–565.

Barretina, J., Caponigro, G., Stransky, N., Venkatesan, K., Margolin, A. A., Kim, S., Wilson, C. J., Lehár, J., Kryukov, G. V., Sonkin, D., Reddy, A., Liu, M., Murray, L., Berger, M. F., Monahan, J. E., Morais, P., Meltzer, J., Korejwa, A., Jané-Valbuena, J., Mapa, F. A., Thibault, J., Bric-Furlong, E., Raman, P., Shipway, A., Engels, I. H., Cheng, J., Yu, G. K., Yu, J., Aspesi, P., de Silva, M., Jagtap, K., Jones, M. D., Wang, L., Hatton, C., Palescandolo, E., Gupta, S., Mahan, S., Sougnez, C., Onofrio, R. C., Liefeld, T., MacConaill, L., Winckler, W., Reich, M., Li, N., Mesirov, J. P., Gabriel, S. B., Getz, G., Ardlie, K., Chan, V., Myer, V. E., Weber, B. L., Porter, J., Warmuth, M., Finan, P., Harris, J. L., Meyerson, M., Golub, T. R., Morrissey, M. P., Sellers, W. R., Schlegel, R. and Garraway, L. A. (2012). The Cancer Cell Line Encyclopedia enables predictive modelling of anticancer drug sensitivity. Nature *483*, 603–607.

Becht, E., Giraldo, N. A., Lacroix, L., Buttard, B., Elarouci, N., Petitprez, F., Selves, J., Laurent-Puig, P., Sautès-Fridman, C., Fridman, W. H. and de Reyniès, A. (2016). Estimating the population abundance of tissue-infiltrating immune and stromal cell populations using gene expression. Genome Biol *17*, 218.

Becht, E., McInnes, L., Healy, J., Dutertre, C.-A., Kwok, I. W. H., Ng, L. G., Ginhoux, F. and Newell, E. W. (2019). Dimensionality reduction for visualizing single-cell data using UMAP. Nat Biotechnol *37*, 38–44.

Bengtsson, A. A. and Ronnblom, L. (2017). Role of interferons in SLE. Best Pract Res Clin Rheumatol *31*, 415–428.

Bengtsson, A. A., Sturfelt, G., Truedsson, L., Blomberg, J., Alm, G., Vallin, H. and

Ronnblom, L. (2000). Activation of type I interferon system in systemic lupus erythematosus correlates with disease activity but not with antiretroviral antibodies. Lupus *9*, 664–71.

Bennett, L., Palucka, A. K., Arce, E., Cantrell, V., Borvak, J., Banchereau, J. and Pascual, V. (2003). Interferon and granulopoiesis signatures in systemic lupus erythematosus blood. J Exp Med *197*, 711–23.

Bilgic, H., Ytterberg, S. R., Amin, S., McNallan, K. T., Wilson, J. C., Koeuth, T., Ellingson, S., Newman, B., Bauer, J. W., Peterson, E. J., Baechler, E. C. and Reed, A. M. (2009). Interleukin-6 and type I interferon-regulated genes and chemokines mark disease activity in dermatomyositis. Arthritis Rheum *60*, 3436–46.

Bindea, G., Mlecnik, B., Tosolini, M., Kirilovsky, A., Waldner, M., Obenauf, A. C., Angell, H., Fredriksen, T., Lafontaine, L., Berger, A., Bruneval, P., Fridman, W. H., Becker, C., Pagès, F., Speicher, M. R., Trajanoski, Z. and Galon, J. (2013). Spatiotemporal dynamics of intratumoral immune cells reveal the immune landscape in human cancer. Immunity *39*, 782–95.

Bombardier, C., Gladman, D. D., Urowitz, M. B., Caron, D. and Chang, C. H. (1992). Derivation of the SLEDAI. A disease activity index for lupus patients. The Committee on Prognosis Studies in SLE. Arthritis Rheum *35*, 630–40.

Borden, E. C. (2019). Interferons α and β in cancer: therapeutic opportunities from new insights. Nat Rev Drug Discov *18*, 219–234.

Boukhaled, G. M., Harding, S. and Brooks, D. G. (2021). Opposing roles of type I interferons in cancer immunity. Annu Rev Pathol *16*, 167–198.

Bouman, B. J., Demerdash, Y., Sood, S., Grünschläger, F., Pilz, F., Itani, A. R., Kuck, A., Marot-Lassauzaie, V., Haas, S., Haghverdi, L. and Essers, M. A. (2024). Single-cell time series analysis reveals the dynamics of HSPC response to inflammation. Life Sci Alliance *7*.

Breheny, P., Stromberg, A. and Lambert, J. (2018). p-Value histograms: inference and diagnostics. High-Throughput *7*, 23.

Burke, J. D. and Young, H. A. (2019). IFN-γ: A cytokine at the right time, is in the right place. Semin Immunol *43*, 101280.

Butler, A., Hoffman, P., Smibert, P., Papalexi, E. and Satija, R. (2018). Integrating single-cell transcriptomic data across different conditions, technologies, and species. Nat Biotechnol *36*, 411–420.

Caielli, S., Wan, Z. and Pascual, V. (2023). Systemic lupus erythematosus pathogenesis: Interferon and beyond. Annu Rev Immunol *41*, 533–560.

Castro, F., Cardoso, A. P., Gonçalves, R. M., Serre, K. and Oliveira, M. J. (2018). Interferon-Gamma at the Crossroads of Tumor Immune Surveillance or Evasion. Front Immunol *9*, 847.

Chang, K., Creighton, C. J., Davis, C., Donehower, L., Drummond, J., Wheeler, D.,

Ally, A., Balasundaram, M., Birol, I., Butterfield, Y. S. N., Chu, A., Chuah, E., Chun, H.-J. E., Dhalla, N., Guin, R., Hirst, M., Hirst, C., Holt, R. A., Jones, S. J. M., Lee, D., Li, H. I., Marra, M. A., Mayo, M., Moore, R. A., Mungall, A. J., Robertson, A. G., Schein, J. E., Sipahimalani, P., Tam, A., Thiessen, N., Varhol, R. J., Beroukhim, R., Bhatt, A. S., Brooks, A. N., Cherniack, A. D., Freeman, S. S., Gabriel, S. B., Helman, E., Jung, J., Meyerson, M., Ojesina, A. I., Pedamallu, C. S., Saksena, G., Schumacher, S. E., Tabak, B., Zack, T., Lander, E. S., Bristow, C. A., Hadjipanayis, A., Haseley, P., Kucherlapati, R., Lee, S., Lee, E., Luquette, L. J., Mahadeshwar, H. S., Pantazi, A., Parfenov, M., Park, P. J., Protopopov, A., Ren, X., Santoso, N., Seidman, J., Seth, S., Song, X., Tang, J., Xi, R., Xu, A. W., Yang, L., Zeng, D., Auman, J. T., Balu, S., Buda, E., Fan, C., Hoadley, K. A., Jones, C. D., Meng, S., Mieczkowski, P. A., Parker, J. S., Perou, C. M., Roach, J., Shi, Y., Silva, G. O., Tan, D., Veluvolu, U., Waring, S., Wilkerson, M. D., Wu, J., Zhao, W., Bodenheimer, T., Hayes, D. N., Hoyle, A. P., Jeffreys, S. R., Mose, L. E., Simons, J. V., Soloway, M. G., Baylin, S. B., Berman, B. P., Bootwalla, M. S., Danilova, L., Herman, J. G., Hinoue, T., Laird, P. W., Rhie, S. K., Shen, H., Triche, T., Weisenberger, D. J., Carter, S. L., Cibulskis, K., Chin, L., Zhang, J., Getz, G., Sougnez, C., Wang, M., Dinh, H., Doddapaneni, H. V., Gibbs, R., Gunaratne, P., Han, Y., Kalra, D., Kovar, C., Lewis, L., Morgan, M., Morton, D., Muzny, D., Reid, J., Xi, L., Cho, J., DiCara, D., Frazer, S., Gehlenborg, N., Heiman, D. I., Kim, J., Lawrence, M. S., Lin, P., Liu, Y., Noble, M. S., Stojanov, P., Voet, D., Zhang, H., Zou, L., Stewart, C., Bernard, B., Bressler, R., Eakin, A., Iype, L., Knijnenburg, T., Kramer, R., Kreisberg, R., Leinonen, K., Lin, J., Liu, Y., Miller, M., Reynolds, S. M., Rovira, H., Shmulevich, I., Thorsson, V., Yang, D., Zhang, W., Amin, S., Wu, C.-J., Wu, C.-C., Akbani, R., Aldape, K., Baggerly, K. A., Broom, B., Casasent, T. D., Cleland, J., Creighton, C., Dodda, D., Edgerton, M., Han, L., Herbrich, S. M., Ju, Z., Kim, H., Lerner, S., Li, J., Liang, H., Liu, W., Lorenzi, P. L., Lu, Y., Melott, J., Mills, G. B., Nguyen, L., Su, X., Verhaak, R., Wang, W., Weinstein, J. N., Wong, A., Yang, Y., Yao, J., Yao, R., Yoshihara, K., Yuan, Y., Yung, A. K., Zhang, N., Zheng, S., Ryan, M., Kane, D. W., Aksoy, B. A., Ciriello, G., Dresdner, G., Gao, J., Gross, B., Jacobsen, A., Kahles, A., Ladanyi, M., Lee, W., Lehmann, K.-V., Miller, M. L., Ramirez, R., Rätsch, G., Reva, B., Sander, C., Schultz, N., Senbabaoglu, Y., Shen, R., Sinha, R., Sumer, S. O., Sun, Y., Taylor, B. S., Weinhold, N., Fei, S., Spellman, P., Benz, C., Carlin, D., Cline, M., Craft, B., Ellrott, K., Goldman, M., Haussler, D., Ma, S., Ng, S., Paull, E., Radenbaugh, A., Salama, S., Sokolov, A., Stuart, J. M., Swatloski, T., Uzunangelov, V., Waltman, P., Yau, C., Zhu, J., Hamilton, S. R., Abbott, S., Abbott, R., Dees, N. D., Delehaunty, K., Ding, L., Dooling, D. J., Eldred, J. M., Fronick, C. C., Fulton, R., Fulton, L. L., Kalicki-Veizer, J., Kanchi, K.-L., Kandoth, C., Koboldt, D. C., Larson, D. E., Ley, T. J., Lin, L., Lu, C., Magrini, V. J., Mardis, E. R., McLellan, M. D., McMichael, J. F., Miller, C. A., O'Laughlin, M., Pohl, C., Schmidt,

H., Smith, S. M., Walker, J., Wallis, J. W., Wendl, M. C., Wilson, R. K., Wylie, T., Zhang, Q., Burton, R., Jensen, M. A., Kahn, A., Pihl, T., Pot, D., Wan, Y., Levine, D. A., Black, A. D., Bowen, J., Network, T. C. G. A. R., Center, G. C., Center, G. D. A., Center, S., Center, D. C., Site, T. S. and Center, B. C. R. (2013). The Cancer Genome Atlas Pan-Cancer analysis project. Nat Genet *45*, 1113–1120.

Chang, W., Gao, W., Liu, D., Luo, B., Li, H., Zhong, L. and Chen, Y. (2024). The upregulation of TGM2 is associated with poor prognosis and the shaping of the inflammatory tumor microenvironment in lung squamous cell carcinoma. Am J Cancer Res *14*, 2823–2838.

Chang, Y. J., Holtzman, M. J. and Chen, C. C. (2002). Interferon-gamma-induced epithelial ICAM-1 expression and monocyte adhesion. Involvement of protein kinase C-dependent c-Src tyrosine kinase activation pathway. J Biol Chem *277*, 7118–26.

Charoentong, P., Finotello, F., Angelova, M., Mayer, C., Efremova, M., Rieder, D., Hackl, H. and Trajanoski, Z. (2017). Pan-cancer immunogenomic analyses reveal genotype-immunophenotype relationships and predictors of response to checkpoint blockade. Cell Rep *18*, 248–262.

Chasset, F., Mathian, A., Dorgham, K., Ribi, C., Trendelenburg, M., Huynh-Do, U., Roux-Lombard, P., Courvoisier, D. S., Amoura, Z., Gorochov, G. and Chizzolini, C. (2022). Serum interferon-α levels and IFN type I-stimulated genes score perform equally to assess systemic lupus erythematosus disease activity. Ann Rheum Dis *81*, 901–903.

Chaussabel, D., Quinn, C., Shen, J., Patel, P., Glaser, C., Baldwin, N., Stichweh, D., Blankenship, D., Li, L., Munagala, I., Bennett, L., Allantaz, F., Mejias, A., Ardura, M., Kaizer, E., Monnet, L., Allman, W., Randall, H., Johnson, D., Lanier, A., Punaro, M., Wittkowski, K. M., White, P., Fay, J., Klintmalm, G., Ramilo, O., Palucka, A. K., Banchereau, J. and Pascual, V. (2008). A modular analysis framework for blood genomics studies: application to systemic lupus erythematosus. Immunity *29*, 150–64.

Chen, H., Yang, K., Pang, L., Fei, J., Zhu, Y. and Zhou, J. (2023). ANKRD22 is a potential novel target for reversing the immunosuppressive effects of PMN-MDSCs in ovarian cancer. J Immunother Cancer *11*.

Choi, Y. H. and Kim, J. K. (2019). Dissecting cellular heterogeneity using single-cell RNA sequencing. Mol Cells *42*, 189–199.

Chow, K. T. and Gale, M., J. (2015). SnapShot: Interferon signaling. Cell *163*, 1808–1808.e1.

Colli, M. L., Ramos-Rodríguez, M., Nakayasu, E. S., Alvelos, M. I., Lopes, M., Hill, J. L. E., Turatsinze, J. V., Coomans de Brachène, A., Russell, M. A., Raurell-Vila, H., Castela, A., Juan-Mateu, J., Webb-Robertson, B. M., Krogvold, L., Dahl-Jorgensen, K., Marselli, L., Marchetti, P., Richardson, S. J., Morgan, N. G., Metz, T. O., Pasquali, L. and Eizirik, D. L. (2020). An integrated multi-omics approach identifies the landscape of interferon-α-mediated responses of human pancreatic beta cells. Nat Commun *11*,

2584.

Cooles, F. A. H. and Isaacs, J. D. (2022). The interferon gene signature as a clinically relevant biomarker in autoimmune rheumatic disease. Lancet Rheumatol *4*, e61–e72.

Cui, C., Xu, C., Yang, W., Chi, Z., Sheng, X., Si, L., Xie, Y., Yu, J., Wang, S., Yu, R., Guo, J. and Kong, Y. (2021). Ratio of the interferon-gamma signature to the immunosuppression signature predicts anti-PD-1 therapy response in melanoma. NPJ Genom Med *6*, 7.

de Cevins, C., Delage, L., Batignes, M., Riller, Q., Luka, M., Remaury, A., Sorin, B., Fali, T., Masson, C., Hoareau, B., Meunier, C., Parisot, M., Zarhrate, M., Pérot, B. P., García-Paredes, V., Carbone, F., Galliot, L., Nal, B., Pierre, P., Canard, L., Boussard, C., Crickx, E., Guillemot, J. C., Bader-Meunier, B., Bélot, A., Quartier, P., Frémond, M. L., Neven, B., Boldina, G., Augé, F., Alain, F., Didier, M., Rieux-Laucat, F. and Ménager, M. M. (2023). Single-cell RNA-sequencing of PBMCs from SAVI patients reveals disease-associated monocytes with elevated integrated stress response. Cell Rep Med *4*, 101333.

De Giovanni, M., Cutillo, V., Giladi, A., Sala, E., Maganuco, C. G., Medaglia, C., Di Lucia, P., Bono, E., Cristofani, C., Consolo, E., Giustini, L., Fiore, A., Eickhoff, S., Kastenmüller, W., Amit, I., Kuka, M. and Iannacone, M. (2020). Spatiotemporal regulation of type I interferon expression determines the antiviral polarization of CD4+ T cells. Nat Immunol *21*, 321–330.

de Kanter, J. K., Lijnzaad, P., Candelli, T., Margaritis, T. and Holstege, F. C. P. (2019). CHETAH: a selective, hierarchical cell type identification method for single-cell RNA sequencing. Nucleic Acids Res *47*, e95.

de Weerd, N. A., Vivian, J. P., Nguyen, T. K., Mangan, N. E., Gould, J. A., Braniff, S.-J., Zaker-Tabrizi, L., Fung, K. Y., Forster, S. C., Beddoe, T., Reid, H. H., Rossjohn, J. and Hertzog, P. J. (2013). Structural basis of a unique interferon-β signaling axis mediated via the receptor IFNAR1. Nat Immunol *14*, 901–907.

Devlin, J. C., Zwack, E. E., Tang, M. S., Li, Z., Fenyo, D., Torres, V. J., Ruggles, K. V. and Loke, P. (2020). Distinct features of human myeloid cell cytokine response profiles identify neutrophil activation by cytokines as a prognostic feature during tuberculosis and cancer. J Immunol *204*, 3389–3399.

Domcke, S. and Shendure, J. (2023). A reference cell tree will serve science better than a reference cell atlas. Cell *186*, 1103–1114.

Domínguez Conde, C., Xu, C., Jarvis, L. B., Rainbow, D. B., Wells, S. B., Gomes, T., Howlett, S. K., Suchanek, O., Polanski, K., King, H. W., Mamanova, L., Huang, N., Szabo, P. A., Richardson, L., Bolt, L., Fasouli, E. S., Mahbubani, K. T., Prete, M., Tuck, L., Richoz, N., Tuong, Z. K., Campos, L., Mousa, H. S., Needham, E. J., Pritchard, S., Li, T., Elmentaite, R., Park, J., Rahmani, E., Chen, D., Menon, D. K., Bayraktar, O. A., James, L. K., Meyer, K. B., Yosef, N., Clatworthy, M. R., Sims, P. A.,

Farber, D. L., Saeb-Parsy, K., Jones, J. L. and Teichmann, S. A. (2022). Cross-tissue immune cell analysis reveals tissue-specific features in humans. Science *376*, eabl5197.

Dummer, R., Brase, J. C., Garrett, J., Campbell, C. D., Gasal, E., Squires, M., Gusenleitner, D., Santinami, M., Atkinson, V., Mandala, M., Chiarion-Sileni, V., Flaherty, K., Larkin, J., Robert, C., Kefford, R., Kirkwood, J. M., Hauschild, A., Schadendorf, D. and Long, G. V. (2020). Adjuvant dabrafenib plus trametinib versus placebo in patients with resected, BRAF(V600)-mutant, stage III melanoma (COMBI-AD): exploratory biomarker analyses from a randomised, phase 3 trial. Lancet Oncol *21*, 358–372.

Dupuy, A. and Simon, R. M. (2007). Critical Review of Published Microarray Studies for Cancer Outcome and Guidelines on Statistical Analysis and Reporting. J Natl Cancer Inst *99*, 147–157.

Duval, C., Bourreau, E., Warrick, E., Bastien, P., Nouveau, S. and Bernerd, F. (2024). A chronic pro-inflammatory environment contributes to the physiopathology of actinic lentigines. Sci Rep *14*, 5256.

Edgar, R., Domrachev, M. and Lash, A. E. (2002). Gene Expression Omnibus: NCBI gene expression and hybridization array data repository. Nucleic Acids Res *30*, 207–10.

Eisen, M. B., Spellman, P. T., Brown, P. O. and Botstein, D. (1998). Cluster analysis and display of genome-wide expression patterns. Proc Natl Acad Sci U S A *95*, 14863–8.

El-Sherbiny, Y. M., Psarras, A., Md Yusof, M. Y., Hensor, E. M. A., Tooze, R., Doody, G., Mohamed, A. A. A., McGonagle, D., Wittmann, M., Emery, P. and Vital, E. M. (2018). A novel two-score system for interferon status segregates autoimmune diseases and correlates with clinical features. Sci Rep *8*, 5793.

Ester, M., Kriegel, H.-P., Sander, J. and Xu, X. (1996). A density-based algorithm for discovering clusters in large spatial databases with noise. In Proceedings of the Second International Conference on Knowledge Discovery and Data Mining KDD'96 pp. 226–231, AAAI Press, Portland, Oregon.

Feng, X., Wu, H., Grossman, J. M., Hanvivadhanakul, P., FitzGerald, J. D., Park, G. S., Dong, X., Chen, W., Kim, M. H., Weng, H. H., Furst, D. E., Gorn, A., McMahon, M., Taylor, M., Brahn, E., Hahn, B. H. and Tsao, B. P. (2006). Association of increased interferon-inducible gene expression with disease activity and lupus nephritis in patients with systemic lupus erythematosus. Arthritis Rheum *54*, 2951–62.

Fenton, S. E., Saleiro, D. and Platanias, L. C. (2021). Type I and II interferons in the anti-tumor immune response. Cancers (Basel) *13*.

Finotello, F. and Trajanoski, Z. (2018). Quantifying tumor-infiltrating immune cells from transcriptomics data. Cancer Immunol Immunother *67*, 1031–1040.

Fujiwara, Y., Sun, Y., Torphy, R. J., He, J., Yanaga, K., Edil, B. H., Schulick, R. D. and Zhu, Y. (2018). Pomalidomide inhibits PD-L1 induction to promote antitumor immunity. Cancer Res *78*, 6655–6665.

Galbraith, N. J., Walker, S. P., Gardner, S. A., Bishop, C., Galandiuk, S. and Polk, H. C. (2020). Interferon-gamma increases monocyte PD-L1 but does not diminish T-cell activation. Cell Immunol *357*, 104197.

Garcin, G., Bordat, Y., Chuchana, P., Monneron, D., Law, H. K., Piehler, J. and Uze, G. (2013). Differential activity of type I interferon subtypes for dendritic cell differentiation. PLoS One *8*, e58465.

Gibson, G. (2022). Perspectives on rigor and reproducibility in single cell genomics. PLoS Genet *18*, e1010210.

Gocher, A. M., Workman, C. J. and Vignali, D. A. A. (2022). Interferon-γ: teammate or opponent in the tumour microenvironment? Nat Rev Immunol *22*, 158–172.

Goel, R. R., Kotenko, S. V. and Kaplan, M. J. (2021). Interferon lambda in inflammation and autoimmune rheumatic diseases. Nat Rev Rheumatol *17*, 349–362.

Goldman, M. J., Craft, B., Hastie, M., Repecka, K., McDade, F., Kamath, A., Banerjee, A., Luo, Y., Rogers, D., Brooks, A. N., Zhu, J. and Haussler, D. (2020). Visualizing and interpreting cancer genomics data via the Xena platform. Nat Biotechnol *38*, 675–678.

Gómez-Bañuelos, E., Goldman, D. W., Andrade, V., Darrah, E., Petri, M. and Andrade, F. (2024). Uncoupling interferons and the interferon signature explains clinical and transcriptional subsets in SLE. Cell Rep Med *5*, 101569.

Govindarajan, R., Duraiyan, J., Kaliyappan, K. and Palanisamy, M. (2012). Microarray and its applications. J Pharm Bioallied Sci *4*, S310–2.

Grabski, I. N. and Irizarry, R. A. (2022). A probabilistic gene expression barcode for annotation of cell types from single-cell RNA-seq data. Biostatistics *23*, 1150–1164.

Grasso, C. S., Tsoi, J., Onyshchenko, M., Abril-Rodriguez, G., Ross-Macdonald, P., Wind-Rotolo, M., Champhekar, A., Medina, E., Torrejon, D. Y., Shin, D. S., Tran, P., Kim, Y. J., Puig-Saus, C., Campbell, K., Vega-Crespo, A., Quist, M., Martignier, C., Luke, J. J., Wolchok, J. D., Johnson, D. B., Chmielowski, B., Hodi, F. S., Bhatia, S., Sharfman, W., Urba, W. J., Slingluff, C. L., J., Diab, A., Haanen, J., Algarra, S. M., Pardoll, D. M., Anagnostou, V., Topalian, S. L., Velculescu, V. E., Speiser, D. E., Kalbasi, A. and Ribas, A. (2020). Conserved interferon-gamma signaling drives clinical response to immune checkpoint blockade therapy in melanoma. Cancer Cell *38*, 500–515 e3.

Hahsler, M., Piekenbrock, M. and Doran, D. (2019). dbscan: Fast density-based clustering with R. Journal of Statistical Software *91*, 1–30.

Hall, J. C., Casciola-Rosen, L., Berger, A. E., Kapsogeorgou, E. K., Cheadle, C., Tzioufas, A. G., Baer, A. N. and Rosen, A. (2012). Precise probes of type II interferon activity define the origin of interferon signatures in target tissues in rheumatic diseases. Proc Natl Acad Sci U S A *109*, 17609–14.

Han, Y., Wang, Y., Dong, X., Sun, D., Liu, Z., Yue, J., Wang, H., Li, T. and Wang, C. (2023). TISCH2: expanded datasets and new tools for single-cell transcriptome analyses of the tumor microenvironment. Nucleic Acids Res *51*, D1425–D1431.

Hao, Y., Hao, S., Andersen-Nissen, E., Mauck, W. M., r., Zheng, S., Butler, A., Lee, M. J., Wilk, A. J., Darby, C., Zager, M., Hoffman, P., Stoeckius, M., Papalexi, E., Mimitou, E. P., Jain, J., Srivastava, A., Stuart, T., Fleming, L. M., Yeung, B., Rogers, A. J., McElrath, J. M., Blish, C. A., Gottardo, R., Smibert, P. and Satija, R. (2021). Integrated analysis of multimodal single-cell data. Cell *184*, 3573–3587.e29.

Hartoularos, G. C., Si, Y., Zhang, F., Kathail, P., Lee, D. S., Ogorodnikov, A., Sun, Y., Song, Y. S., Kang, H. M. and Ye, C. J. (2023). Reference-free multiplexed single-cell sequencing identifies genetic modifiers of the human immune response. bioRxiv.

Hastie, T., Tibshirani, R. and Friedman, J. (2009). Random Forests pp. 587–604. New York, NY: Springer New York.

Ianevski, A., Giri, A. K. and Aittokallio, T. (2022). Fully-automated and ultra-fast cell-type identification using specific marker combinations from single-cell transcriptomic data. Nat Commun , *13*, 1246.

Isaacs, A. and Lindenmann, J. (1957). Virus interference. I. The interferon. Proc R Soc Lond B Biol Sci , *147*, 258–67.

Itadani, H., Mizuarai, S. and Kotani, H. (2008). Can systems biology understand pathway activation? Gene expression signatures as surrogate markers for understanding the complexity of pathway activation. Curr Genomics , *9*, 349–60.

Ivashkiv, L. B. (2018). IFNγ: signalling, epigenetics and roles in immunity, metabolism, disease and cancer immunotherapy. Nat Rev Immunol , *18*, 545–558.

Jabs, W. J., Hennig, C., Zawatzky, R. and Kirchner, H. (1999). Failure to detect antiviral activity in serum and plasma of healthy individuals displaying high activity in ELISA for IFN-alpha and IFN-beta. J Interferon Cytokine Res , *19*, 463–9.

James, C. M., Abdad, M. Y., Mansfield, J. P., Jacobsen, H. K., Vind, A. R., Stumbles, P. A. and Bartlett, E. J. (2007). Differential activities of alpha/beta IFN subtypes against influenza virus in vivo and enhancement of specific immune responses in DNA vaccinated mice expressing haemagglutinin and nucleoprotein. Vaccine , *25*, 1856–67.

Jankowski, J., Lee, H. K., Wilflingseder, J. and Hennighausen, L. (2021). Interferon-regulated genetic programs and jak/stat pathway activate the intronic promoter of the short ace2 isoform in renal proximal tubules. bioRxiv.

Jorgovanovic, D., Song, M., Wang, L. and Zhang, Y. (2020). Roles of IFN-γ in tumor progression and regression: a review. Biomark Res , *8*, 49.

Kambayashi, T., Assarsson, E., Lukacher, A. E., Ljunggren, H. G. and Jensen, P. E. (2003). Memory CD8+ T cells provide an early source of IFN-gamma. J Immunol , *170*, 2399–408.

Karachaliou, N., Gonzalez-Cao, M., Crespo, G., Drozdowskyj, A., Aldeguer, E., Gimenez-Capitan, A., Teixido, C., Molina-Vila, M. A., Viteri, S., De Los Llanos Gil, M., Algarra, S. M., Perez-Ruiz, E., Marquez-Rodas, I., Rodriguez-Abreu, D., Blanco, R., Puertolas, T., Royo, M. A. and Rosell, R. (2018). Interferon gamma, an important marker of

response to immune checkpoint blockade in non-small cell lung cancer and melanoma patients. Ther Adv Med Oncol , *10*, 1758834017749748.

Karagiannis, T. T., Cleary, J. P., J., Gok, B., Henderson, A. J., Martin, N. G., Yajima, M., Nelson, E. C. and Cheng, C. S. (2020). Single cell transcriptomics reveals opioid usage evokes widespread suppression of antiviral gene program. Nat Commun , *11*, 2611.

Kartha, V. K., Duarte, F. M., Hu, Y., Ma, S., Chew, J. G., Lareau, C. A., Earl, A., Burkett, Z. D., Kohlway, A. S., Lebofsky, R. and Buenrostro, J. D. (2022). Functional inference of gene regulation using single-cell multi-omics. Cell Genom , *2*.

Katze, M. G., He, Y. and Gale, M., J. (2002). Viruses and interferon: a fight for supremacy. Nat Rev Immunol , *2*, 675–87.

Keskinen, P., Ronni, T., Matikainen, S., Lehtonen, A. and Julkunen, I. (1997). Regulation of HLA class I and II expression by interferons and influenza A virus in human peripheral blood mononuclear cells. Immunology , *91*, 421–9.

Kim, N., Kim, H. K., Lee, K., Hong, Y., Cho, J. H., Choi, J. W., Lee, J.-I., Suh, Y.-L., Ku, B. M., Eum, H. H., Choi, S., Choi, Y.-L., Joung, J.-G., Park, W.-Y., Jung, H. A., Sun, J.-M., Lee, S.-H., Ahn, J. S., Park, K., Ahn, M.-J. and Lee, H.-O. (2020). Single-cell RNA sequencing demonstrates the molecular and cellular reprogramming of metastatic lung adenocarcinoma. Nat Commun , *11*, 2285.

Kim, S. T., Cristescu, R., Bass, A. J., Kim, K. M., Odegaard, J. I., Kim, K., Liu, X. Q., Sher, X., Jung, H., Lee, M., Lee, S., Park, S. H., Park, J. O., Park, Y. S., Lim, H. Y., Lee, H., Choi, M., Talasaz, A., Kang, P. S., Cheng, J., Loboda, A., Lee, J. and Kang, W. K. (2018). Comprehensive molecular characterization of clinical responses to PD-1 inhibition in metastatic gastric cancer. Nat Med , *24*, 1449–1458.

Kiselev, V. Y., Andrews, T. S. and Hemberg, M. (2019). Challenges in unsupervised clustering of single-cell RNA-seq data. Nat Rev Genet , *20*, 273–282.

Knox, J. J., Myles, A. and Cancro, M. P. (2019). T-bet(+) memory B cells: Generation, function, and fate. Immunol Rev , *288*, 149–160.

Kobak, D. and Berens, P. (2019). The art of using t-SNE for single-cell transcriptomics. Nat Commun , *10*, 5416.

Kosmidis, C., Sapalidis, K., Koletsa, T., Kosmidou, M., Efthimiadis, C., Anthimidis, G., Varsamis, N., Michalopoulos, N., Koulouris, C., Atmatzidis, S., Liavas, L., Strati, T. M., Koimtzis, G., Tsakalidis, A., Mantalovas, S., Zarampouka, K., Florou, M., Giannakidis, D. E., Georgakoudi, E., Baka, S., Zarogoulidis, P., Man, Y. G. and Kesisoglou, I. (2018). Interferon-γ and colorectal cancer: an up-to date. J Cancer , *9*, 232–238.

Kotliarov, Y., Sparks, R., Martins, A. J., Mulè, M. P., Lu, Y., Goswami, M., Kardava, L., Banchereau, R., Pascual, V. and Biancotto, A. (2020). Broad immune activation underlies shared set point signatures for vaccine responsiveness in healthy individuals and disease activity in patients with lupus. Nat Med , *26*, 618–629.

Kratz, A. and Carninci, P. (2014). The devil in the details of RNA-seq. Nat Biotechnol , *32*, 882–4.

Kreis, J., Aybey, B., Geist, F., Brors, B. and Staub, E. (2024). Stromal Signals Dominate Gene Expression Signature Scores That Aim to Describe Cancer Cell-intrinsic Stemness or Mesenchymality Characteristics. Cancer Res Commun , *4*, 516–529.

Kreis, J., Nedić, B., Mazur, J., Urban, M., Schelhorn, S. E., Grombacher, T., Geist, F., Brors, B., Zühlsdorf, M. and Staub, E. (2021). RosettaSX: Reliable gene expression signature scoring of cancer models and patients. Neoplasia , *23*, 1069–1077.

Lafzi, A., Moutinho, C., Picelli, S. and Heyn, H. (2018). Tutorial: guidelines for the experimental design of single-cell RNA sequencing studies. Nat Protoc , *13*, 2742–2757.

Lahnemann, D., Koster, J., Szczurek, E., McCarthy, D. J., Hicks, S. C., Robinson, M. D., Vallejos, C. A., Campbell, K. R., Beerenwinkel, N., Mahfouz, A., Pinello, L., Skums, P., Stamatakis, A., Attolini, C. S., Aparicio, S., Baaijens, J., Balvert, M., Barbanson, B., Cappuccio, A., Corleone, G., Dutilh, B. E., Florescu, M., Guryev, V., Holmer, R., Jahn, K., Lobo, T. J., Keizer, E. M., Khatri, I., Kielbasa, S. M., Korbel, J. O., Kozlov, A. M., Kuo, T. H., Lelieveldt, B. P. F., Mandoiu, I., Marioni, J. C., Marschall, T., Molder, F., Niknejad, A., Raczkowska, A., Reinders, M., Ridder, J., Saliba, A. E., Somarakis, A., Stegle, O., Theis, F. J., Yang, H., Zelikovsky, A., McHardy, A. C., Raphael, B. J., Shah, S. P. and Schonhuth, A. (2020). Eleven grand challenges in single-cell data science. Genome Biol , *21*, 31.

Lazear, H. M., Schoggins, J. W. and Diamond, M. S. (2019). Shared and Distinct Functions of Type I and Type III Interferons. Immunity , *50*, 907–923.

Lee, A. J. and Ashkar, A. A. (2018). The dual nature of type I and Type II interferons. Front Immunol , *9*, 2061.

Lee, H. K., Jung, O. and Hennighausen, L. (2020). Activation of interferon-stimulated transcriptomes and ace2 isoforms in human airway epithelium is curbed by janus kinase inhibitors. Preprint.

Li, H., van der Leun, A. M., Yofe, I., Lubling, Y., Gelbard-Solodkin, D., van Akkooi, A. C. J., van den Braber, M., Rozeman, E. A., Haanen, J. B. A. G., Blank, C. U., Horlings, H. M., David, E., Baran, Y., Bercovich, A., Lifshitz, A., Schumacher, T. N., Tanay, A. and Amit, I. (2020). Dysfunctional CD8 T Cells form a proliferative, dynamically regulated compartment within human melanoma. Cell , *181*, 747.

Liaw, A. and Wiener, M. (2002). Classification and regression by randomForest. R news , *2*, 18–22.

Liberzon, A., Birger, C., Thorvaldsdottir, H., Ghandi, M., Mesirov, J. P. and Tamayo, P. (2015). The Molecular Signatures Database (MSigDB) hallmark gene set collection. Cell Syst , *1*, 417–425.

Lim, J., Chin, V., Fairfax, K., Moutinho, C., Suan, D., Ji, H. and Powell, J. E. (2023). Transitioning single-cell genomics into the clinic. Nat Rev Genet , *24*, 573–584.

Linderman, G. C. (2021). Dimensionality reduction of single-cell RNA-seq data, pp. 331–342. New York, NY: Springer US.

Liu, M., Liu, J., Hao, S., Wu, P., Zhang, X., Xiao, Y., Jiang, G. and Huang, X. (2018). Higher activation of the interferon-gamma signaling pathway in systemic lupus erythematosus patients with a high type I IFN score: relation to disease activity. Clin Rheumatol , *37*, 2675–2684.

Lonsdale, J., Thomas, J., Salvatore, M., Phillips, R., Lo, E., Shad, S., Hasz, R., Walters, G., Garcia, F., Young, N., Foster, B., Moser, M., Karasik, E., Gillard, B., Ramsey, K., Sullivan, S., Bridge, J., Magazine, H., Syron, J., Fleming, J., Siminoff, L., Traino, H., Mosavel, M., Barker, L., Jewell, S., Rohrer, D., Maxim, D., Filkins, D., Harbach, P., Cortadillo, E., Berghuis, B., Turner, L., Hudson, E., Feenstra, K., Sobin, L., Robb, J., Branton, P., Korzeniewski, G., Shive, C., Tabor, D., Qi, L., Groch, K., Nampally, S., Buia, S., Zimmerman, A., Smith, A., Burges, R., Robinson, K., Valentino, K., Bradbury, D., Cosentino, M., Diaz-Mayoral, N., Kennedy, M., Engel, T., Williams, P., Erickson, K., Ardlie, K., Winckler, W., Getz, G., DeLuca, D., MacArthur, D., Kellis, M., Thomson, A., Young, T., Gelfand, E., Donovan, M., Meng, Y., Grant, G., Mash, D., Marcus, Y., Basile, M., Liu, J., Zhu, J., Tu, Z., Cox, N. J., Nicolae, D. L., Gamazon, E. R., Im, H. K., Konkashbaev, A., Pritchard, J., Stevens, M., Flutre, T., Wen, X., Dermitzakis, E. T., Lappalainen, T., Guigo, R., Monlong, J., Sammeth, M., Koller, D., Battle, A., Mostafavi, S., McCarthy, M., Rivas, M., Maller, J., Rusyn, I., Nobel, A., Wright, F., Shabalin, A., Feolo, M., Sharopova, N., Sturcke, A., Paschal, J., Anderson, J. M., Wilder, E. L., Derr, L. K., Green, E. D., Struewing, J. P., Temple, G., Volpi, S., Boyer, J. T., Thomson, E. J., Guyer, M. S., Ng, C., Abdallah, A., Colantuoni, D., Insel, T. R., Koester, S. E., Little, A. R., Bender, P. K., Lehner, T., Yao, Y., Compton, C. C., Vaught, J. B., Sawyer, S., Lockhart, N. C., Demchok, J. and Moore, H. F. (2013). The Genotype-Tissue Expression (GTEx) project. Nat Genet , *45*, 580–585.

Love, M. I., Huber, W. and Anders, S. (2014). Moderated estimation of fold change and dispersion for RNA-seq data with DESeq2. Genome Biol , *15*, 550.

Luecken, M. D., Büttner, M., Chaichoompu, K., Danese, A., Interlandi, M., Mueller, M. F., Strobl, D. C., Zappia, L., Dugas, M., Colomé-Tatché, M. and Theis, F. J. (2022). Benchmarking atlas-level data integration in single-cell genomics. Nat Methods , *19*, 41–50.

Luecken, M. D. and Theis, F. J. (2019). Current best practices in single-cell RNA-seq analysis: a tutorial. Mol Syst Biol , *15*, e8746.

Luo, B., Zheng, H., Liang, G., Luo, Y., Zhang, Q. and Li, X. (2024). HMGB3 Contributes to Anti-PD-1 Resistance by Inhibiting IFN-γ-Driven Ferroptosis in TNBC. Mol Carcinog , *64*.

Maechler, M. (2018). Cluster: cluster analysis basics and extensions.

Magen, A., Nie, J., Ciucci, T., Tamoutounour, S., Zhao, Y., Mehta, M., Tran, B., Mc-

Gavern, D. B., Hannenhalli, S. and Bosselut, R. (2019). Single-cell profiling defines transcriptomic signatures specific to tumor-Reactive versus virus-responsive CD4(+) T Cells. Cell Rep , *29*, 3019–3032.e6.

Mariathasan, S., Turley, S. J., Nickles, D., Castiglioni, A., Yuen, K., Wang, Y., Kadel, E. E., I., Koeppen, H., Astarita, J. L., Cubas, R., Jhunjhunwala, S., Banchereau, R., Yang, Y., Guan, Y., Chalouni, C., Ziai, J., Senbabaoglu, Y., Santoro, S., Sheinson, D., Hung, J., Giltnane, J. M., Pierce, A. A., Mesh, K., Lianoglou, S., Riegler, J., Carano, R. A. D., Eriksson, P., Hoglund, M., Somarriba, L., Halligan, D. L., van der Heijden, M. S., Loriot, Y., Rosenberg, J. E., Fong, L., Mellman, I., Chen, D. S., Green, M., Derleth, C., Fine, G. D., Hegde, P. S., Bourgon, R. and Powles, T. (2018). TGFbeta attenuates tumour response to PD-L1 blockade by contributing to exclusion of T cells. Nature , *554*, 544–548.

McInnes, L. and Healy, J. (2018). UMAP: Uniform manifold approximation and projection for dimension reduction. ArXiv , *abs/1802.03426*.

McKenzie, A. (2016). bayesbio: Miscellaneous Functions for Bioinformatics and Bayesian Statistics.

McNab, F., Mayer-Barber, K., Sher, A., Wack, A. and O'Garra, A. (2015). Type I interferons in infectious disease. Nat Rev Immunol , *15*, 87–103.

Melville, J., Lun, A., Djekidel, M. N. and Hao, Y. (2020). uwot: The uniform manifold approximation and projection (UMAP) method for dimensionality reduction. R package version 0.1 , *10*.

Mesev, E. V., LeDesma, R. A. and Ploss, A. (2019). Decoding type I and III interferon signalling during viral infection. Nat Microbiol , *4*, 914–924.

Michielsen, L., Lotfollahi, M., Strobl, D., Sikkema, L., Reinders, M. J. T., Theis, F. J. and Mahfouz, A. (2023). Single-cell reference mapping to construct and extend cell-type hierarchies. NAR Genom Bioinform , *5*.

Mo, X., Zhang, H., Preston, S., Martin, K., Zhou, B., Vadalia, N., Gamero, A. M., Soboloff, J., Tempera, I. and Zaidi, M. R. (2018). Interferon-gamma signaling in melanocytes and melanoma cells regulates expression of CTLA-4. Cancer Res , *78*, 436–450.

Morrow, A. N., Schmeisser, H., Tsuno, T. and Zoon, K. C. (2011). A novel role for IFN-stimulated gene factor 3II in IFN-γ signaling and induction of antiviral activity in human cells. J Immunol , *186*, 1685–93.

Newberg, L. A., Chen, X., Kodira, C. D. and Zavodszky, M. I. (2018). Computational de novo discovery of distinguishing genes for biological processes and cell types in complex tissues. PLoS One , *13*, e0193067.

Newman, A. M., Liu, C. L., Green, M. R., Gentles, A. J., Feng, W., Xu, Y., Hoang, C. D., Diehn, M. and Alizadeh, A. A. (2015). Robust enumeration of cell subsets from tissue expression profiles. Nat Methods , *12*, 453–457.

Nies, H. W., Zakaria, Z., Mohamad, M. S., Chan, W. H., Zaki, N., Sinnott, R. O., Napis, S., Chamoso, P., Omatu, S. and Corchado, J. M. (2019). A Review of Computational Methods for Clustering Genes with Similar Biological Functions. Processes , *7*.

Nieto, P., Elosua-Bayes, M., Trincado, J. L., Marchese, D., Massoni-Badosa, R., Salvany, M., Henriques, A., Nieto, J., Aguilar-Fernández, S., Mereu, E., Moutinho, C., Ruiz, S., Lorden, P., Chin, V. T., Kaczorowski, D., Chan, C. L., Gallagher, R., Chou, A., Planas-Rigol, E., Rubio-Perez, C., Gut, I., Piulats, J. M., Seoane, J., Powell, J. E., Batlle, E. and Heyn, H. (2021). A single-cell tumor immune atlas for precision oncology. Genome Res , *31*, 1913–1926.

Nirmal, A. J., Regan, T., Shih, B. B., Hume, D. A., Sims, A. H. and Freeman, T. C. (2018). Immune cell gene signatures for profiling the microenvironment of solid tumors. Cancer Immunol Res , *6*, 1388–1400.

Okoniewski, M. J. and Miller, C. J. (2006). Hybridization interactions between probesets in short oligo microarrays lead to spurious correlations. BMC Bioinformatics , *7*, 276.

Pallotta, M. T., Rossini, S., Suvieri, C., Coletti, A., Orabona, C., Macchiarulo, A., Volpi, C. and Grohmann, U. (2022). Indoleamine 2,3-dioxygenase 1 (IDO1): an up-to-date overview of an eclectic immunoregulatory enzyme. FEBS J , *289*, 6099–6118.

Pasquini, G., Rojo Arias, J. E., Schäfer, P. and Busskamp, V. (2021). Automated methods for cell type annotation on scRNA-seq data. Comput Struct Biotechnol J , *19*, 961–969.

Pearson, K. (1901). LIII. On lines and planes of closest fit to systems of points in space. The London, Edinburgh, and Dublin Philosophical Magazine and Journal of Science , *2*, 559–572.

Peng, S. L., Szabo, S. J. and Glimcher, L. H. (2002). T-bet regulates IgG class switching and pathogenic autoantibody production. Proc Natl Acad Sci U S A , *99*, 5545–5550.

Perry, A. K., Chen, G., Zheng, D., Tang, H. and Cheng, G. (2005). The host type I interferon response to viral and bacterial infections. Cell Res , *15*, 407–22.

Pertsovskaya, I., Abad, E., Domedel-Puig, N., Garcia-Ojalvo, J. and Villoslada, P. (2013). Transient oscillatory dynamics of interferon beta signaling in macrophages. BMC Syst Biol , *7*, 59.

Pinto, E. F. and Andrade, C. (2016). Interferon-related depression: A primer on mechanisms, treatment, and prevention of a common clinical problem. Curr Neuropharmacol , *14*, 743–8.

Platanias, L. C. (2005). Mechanisms of type-I- and type-II-interferon-mediated signalling. Nat Rev Immunol , *5*, 375–86.

Qi, Y. (2012). Random Forest for Bioinformatics, pp. 307–323. New York, NY: Springer New York.

Rahnenführer, J., Domingues, F. S., Maydt, J. and Lengauer, T. (2004). Calculating the statistical significance of changes in pathway activity from gene expression data. Stat Appl Genet Mol Biol , *3*, Article16.

Rai, T. S., Glass, M., Cole, J. J., Rather, M. I., Marsden, M., Neilson, M., Brock, C., Humphreys, I. R., Everett, R. D. and Adams, P. D. (2017). Histone chaperone HIRA deposits histone H3.3 onto foreign viral DNA and contributes to anti-viral intrinsic immunity. Nucleic Acids Res , *45*, 11673–11683.

Regev, A., Teichmann, S. A., Lander, E. S., Amit, I., Benoist, C., Birney, E., Bodenmiller, B., Campbell, P., Carninci, P., Clatworthy, M., Clevers, H., Deplancke, B., Dunham, I., Eberwine, J., Eils, R., Enard, W., Farmer, A., Fugger, L., Gottgens, B., Hacohen, N., Haniffa, M., Hemberg, M., Kim, S., Klenerman, P., Kriegstein, A., Lein, E., Linnarsson, S., Lundberg, E., Lundeberg, J., Majumder, P., Marioni, J. C., Merad, M., Mhlanga, M., Nawijn, M., Netea, M., Nolan, G., Pe'er, D., Phillipakis, A., Ponting, C. P., Quake, S., Reik, W., Rozenblatt-Rosen, O., Sanes, J., Satija, R., Schumacher, T. N., Shalek, A., Shapiro, E., Sharma, P., Shin, J. W., Stegle, O., Stratton, M., Stubbington, M. J. T., Theis, F. J., Uhlen, M., van Oudenaarden, A., Wagner, A., Watt, F., Weissman, J., Wold, B., Xavier, R., Yosef, N. and Human Cell Atlas Meeting, P. (2017). The Human Cell Atlas. Elife , *6*.

Reyes, M., Vickers, D., Billman, K., Eisenhaure, T., Hoover, P., Browne, E. P., Rao, D. A., Hacohen, N. and Blainey, P. C. (2019). Multiplexed enrichment and genomic profiling of peripheral blood cells reveal subset-specific immune signatures. Sci Adv , *5*, eaau9223.

Rice, G. I., Forte, G. M., Szynkiewicz, M., Chase, D. S., Aeby, A., Abdel-Hamid, M. S., Ackroyd, S., Allcock, R., Bailey, K. M., Balottin, U., Barnerias, C., Bernard, G., Bodemer, C., Botella, M. P., Cereda, C., Chandler, K. E., Dabydeen, L., Dale, R. C., De Laet, C., De Goede, C. G., Del Toro, M., Effat, L., Enamorado, N. N., Fazzi, E., Gener, B., Haldre, M., Lin, J. P., Livingston, J. H., Lourenco, C. M., Marques, W., J., Oades, P., Peterson, P., Rasmussen, M., Roubertie, A., Schmidt, J. L., Shalev, S. A., Simon, R., Spiegel, R., Swoboda, K. J., Temtamy, S. A., Vassallo, G., Vilain, C. N., Vogt, J., Wermenbol, V., Whitehouse, W. P., Soler, D., Olivieri, I., Orcesi, S., Aglan, M. S., Zaki, M. S., Abdel-Salam, G. M., Vanderver, A., Kisand, K., Rozenberg, F., Lebon, P. and Crow, Y. J. (2013). Assessment of interferon-related biomarkers in Aicardi-Goutieres syndrome associated with mutations in TREX1, RNASEH2A, RNASEH2B, RNASEH2C, SAMHD1, and ADAR: a case-control study. Lancet Neurol , *12*, 1159–69.

Ritchie, M. E., Phipson, B., Wu, D., Hu, Y., Law, C. W., Shi, W. and Smyth, G. K. (2015). limma powers differential expression analyses for RNA-sequencing and microarray studies. Nucleic Acids Res , *43*, e47.

Rooney, M. S., Shukla, S. A., Wu, C. J., Getz, G. and Hacohen, N. (2015). Molecular and genetic properties of tumors associated with local immune cytolytic activity. Cell , *160*, 48–61.

Rubtsova, K., Rubtsov, A. V., Thurman, J. M., Mennona, J. M., Kappler, J. W. and

Marrack, P. (2017). B cells expressing the transcription factor T-bet drive lupus-like autoimmunity. J Clin Invest , *127*, 1392–1404.

Rucker, G. (2012). Network meta-analysis, electrical networks and graph theory. Res Synth Methods , *3*, 312–24.

Satija, R. (2016). Seurat: R toolkit for single cell genomics. http://www.satijalab.org/seurat.html. http://www.satijalab.org/seurat.html.

Schelker, M., Feau, S., Du, J., Ranu, N., Klipp, E., MacBeath, G., Schoeberl, B. and Raue, A. (2017). Estimation of immune cell content in tumour tissue using single-cell RNA-seq data. Nat Commun , *8*, 2032.

Schneider, W. M., Chevillotte, M. D. and Rice, C. M. (2014). Interferon-stimulated genes: a complex web of host defenses. Annu Rev Immunol , *32*, 513–545.

Schreiber, G. (2017). The molecular basis for differential type I interferon signaling. J Biol Chem , *292*, 7285–7294.

Schroder, K., Hertzog, P. J., Ravasi, T. and Hume, D. A. (2003). Interferon-γ: an overview of signals, mechanisms and functions. J Leukoc Biol , *75*, 163–189.

Sharma, P., Retz, M., Siefker-Radtke, A., Baron, A., Necchi, A., Bedke, J., Plimack, E. R., Vaena, D., Grimm, M. O., Bracarda, S., Arranz, J. A., Pal, S., Ohyama, C., Saci, A., Qu, X., Lambert, A., Krishnan, S., Azrilevich, A. and Galsky, M. D. (2017). Nivolumab in metastatic urothelial carcinoma after platinum therapy (CheckMate 275): a multicentre, single-arm, phase 2 trial. Lancet Oncol , *18*, 312–322.

Sindhava, V. J., Oropallo, M. A., Moody, K., Naradikian, M., Higdon, L. E., Zhou, L., Myles, A., Green, N., Nündel, K., Stohl, W., Schmidt, A. M., Cao, W., Dorta-Estremera, S., Kambayashi, T., Marshak-Rothstein, A. and Cancro, M. P. (2017). A TLR9-dependent checkpoint governs B cell responses to DNA-containing antigens. J Clin Invest , *127*, 1651–1663.

Soon, W. W., Hariharan, M. and Snyder, M. P. (2013). High-throughput sequencing for biology and medicine. Mol Syst Biol , *9*, 640.

Sprang, M., Andrade-Navarro, M. A. and Fontaine, J.-F. (2022). Batch effect detection and correction in RNA-seq data using machine-learning-based automated assessment of quality. BMC Bioinformatics , *23*, 279.

Sri-Ngern-Ngam, K., Keawvilai, P., Pisitkun, T. and Palaga, T. (2022). Upregulation of programmed cell death 1 by interferon gamma and its biological functions in human monocytes. Biochem Biophys Rep , *32*, 101369.

Staub, E. (2012). An interferon response gene expression signature is activated in a subset of medulloblastomas. Transl Oncol , *5*, 297–304.

Stears, R. L., Martinsky, T. and Schena, M. (2003). Trends in microarray analysis. Nat Med , *9*, 140–5.

Stuart, T., Butler, A., Hoffman, P., Hafemeister, C., Papalexi, E., Mauck, W. M., r., Hao, Y., Stoeckius, M., Smibert, P. and Satija, R. (2019). Comprehensive Integration

of Single-Cell Data. Cell , *177*, 1888–1902.e21.

Sturm, G., Finotello, F., Petitprez, F., Zhang, J. D., Baumbach, J., Fridman, W. H., List, M. and Aneichyk, T. (2019). Comprehensive evaluation of transcriptome-based cell-type quantification methods for immuno-oncology. Bioinformatics , *35*, i436–i445.

Sun, X., Lin, X., Li, Z. and Wu, H. (2022). A comprehensive comparison of supervised and unsupervised methods for cell type identification in single-cell RNA-seq. Brief Bioinform , *23*.

Suvà, M. L. and Tirosh, I. (2019). Single-cell RNA sequencing in cancer: Lessons learned and emerging challenges. Mol Cell , *75*, 7–12.

Swiecki, M. and Colonna, M. (2011). Type I interferons: diversity of sources, production pathways and effects on immune responses. Curr Opin Virol , *1*, 463–75.

Tang, F., Barbacioru, C., Wang, Y., Nordman, E., Lee, C., Xu, N., Wang, X., Bodeau, J., Tuch, B. B., Siddiqui, A., Lao, K. and Surani, M. A. (2009). mRNA-Seq whole-transcriptome analysis of a single cell. Nat Med , *6*, 377–82.

Taylor, M. W. (2014). Interferons, vol. 1,. Springer Cham.

Thomas, C., Moraga, I., Levin, D., Krutzik, P. O., Podoplelova, Y., Trejo, A., Lee, C., Yarden, G., Vleck, S. E., Glenn, J. S., Nolan, G. P., Piehler, J., Schreiber, G. and Garcia, K. C. (2011). Structural linkage between ligand discrimination and receptor activation by type I interferons. Cell *146*, 621–32.

Toro-Domínguez, D., Martorell-Marugán, J., Goldman, D., Petri, M., Carmona-Sáez, P. and Alarcón-Riquelme, M. E. (2018). Stratification of Systemic Lupus Erythematosus Patients Into Three Groups of Disease Activity Progression According to Longitudinal Gene Expression. Arthritis Rheumatol *70*, 2025–2035.

Trapnell, C. (2015). Defining cell types and states with single-cell genomics. Genome Res *25*, 1491–8.

Uhlitz, F., Bischoff, P., Peidli, S., Sieber, A., Trinks, A., Lüthen, M., Obermayer, B., Blanc, E., Ruchiy, Y., Sell, T., Mamlouk, S., Arsie, R., Wei, T., Klotz-Noack, K., Schwarz, R. F., Sawitzki, B., Kamphues, C., Beule, D., Landthaler, M., Sers, C., Horst, D., Blüthgen, N. and Morkel, M. (2021). Mitogen-activated protein kinase activity drives cell trajectories in colorectal cancer. EMBO Mol Med *13*, e14123.

Van Allen, E. M., Miao, D., Schilling, B., Shukla, S. A., Blank, C., Zimmer, L., Sucker, A., Hillen, U., Foppen, M. H. G., Goldinger, S. M., Utikal, J., Hassel, J. C., Weide, B., Kaehler, K. C., Loquai, C., Mohr, P., Gutzmer, R., Dummer, R., Gabriel, S., Wu, C. J., Schadendorf, D. and Garraway, L. A. (2015). Genomic correlates of response to CTLA-4 blockade in metastatic melanoma. Science *350*, 207–211.

Van den Berge, K., Hembach, K. M., Soneson, C., Tiberi, S., Clement, L., Love, M. I., Patro, R. and Robinson, M. D. (2019). RNA sequencing data: Hitchhiker's guide to expression analysis. Annu Rev Biomed Data Sci *2*, 139–173.

van der Maaten, L. and Hinton, G. (2008). Viualizing data using t-SNE. Journal of

Machine Learning Research *9*, 2579–2605.

Vijaymeena, M. and Kavitha, K. (2016). A survey on similarity measures in text mining. Machine Learning and Applications: An International Journal *3*, 19–28.

Waddell, S. J., Popper, S. J., Rubins, K. H., Griffiths, M. J., Brown, P. O., Levin, M. and Relman, D. A. (2010). Dissecting interferon-induced transcriptional programs in human peripheral blood cells. PLoS One *5*, e9753.

Walsh, R. J., Kong, S. W., Yao, Y., Jallal, B., Kiener, P. A., Pinkus, J. L., Beggs, A. H., Amato, A. A. and Greenberg, S. A. (2007). Type I interferon-inducible gene expression in blood is present and reflects disease activity in dermatomyositis and polymyositis. Arthritis Rheum *56*, 3784–92.

Wang, Z., Gerstein, M. and Snyder, M. (2009). RNA-Seq: a revolutionary tool for transcriptomics. Nat Rev Genet *10*, 57–63.

Winter, C., Kosch, R., Ludlow, M., Osterhaus, A. and Jung, K. (2019). Network meta-analysis correlates with analysis of merged independent transcriptome expression data. BMC Bioinformatics *20*, 144.

Wu, S. Z., Al-Eryani, G., Roden, D. L., Junankar, S., Harvey, K., Andersson, A., Thennavan, A., Wang, C., Torpy, J. R., Bartonicek, N., Wang, T., Larsson, L., Kaczorowski, D., Weisenfeld, N. I., Uytingco, C. R., Chew, J. G., Bent, Z. W., Chan, C.-L., Gnanasambandapillai, V., Dutertre, C.-A., Gluch, L., Hui, M. N., Beith, J., Parker, A., Robbins, E., Segara, D., Cooper, C., Mak, C., Chan, B., Warrier, S., Ginhoux, F., Millar, E., Powell, J. E., Williams, S. R., Liu, X. S., O'Toole, S., Lim, E., Lundeberg, J., Perou, C. M. and Swarbrick, A. (2021). A single-cell and spatially resolved atlas of human breast cancers. Nat Genet *53*, 1334–1347.

Wu, T. D., Madireddi, S., de Almeida, P. E., Banchereau, R., Chen, Y.-J. J., Chitre, A. S., Chiang, E. Y., Iftikhar, H., O'Gorman, W. E., Au-Yeung, A., Takahashi, C., Goldstein, L. D., Poon, C., Keerthivasan, S., de Almeida Nagata, D. E., Du, X., Lee, H.-M., Banta, K. L., Mariathasan, S., Das Thakur, M., Huseni, M. A., Ballinger, M., Estay, I., Caplazi, P., Modrusan, Z., Delamarre, L., Mellman, I., Bourgon, R. and Grogan, J. L. (2020). Peripheral T cell expansion predicts tumour infiltration and clinical response. Nature *579*, 274–278.

Xia, B. and Yanai, I. (2019). A periodic table of cell types. Development *146*.

Xie, B., Jiang, Q., Mora, A. and Li, X. (2021). Automatic cell type identification methods for single-cell RNA sequencing. Comput Struct Biotechnol J *19*, 5874–5887.

Xu, R. and Wunsch, D. (2005). Survey of clustering algorithms. IEEE Transactions on Neural Networks *16*, 645–678.

Yan, K., Lu, Y., Yan, Z. and Wang, Y. (2021). 9-Gene signature correlated with CD8(+) T cell infiltration activated by IFN-γ: A biomarker of immune checkpoint therapy response in melanoma. Front Immunol *12*, 622563.

Zeng, H. (2022). What is a cell type and how to define it? Cell *185*, 2739–2755.

Zhang, J. M., Kamath, G. M. and Tse, D. N. (2019a). Valid post-clustering differential analysis for single-cell RNA-seq. Cell Syst *9*, 383–392.e6.

Zhang, Q., He, Y., Luo, N., Patel, S. J., Han, Y., Gao, R., Modak, M., Carotta, S., Haslinger, C., Kind, D., Peet, G. W., Zhong, G., Lu, S., Zhu, W., Mao, Y., Xiao, M., Bergmann, M., Hu, X., Kerkar, S. P., Vogt, A. B., Pflanz, S., Liu, K., Peng, J., Ren, X. and Zhang, Z. (2019b). Landscape and dynamics of single immune cells in hepatocellular carcinoma. Cell *179*, 829–845.e20.

Zhang, X., Lan, Y., Xu, J., Quan, F., Zhao, E., Deng, C., Luo, T., Xu, L., Liao, G., Yan, M., Ping, Y., Li, F., Shi, A., Bai, J., Zhao, T., Li, X. and Xiao, Y. (2019c). CellMarker: a manually curated resource of cell markers in human and mouse. Nucleic Acids Res *47*, D721–d728.

Zhao, X., Wu, S., Fang, N., Sun, X. and Fan, J. (2019). Evaluation of single-cell classifiers for single-cell RNA sequencing data sets. Brief Bioinform *21*, 1581–1595.

Zheng, G. X., Terry, J. M., Belgrader, P., Ryvkin, P., Bent, Z. W., Wilson, R., Ziraldo, S. B., Wheeler, T. D., McDermott, G. P., Zhu, J., Gregory, M. T., Shuga, J., Montesclaros, L., Underwood, J. G., Masquelier, D. A., Nishimura, S. Y., Schnall-Levin, M., Wyatt, P. W., Hindson, C. M., Bharadwaj, R., Wong, A., Ness, K. D., Beppu, L. W., Deeg, H. J., McFarland, C., Loeb, K. R., Valente, W. J., Ericson, N. G., Stevens, E. A., Radich, J. P., Mikkelsen, T. S., Hindson, B. J. and Bielas, J. H. (2017). Massively parallel digital transcriptional profiling of single cells. Nat Commun *8*, 14049.

Zhu, H., Hu, X., Feng, S., Li, Y., Zhang, Y., Qiu, S., Chen, R., Ye, Y., Gu, L., Jian, Z., Xu, X. and Xiong, X. (2022). APOL4, a Novel Immune-Related Prognostic Biomarker for Glioma. J Clin Med *11*.

Zhu, X., Zhang, J., Xu, Y., Wang, J., Peng, X. and Li, H.-D. (2020). Single-Cell Clustering Based on Shared Nearest Neighbor and Graph Partitioning. Interdiscip Sci *12*, 117–130.

Ziegler, C. G. K., Allon, S. J., Nyquist, S. K., Mbano, I. M., Miao, V. N., Tzouanas, C. N., Cao, Y., Yousif, A. S., Bals, J., Hauser, B. M., Feldman, J., Muus, C., Wadsworth, M. H., n., Kazer, S. W., Hughes, T. K., Doran, B., Gatter, G. J., Vukovic, M., Taliaferro, F., Mead, B. E., Guo, Z., Wang, J. P., Gras, D., Plaisant, M., Ansari, M., Angelidis, I., Adler, H., Sucre, J. M. S., Taylor, C. J., Lin, B., Waghray, A., Mitsialis, V., Dwyer, D. F., Buchheit, K. M., Boyce, J. A., Barrett, N. A., Laidlaw, T. M., Carroll, S. L., Colonna, L., Tkachev, V., Peterson, C. W., Yu, A., Zheng, H. B., Gideon, H. P., Winchell, C. G., Lin, P. L., Bingle, C. D., Snapper, S. B., Kropski, J. A., Theis, F. J., Schiller, H. B., Zaragosi, L. E., Barbry, P., Leslie, A., Kiem, H. P., Flynn, J. L., Fortune, S. M., Berger, B., Finberg, R. W., Kean, L. S., Garber, M., Schmidt, A. G., Lingwood, D., Shalek, A. K. and Ordovas-Montanes, J. (2020). SARS-CoV-2 Receptor ACE2 Is an Interferon-Stimulated Gene in Human Airway Epithelial Cells and Is Detected in Specific Cell Subsets across Tissues. Cell *181*, 1016–1035.e19.

Zilionis, R., Engblom, C., Pfirschke, C., Savova, V., Zemmour, D., Saatcioglu, H. D.,

Krishnan, I., Maroni, G., Meyerovitz, C. V., Kerwin, C. M., Choi, S., Richards, W. G., De Rienzo, A., Tenen, D. G., Bueno, R., Levantini, E., Pittet, M. J. and Klein, A. M. (2019). Single-cell transcriptomics of human and mouse lung cancers reveals conserved myeloid populations across individuals and species. Immunity *50*, 1317–1334.e10.

Zou, C.-Y., Guan, G.-F., Zhu, C., Liu, T.-Q., Guo, Q., Cheng, W. and Wu, A.-H. (2019). Costimulatory checkpoint SLAMF8 is an independent prognosis factor in glioma. CNS Neurosci Ther *25*, 333–342.

A Appendix

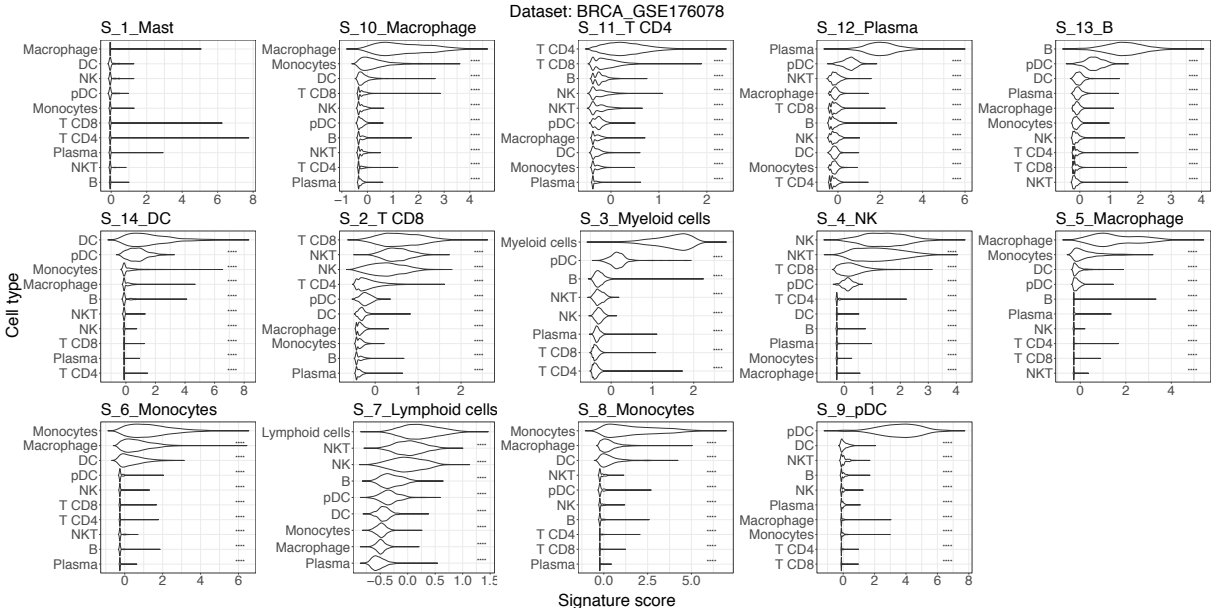
Dataset: BRCA_GSE176078
S_1_Mast
S_10_Macrophage
S_11_T CD4
S_12_Plasma
S_13_B
S_14_DC
S_2_T CD8
S_3_Myeloid cells
S_4_NK
S_5_Macrophage
S_6_Monocytes
S_7_Lymphoid cells
S_8_Monocytes
S_9_pDC
Cell type
Signature score

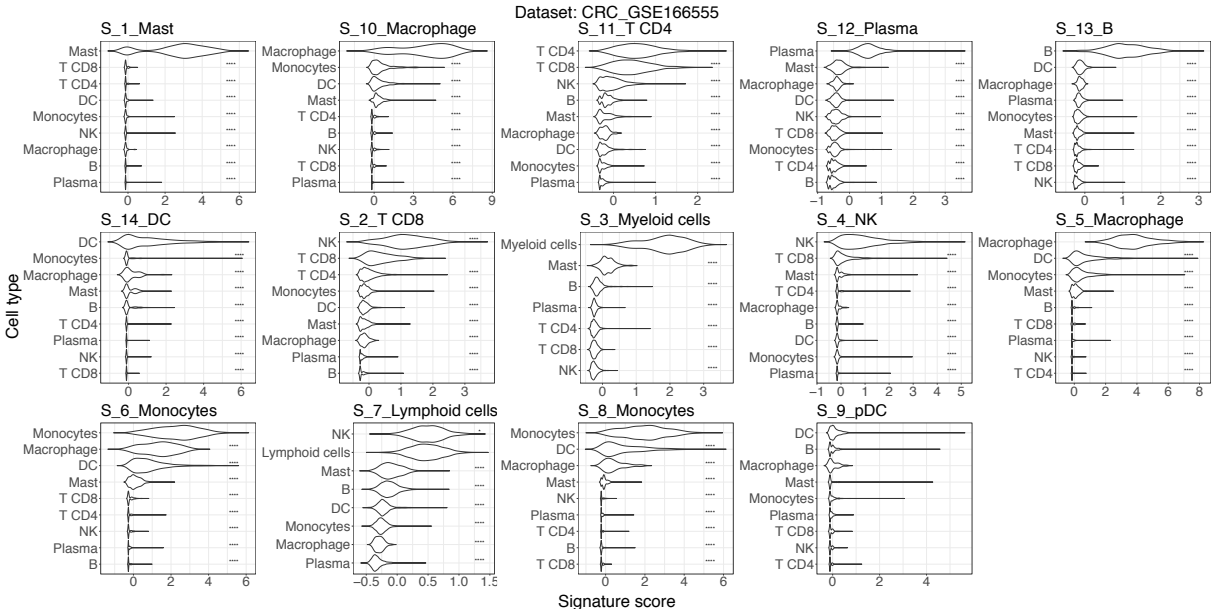
Dataset: CRC_GSE166555
S_1_Mast
S_10_Macrophage
S_11_T CD4
S_12_Plasma
S_13_B
S_14_DC
S_2_T CD8
S_3_Myeloid cells
S_4_NK
S_5_Macrophage
S_6_Monocytes
S_7_Lymphoid cells
S_8_Monocytes
S_9_pDC
Cell type
Signature score

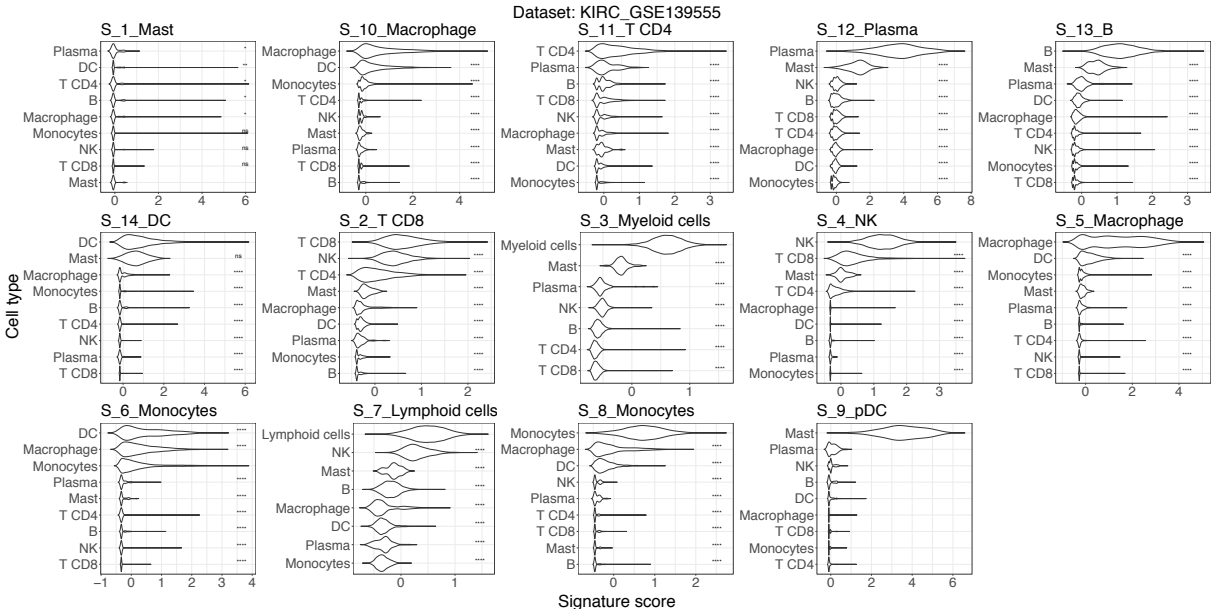
Dataset: KIRC_GSE139555
S_1_Mast
S_10_Macrophage
S_11_T CD4
S_12_Plasma
S_13_B
S_14_DC
S_2_T CD8
S_3_Myeloid cells
S_4_NK
S_5_Macrophage
S_6_Monocytes
S_7_Lymphoid cells
S_8_Monocytes
S_9_pDC
Cell type
Signature score

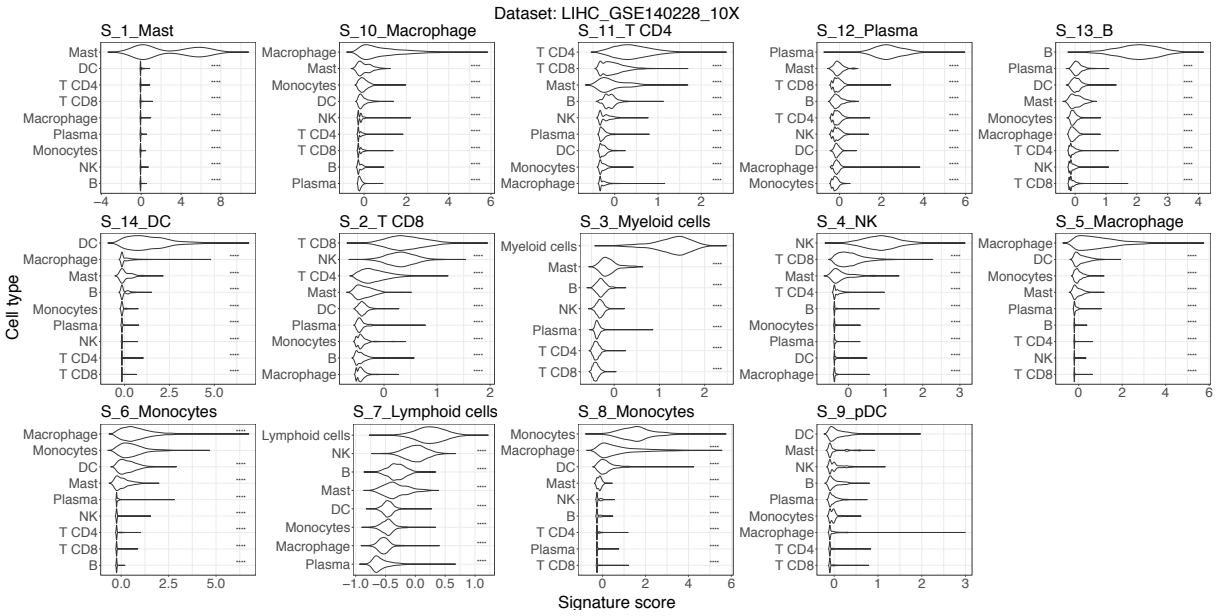
Dataset: LIHC_GSE140228_10X
S_1_Mast
S_10_Macrophage
S_11_T CD4
S_12_Plasma
S_13_B
S_14_DC
S_2_T CD8
S_3_Myeloid cells
S_4_NK
S_5_Macrophage
S_6_Monocytes
S_7_Lymphoid cells
S_8_Monocytes
S_9_pDC
Cell type
Signature score

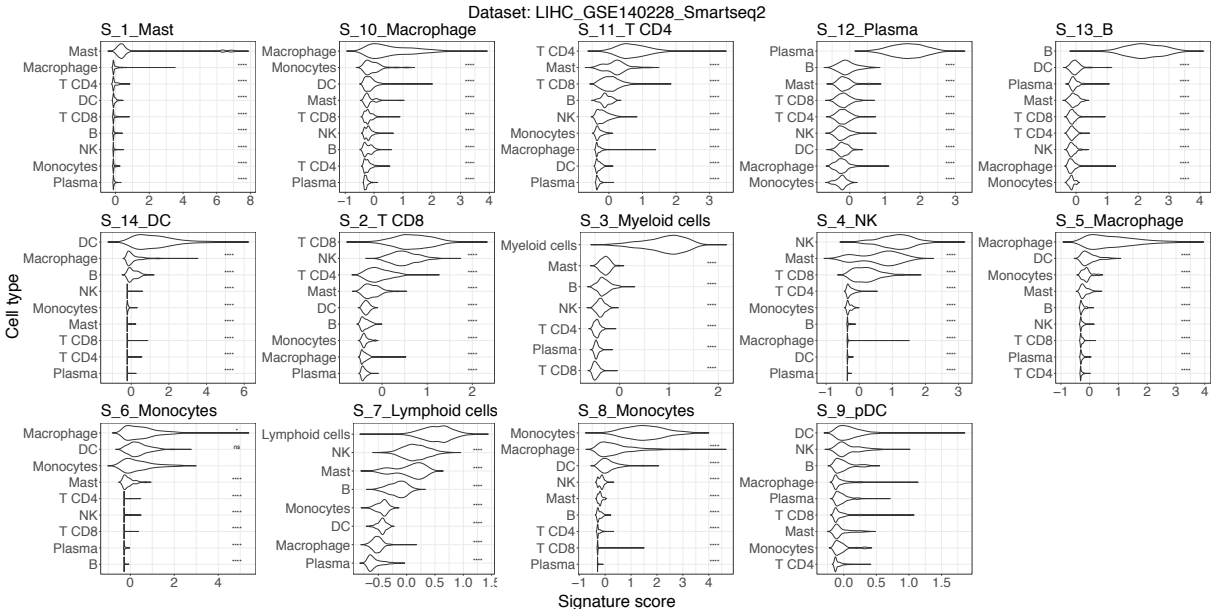
Dataset: LIHC_GSE140228_Smartseq2
S_1_Mast
S_10_Macrophage
S_11_T CD4
S_12_Plasma
S_13_B
S_14_DC
S_2_T CD8
S_3_Myeloid cells
S_4_NK
S_5_Macrophage
S_6_Monocytes
S_7_Lymphoid cells
S_8_Monocytes
S_9_pDC
Cell type
Signature score

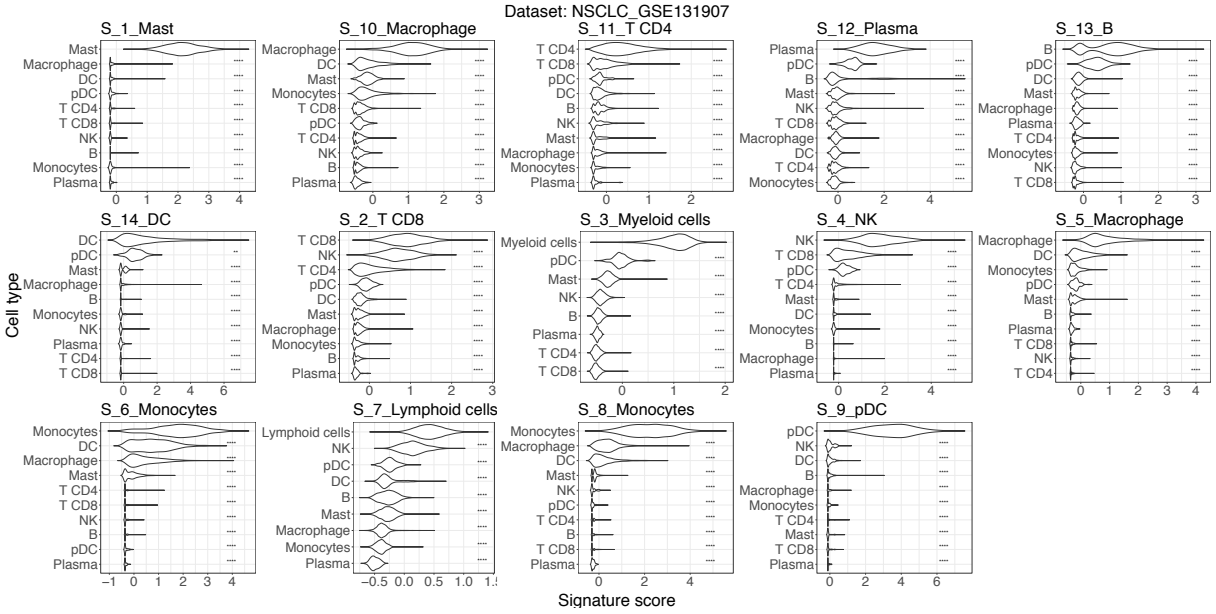
Dataset: NSCLC_GSE131907
S_1_Mast
S_10_Macrophage
S_11_T CD4
S_12_Plasma
S_13_B
S_14_DC
S_2_T CD8
S_3_Myeloid cells
S_4_NK
S_5_Macrophage
S_6_Monocytes
S_7_Lymphoid cells
S_8_Monocytes
S_9_pDC
Cell type
Signature score

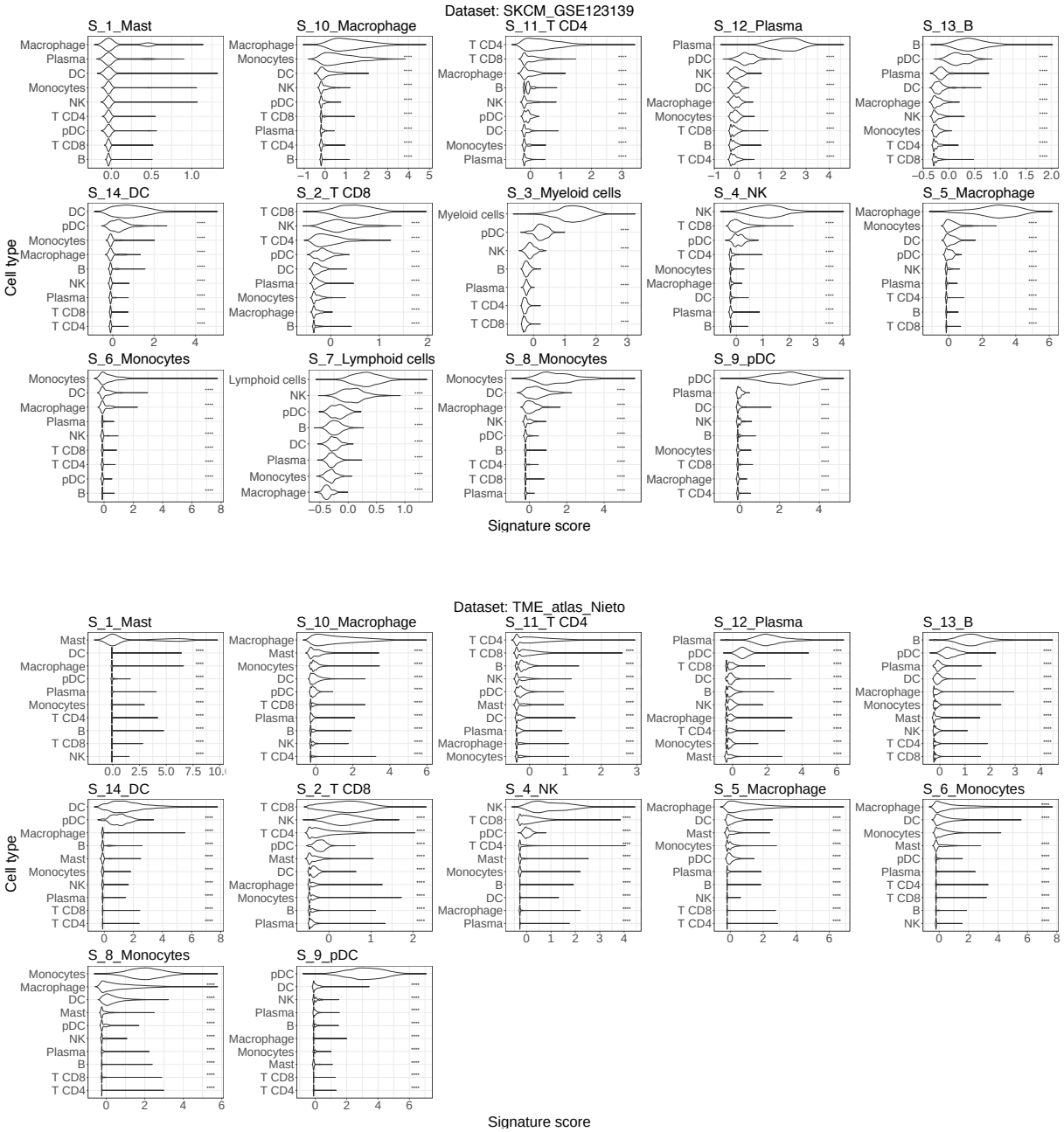

Figure A.1: Violin plots for validating the gene signatures in the discovery and validation datasets.

Mean signature scores are calculated for each signature and each cell in discovery and validation datasets. High expression of a gene set in the corresponding cell type is tested using Wilcoxon rank sum tests (non-significant ($p > 0.05$) - not shown; * = $p < 0.05$, ** = $p < 0.01$). (Reprinted from Aybey et al. (2023))

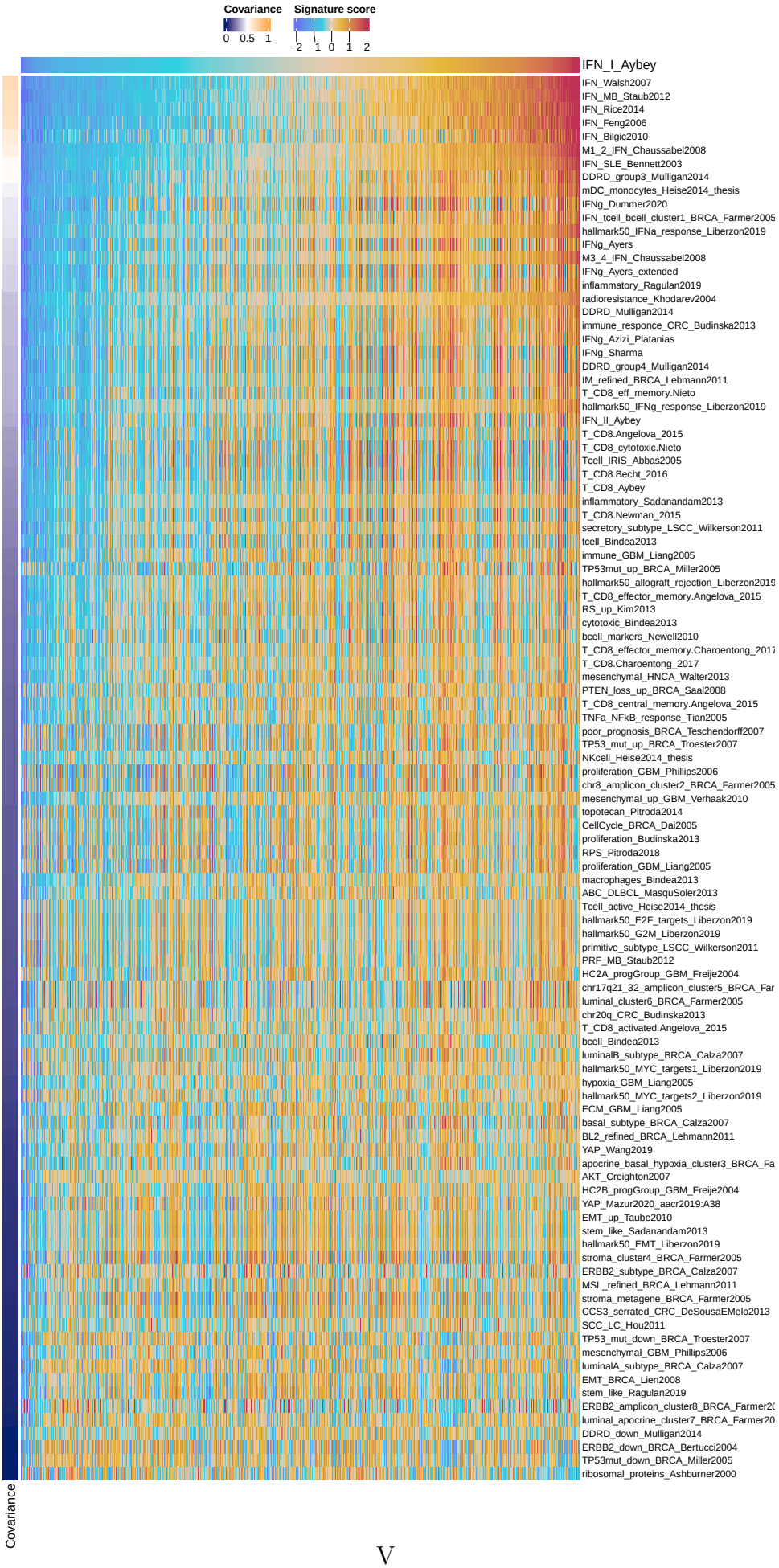
Covariance
0 0.5 1
Signature score
−2 −1 0 1 2
IFN_I_Aybey
IFN_Walsh2007
IFN_MB_Staub2012
IFN_Rice2014
IFN_Feng2006
IFN_Bilgic2010
M1_2_IFN_Chaussabel2008
IFN_SLE_Bennett2003
DDRD_group3_Mulligan2014
mDC_monocytes_Heise2014_thesis
IFNg_Dummer2020
IFN_tcell_bcell_cluster1_BRCA_Farmer2005
hallmark50_IFNa_response_Liberzon2019
IFNg_Ayers
M3_4_IFN_Chaussabel2008
IFNg_Ayers_extended
inflammatory_Ragulan2019
radioresistance_Khodarev2004
DDRD_Mulligan2014
immune_responce_CRC_Budinska2013
IFNg_Azizi_Platanias
IFNg_Sharma
DDRD_group4_Mulligan2014
IM_refined_BRCA_Lehmann2011
T_CD8_eff_memory.Nieto
hallmark50_IFNg_response_Liberzon2019
IFN_II_Aybey
T_CD8.Angelova_2015
T_CD8_cytotoxic.Nieto
Tcell_IRIS_Abbas2005
T_CD8.Becht_2016
T_CD8_Aybey
inflammatory_Sadanandam2013
T_CD8.Newman_2015
secretory_subtype_LSCC_Wilkerson2011
tcell_Bindea2013
immune_GBM_Liang2005
TP53mut_up_BRCA_Miller2005
hallmark50_allograft_rejection_Liberzon2019
T_CD8_effector_memory.Angelova_2015
RS_up_Kim2013
cytotoxic_Bindea2013
bcell_markers_Newell2010
T_CD8_effector_memory.Charoentong_2017
T_CD8.Charoentong_2017
mesenchymal_HNCA_Walter2013
PTEN_loss_up_BRCA_Saal2008
T_CD8_central_memory.Angelova_2015
TNFa_NFkB_response_Tian2005
poor_prognosis_BRCA_Teschendorff2007
TP53_mut_up_BRCA_Troester2007
NKcell_Heise2014_thesis
proliferation_GBM_Phillips2006
chr8_amplicon_cluster2_BRCA_Farmer2005
mesenchymal_up_GBM_Verhaak2010
topotecan_Pitroda2014
CellCycle_BRCA_Dai2005
proliferation_Budinska2013
RPS_Pitroda2018
proliferation_GBM_Liang2005
macrophages_Bindea2013
ABC_DLBCL_MasquSoler2013
Tcell_active_Heise2014_thesis
hallmark50_E2F_targets_Liberzon2019
hallmark50_G2M_Liberzon2019
primitive_subtype_LSCC_Wilkerson2011
PRF_MB_Staub2012
HC2A_progGroup_GBM_Freije2004
chr17q21_32_amplicon_cluster5_BRCA_Far
luminal_cluster6_BRCA_Farmer2005
chr20q_CRC_Budinska2013
T_CD8_activated.Angelova_2015
bcell_Bindea2013
luminalB_subtype_BRCA_Calza2007
hallmark50_MYC_targets1_Liberzon2019
hypoxia_GBM_Liang2005
hallmark50_MYC_targets2_Liberzon2019
ECM_GBM_Liang2005
basal_subtype_BRCA_Calza2007
BL2_refined_BRCA_Lehmann2011
YAP_Wang2019
apocrine_basal_hypoxia_cluster3_BRCA_Fa
AKT_Creighton2007
HC2B_progGroup_GBM_Freije2004
YAP_Mazur2020_aacr2019:A38
EMT_up_Taube2010
stem_like_Sadanandam2013
hallmark50_EMT_Liberzon2019
stroma_cluster4_BRCA_Farmer2005
ERBB2_subtype_BRCA_Calza2007
MSL_refined_BRCA_Lehmann2011
stroma_metagene_BRCA_Farmer2005
CCS3_serrated_CRC_DeSousaEMelo2013
SCC_LC_Hou2011
TP53_mut_down_BRCA_Troester2007
mesenchymal_GBM_Phillips2006
luminalA_subtype_BRCA_Calza2007
EMT_BRCA_Lien2008
stem_like_Ragulan2019
ERBB2_amplicon_cluster8_BRCA_Farmer2(
luminal_apocrine_cluster7_BRCA_Farmer20
DDRD_down_Mulligan2014
ERBB2_down_BRCA_Bertucci2004
TP53mut_down_BRCA_Miller2005
ribosomal_proteins_Ashburner2000
Covariance

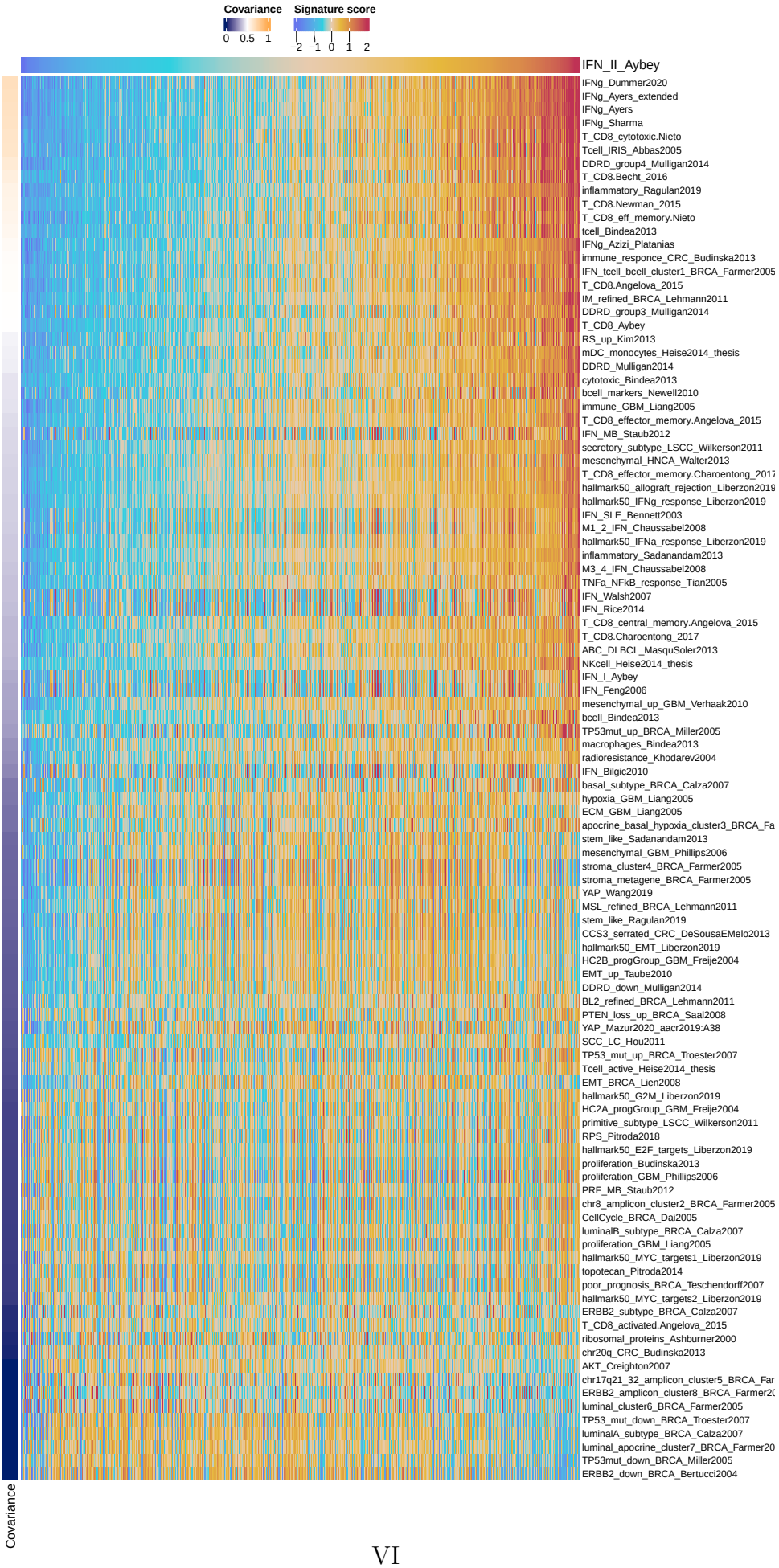
Covariance
0 0.5 1
Signature score
−2 −1 0 1 2
IFN_II_Aybey
IFNg_Dummer2020
IFNg_Ayers_extended
IFNg_Ayers
IFNg_Sharma
T_CD8_cytotoxic.Nieto
Tcell_IRIS_Abbas2005
DDRD_group4_Mulligan2014
T_CD8.Becht_2016
inflammatory_Ragulan2019
T_CD8.Newman_2015
T_CD8_eff_memory.Nieto
tcell_Bindea2013
IFNg_Azizi_Platanias
immune_responce_CRC_Budinska2013
IFN_tcell_bcell_cluster1_BRCA_Farmer2005
T_CD8.Angelova_2015
IM_refined_BRCA_Lehmann2011
DDRD_group3_Mulligan2014
T_CD8_Aybey
RS_up_Kim2013
mDC_monocytes_Heise2014_thesis
DDRD_Mulligan2014
cytotoxic_Bindea2013
bcell_markers_Newell2010
immune_GBM_Liang2005
T_CD8_effector_memory.Angelova_2015
IFN_MB_Staub2012
secretory_subtype_LSCC_Wilkerson2011
mesenchymal_HNCA_Walter2013
T_CD8_effector_memory.Charoentong_2017
hallmark50_allograft_rejection_Liberzon2019
hallmark50_IFNg_response_Liberzon2019
IFN_SLE_Bennett2003
M1_2_IFN_Chaussabel2008
hallmark50_IFNa_response_Liberzon2019
inflammatory_Sadanandam2013
M3_4_IFN_Chaussabel2008
TNFa_NFkB_response_Tian2005
IFN_Walsh2007
IFN_Rice2014
T_CD8_central_memory.Angelova_2015
T_CD8.Charoentong_2017
ABC_DLBCL_MasquSoler2013
NKcell_Heise2014_thesis
IFN_I_Aybey
IFN_Feng2006
mesenchymal_up_GBM_Verhaak2010
bcell_Bindea2013
TP53mut_up_BRCA_Miller2005
macrophages_Bindea2013
radioresistance_Khodarev2004
IFN_Bilgic2010
basal_subtype_BRCA_Calza2007
hypoxia_GBM_Liang2005
ECM_GBM_Liang2005
apocrine_basal_hypoxia_cluster3_BRCA_Fa
stem_like_Sadanandam2013
mesenchymal_GBM_Phillips2006
stroma_cluster4_BRCA_Farmer2005
stroma_metagene_BRCA_Farmer2005
YAP_Wang2019
MSL_refined_BRCA_Lehmann2011
stem_like_Ragulan2019
CCS3_serrated_CRC_DeSousaEMelo2013
hallmark50_EMT_Liberzon2019
HC2B_progGroup_GBM_Freije2004
EMT_up_Taube2010
DDRD_down_Mulligan2014
BL2_refined_BRCA_Lehmann2011
PTEN_loss_up_BRCA_Saal2008
YAP_Mazur2020_aacr2019:A38
SCC_LC_Hou2011
TP53_mut_up_BRCA_Troester2007
Tcell_active_Heise2014_thesis
EMT_BRCA_Lien2008
hallmark50_G2M_Liberzon2019
HC2A_progGroup_GBM_Freije2004
primitive_subtype_LSCC_Wilkerson2011
RPS_Pitroda2018
hallmark50_E2F_targets_Liberzon2019
proliferation_Budinska2013
proliferation_GBM_Phillips2006
PRF_MB_Staub2012
chr8_amplicon_cluster2_BRCA_Farmer2005
CellCycle_BRCA_Dai2005
luminalB_subtype_BRCA_Calza2007
proliferation_GBM_Liang2005
hallmark50_MYC_targets1_Liberzon2019
topotecan_Pitroda2014
poor_prognosis_BRCA_Teschendorff2007
hallmark50_MYC_targets2_Liberzon2019
ERBB2_subtype_BRCA_Calza2007
T_CD8_activated.Angelova_2015
ribosomal_proteins_Ashburner2000
chr20q_CRC_Budinska2013
AKT_Creighton2007
chr17q21_32_amplicon_cluster5_BRCA_Far
ERBB2_amplicon_cluster8_BRCA_Farmer2(
luminal_cluster6_BRCA_Farmer2005
TP53_mut_down_BRCA_Troester2007
luminalA_subtype_BRCA_Calza2007
luminal_apocrine_cluster7_BRCA_Farmer20
TP53mut_down_BRCA_Miller2005
ERBB2_down_BRCA_Bertucci2004
Covariance

Figure A.2: RosettaSX analysis showing relation of all coherent signatures to my IFN GESs in TCGA BRCA cohort.

A similar analysis from Kreis et al. (2021) is performed using all published signatures compiled by Kreis et al. (2021) and additional published $CD8^+$ T cell and IFN-II signatures. Mean signature scores are calculated only for coherent signatures (coherence score > 0.2). All coherent signatures are depicted as opposed to top 20 signatutes with the highest covariance in Figure 3.9. Covariance between each of my IFN signatures and coherent signatures are calculated. Mean signature scores are shown from low (blue) to high (red). Covariance values are shown from low (dark blue) to high (orange).